National Library of Canada

Acquisitions and Bibliographic Services Branch

395 Wellington Street
Ottawa, Ontario
K1A 0N4

Bibliothèque nationale du Canada

Direction des acquisitions et des services bibliographiques

395, rue Wellington
Ottawa (Ontario)
K1A 0N4

Your file Votre référence

Our file Notre référence

NOTICE

The quality of this microform is heavily dependent upon the quality of the original thesis submitted for microfilming. Every effort has been made to ensure the highest quality of reproduction possible.

If pages are missing, contact the university which granted the degree.

Some pages may have indistinct print especially if the original pages were typed with a poor typewriter ribbon or if the university sent us an inferior photocopy.

AVIS

La qualité de cette microforme dépend grandement de la qualité de la thèse soumise au microfilmage. Nous avons tout fait pour assurer une qualité supérieure de reproduction.

S'il manque des pages, veuillez communiquer avec l'université qui a conféré le grade.

La qualité d'impression de certaines pages peut laisser à désirer, surtout si les pages originales ont été dactylographiées à l'aide d'un ruban usé ou si l'université nous a fait parvenir une photocopie de qualité inférieure.

Canada

Laser Nonlinearity Compensation for Subcarrier Multiplexed Optical Transmission Systems

By

Niloufar Tayebi, B.A.Sc.

A thesis submitted to the
School of Graduate Studies and Research
University of Ottawa
in partial fulfillment of the requirements
for the degree of

Master of Applied Science

Ottawa-Carleton Institute for Electrical Engineering

Department of Electrical Engineering
Faculty of Engineering
University of Ottawa

ISBN 0-315-85765-X

Canada

UNIVERSITÉ D'OTTAWA
UNIVERSITY OF OTTAWA

Acknowledgements

I wish to express my sincere gratitude to my academic supervisor Dr. Mohsen Kavehrad for his help and encouragement during the course of the M.A.Sc. program.

Thanks to all professors, colleages and friends at the Department of Electrical Engineering, University of Ottawa for their helpful discussions.

This research was partially supported by the Telecommunications Research institute of Ontario, Photonic Networks and Systems Thrust and in parts by the Natural Science and Engineering Research Council of Canada.

Contents

List of Figures

List of Tables

Acronyms

AM-VSB ..... Amplitude Modulation-Vestigial Side-Band

CATV ..... Cable Television

CNR ..... Carrier-to-Noise Ratio

CSO ..... Composite Second Order

CTB ..... Composite Triple Beat

DFB ..... Distributed Feedback

FDM ..... Frequency Division Multiplexing

FM ..... Frequency Modulation

HDTV ..... High Definition Television

ILD ..... Injection Laser Diode

IMD ..... Intermodulation Distortion

IMP ..... Intermodulation Product

LD ..... Laser Diode

LED ..... Light-Emitting Diode

OMD ..... Optical Modulation Depth

QAM ..... Quadrature Amplitude Modulation

RIN ..... Relative Intensity Noise

Sig. Sp. ..... Signal Spontaneous beat noise

SNR ..... Signal-to Noise Ratio

TE ..... Transverse Electric

TM ..... Transverse Magnetic

WDM ..... Wavelength Division Multiplexing

Abstract

Subcarrier multiplexing efficiently uses the available fiber bandwidth in video transmission. Semiconductor lasers are usually used as optical transmitters in such systems. A semiconductor laser exhibits nonlinear characteristics. Nonlinearity degrades system performance. For nonlinearity compensation, a nonlinear predistortion block is assumed to be incorporated prior to the laser. Characteristics of this nonlinear block invert those of the laser. Performance of the subcarrier multiplexed system with and without predistortion is evaluated by harmonic distortion and intermodulation distortion analyses. Nonlinear distortion level decreases significantly when predistortion is employed prior to the laser. This enhancement results in system requirements for carrier-to-noise ratio being met.

Chapter I

Introduction

1.1 Introduction

Subcarrier Multiplexing is an efficient use of the available fiber bandwidth in video transmission. Video signals modulate carriers which are equally spaced in the available bandwidth. Fig.1.1 depicts a block diagram for a subcarrier multiplexing system. Modulated carriers are combined to form the electric input signal to the laser. The output optical signal reaches the receiver via fiber. At the receiver a photodetector converts the optical power to an electrical signal. The electrical signal is demultiplexed by the bandpass filters and then demodulated.

A semiconductor laser has nonlinear characteristics. The input current of a semiconductor laser has to exceed a certain threshold level in order for any optical output to result. Laser light-current (L/I) characteristic is shown in Fig.1.2. Nonlinearity causes generation of new frequencies. Applying a large signal to the system causes Nonlinear Distortion (ND). In the case when there are several small input signals, their phasor sum results in a signal that is equivalent to a large signal applied to the system. So the overall effect of them is like the effect of a large signal that yields Nonlinear Distortion. In CATV transmission, several subcarriers are multiplexed to modulate a single laser diode light. Each of the subcarriers current can be represented by a phasor which has a particular amplitude, frequency and phase. The *total* current that forms the input current to the laser, is the phasor sum of the amplitude and the phase of subcarriers. If this sum, or *total* current, exceeds the range between the bias current and threshold current, zero-level clipping occurs in the output power. This is shown in Fig.1.3.

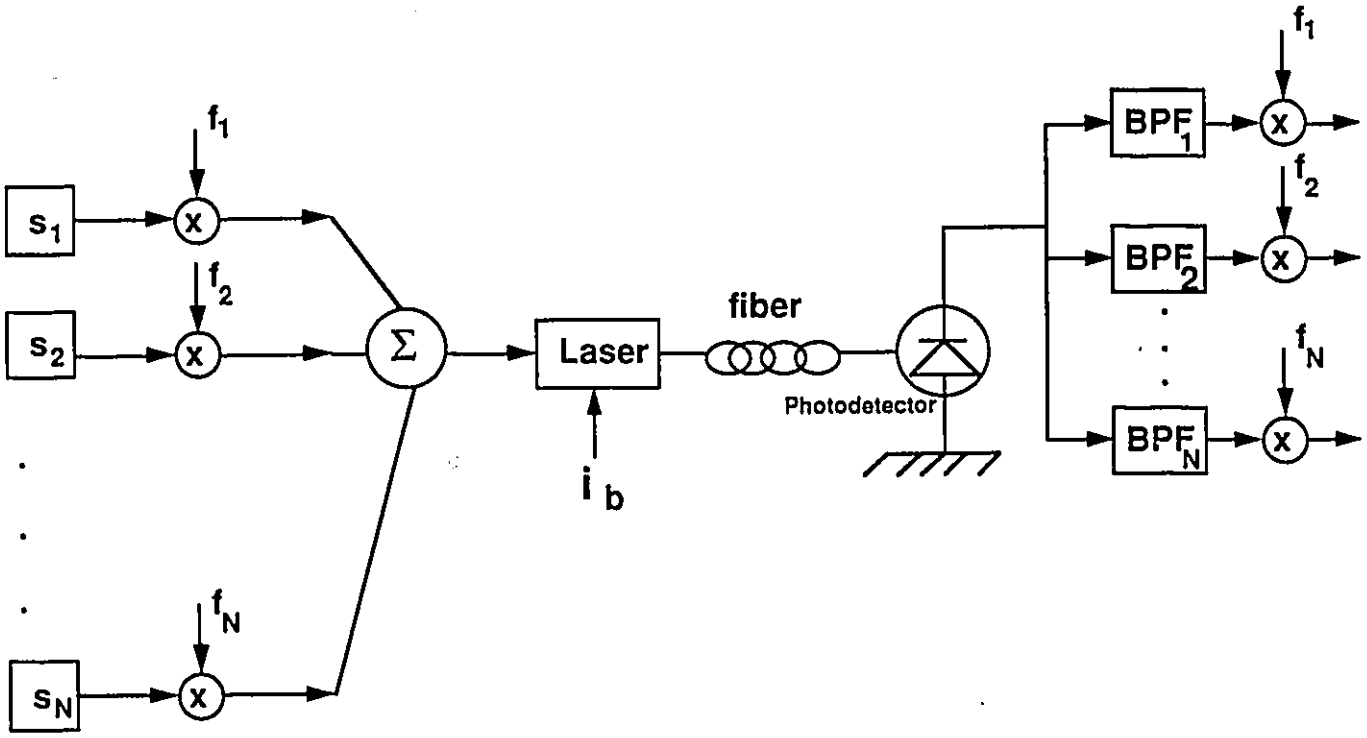

Figure 1.1. Block diagram of a subcarrier multiplexing system

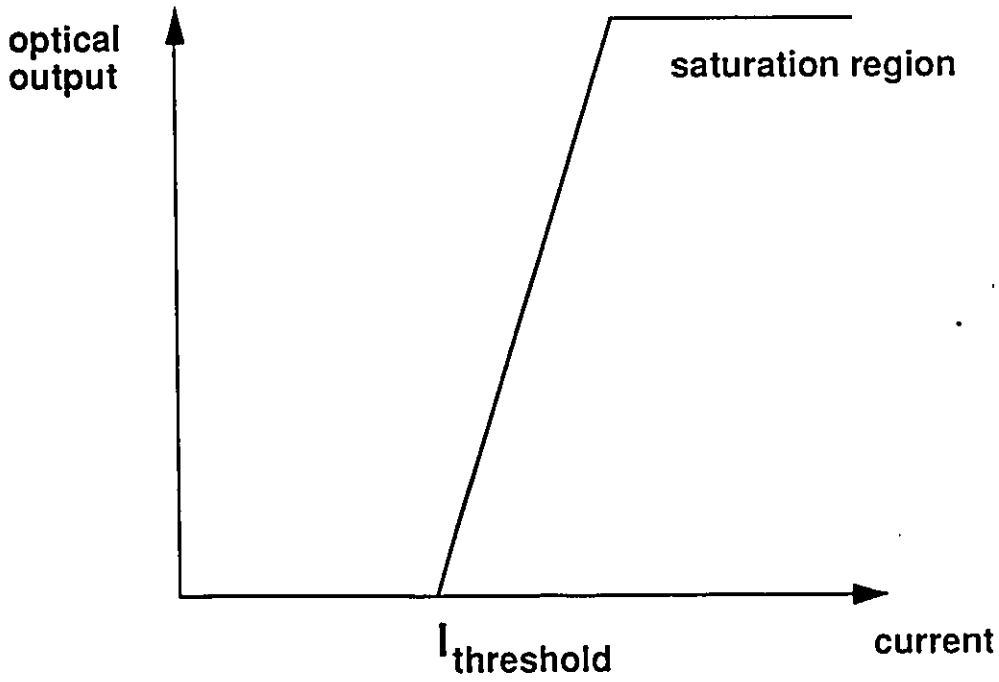

Figure 1.2. Input-output characteristic of a laser diode.

Here, the *total* modulated current that is applied to the laser diode is i_{total} whose amplitude can be larger than the range between bias current and the laser threshold current. In this case, zero-level clipping occurs at the output optical power. If the number of carriers is small, the *total* modulated current does not go below the threshold current and no clippping occurs. Optical modulation depth is defined to be:

$$m = \frac{I_p}{I_b - I_{th}} \tag{1.1}$$

where I_p is the peak amplitude of the input current, I_b is the bias current of the laser and I_{th} is the threshold current. When the number of carriers is not small, we can choose a small modulation depth for each carrier so that the effective optical modulation depth (OMD) is not so large to cause the total current to go below the threshold. The effective modulation index is

$$m_t = \sqrt{\sum_{i=1}^{N} {m_i}^2} \tag{1.2}$$

where N is the number of subcarriers, m_i is the optical modulation depth of the i_{th} carrier[1]. If N is increased, m_t is increased so we can have larger modulation indices leading to a lesser transmitted power.

On the other hand, as the input-output characteristics of the laser shown in Fig.1.2 suggests, the output optical power saturates for large values of input current. This is another source of nonlinearity in the characteristics of the laser. The first source of nonlinearity in semiconductor lasers is due to the threshold current which cannot be linearized since this is an inherent property of the semiconductor lasers [2]. The second source is due to saturation which depends on the value of the total input current. The total value depends on the number of subcarriers and the individual modulation indices.

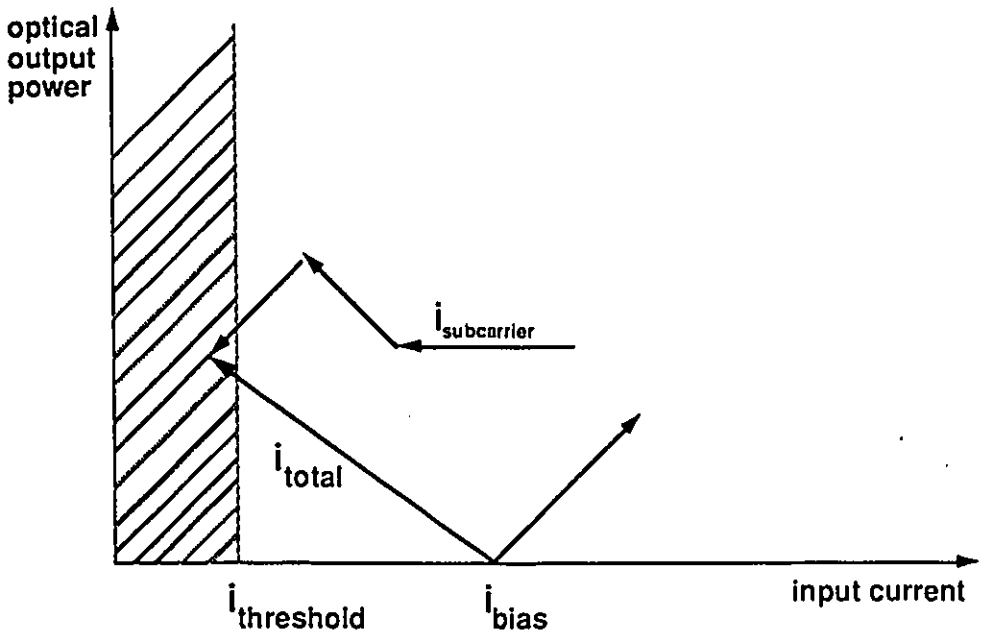

Figure 1.3. Total current in multiplexing is the phasor sum of the subcarrier currents.

Linearization of the laser characteristic yields in using a larger number of channels without the problem that was mentioned and also larger modulation indices can be used easing the power budget requirements. This can be done by introducing a predistortion block prior to laser diode. The predistortion characteristic inverts that of the laser diode. Hence, the overall system exhibits less nonlinearity than the laser diode itself. In other words, nonlinearity of the laser has been compensated.

1.2 Proposed Approach

A laser diode has an input in the form of an electric current and an output in the form of light or photons. So it can be analyzed like other systems by its input-output characteristic. This characteristic is represented in the form of the curves shown in Fig.1.2. This is a solid presentation of a laser. When input current to a semiconductor laser is more than the threshold current, stimulated emission of photons starts. The density of the electron carriers and the density of emitted photons are measures as input and output signals of a laser diode. Electron carriers are in the conduction band of the semiconductor material and the emitted photons are in the lasing mode or stimulated state of the material. Otherwise, the output is just spontaneous emission of photons. Dynamic behaviour of a semiconductor laser is expressed by a set of nonlinear differential equations known as rate equations. Rate equations relate output photon density to the input injected current and take into account the parameters which are due to material properties or are external parameters applied to the laser. For a single-mode laser rate equations are:

$$\frac{dN}{dt} = \frac{I_o}{V} - \frac{N}{\tau_s} - g(N - N_o)(1 - \epsilon S)S \qquad (1.3.a)$$

$$\frac{dS}{dt} = \Gamma g(N - N_o)(1 - \epsilon S)S - \frac{S}{\tau_{ph}} + \Gamma\beta\frac{N}{\tau_s} \qquad (1.3.b)$$

with

$S =$ density of photons in lasing mode

$N =$ density of electrons in the conduction band of the semiconductor

$N_o =$ Transparent carrier density

$I_o =$ injection current

$g =$ optical power gain

$V =$ volume of the active laser region times electronic charge

$\tau_s =$ spontaneous electron lifetime

$\tau_{ph} =$ photon lifetime

$\beta =$ probability of spontaneous emission of a photon in lasing mode

$\epsilon =$ power gain compression parameter

$\Gamma =$ Optical confinement factor

To linearize the characteristic in the active region we need a model. Since laser non-linearity has memory, a Volterra-Series expansion has been shown to be an appropriate model for the system [3].

For practical application of the Volterra series for system representation, the system must be a weakly nonlinear one. In this way, only a few Volterra transfer functions need be taken into account. If the system has a strong nonlinearity in its characteristic such as kinks, jumps or hard limitations, it cannot be expressed by a few Volterra transfer

functions and the associated series representation converges very slowly in this case.

Semiconductor lasers exhibit a weak nonlinearity when the current is well above threshold. Therefore, Volterra transfer functions of low order are employed in their modelling. In this case, up to a third order transfer function modelling is adequate [3],[4]. An inverse system is proposed based on the Volterra transfer functions which models the laser predistortion characteristics.

1.3 Contributions

For nonlinearity compensation, we introduced a predistortion block to be incorporated prior to the laser. The characteristics of this predistortion block inverts those of the laser. The performance of the subcarrier multiplexed system with and without predistortion is evaluated by harmonic distortion and intermodulation analyses. The proposed predistortion reduces the amount of nonlinear distortion, significantly. We carried out the harmonic distortion analysis by applying a single-frequency tone to the input and observing the amount of harmonic distortion at the output. However, we evaluated the intermodulation distortion at the output in a frequency domain approach. Both analyses showed significant reduction of nonlinear noises.

We applied the proposed system to different modulation schemes utilized in CATV transmission. Without the predistortion block, the requirements for CNR (carrier-to-noise ratio) for some systems are not met. The reason is of course the nonlinear distortion which degrades the system performance. We showed that with the predistortion block these requirements are met, due to the reduction of nonlinear noise in the system.

1.4 Thesis Organization

Chapter 2 provides a review of the related work. Laser nonlinearity modelling has been introduced. The amount of nonlinear distortion noise with these models has been compared with experimental results. The comparisons have shown agreements, so these models can predict nonlinear behaviour.

Chapter 3 provides an analysis of the rate equations and introduces the Volterra transfer functions that model the dynamic behaviour of the laser. The inverse system which is also based on Volterra transfer functions is also introduced.

The performance of both systems is evaluated by harmonic distortion analysis and intermodulation distortion analysis in chapter 4.

Chapter 5 is a summary of the method for implementation of the proposed predistortion block.

Chapter 6 presents the results that were obtained by computer simulations. The simulating programs run on a Sun Workstation. The accuracy of these results is discussed. In this chapter, performance comparison of the nonlinear laser system and the linearized system will be demonstrated, as well.

The overall conclusions of this work and some suggestions for future research are discussed in chapter 7.

Chapter 2

Review of Related Work

This chapter is a brief review of the related work. Some terms and definitions that have been used are explained. A schematic of a complete subcarrier multiplexing system is shown in Fig.1.1 in the introductory chapter. Consider the transmission laser and photodetector system shown in Fig.2.1.

In performance analysis of an analog system, the ratio of rms carrier power to rms noise power at the output of the optical receiver is calculated. There are different sources of noise in a system. Noise power is the sum of powers of *source noise* or transmission laser noise, *receiver noise* or photodiode noise, *amplifier noise* and in case of multiplexing systems *intermodulation noise.* When multiple carrier frequencies pass through a nonlinear device such as a laser diode, signal products other than the fundamental or original frequencies can be produced which are called intermodulation (IM) products. Third-order types are at frequencies $f_i + f_j - f_k$, also known as triple-beat IM products and $2f_i - f_j$, which are known as two-tone third-order IM products. If a passband signal contains a larger number of equally spaced carriers, several IM terms will exist at or near the same frequency. This is known as *beat-stacking.* Beat-stacking is measured in *composite-second-order (CSO)* and *composite-triple-beat (CTB).* CSO is defined as the ratio of the peak carrier power to the peak power in the composite 2nd-order IM tone at the carrier frequency. CTB is the ratio of the peak carrier power to the peak power in the composite 3rd-order IM tone at the carrier frequency.

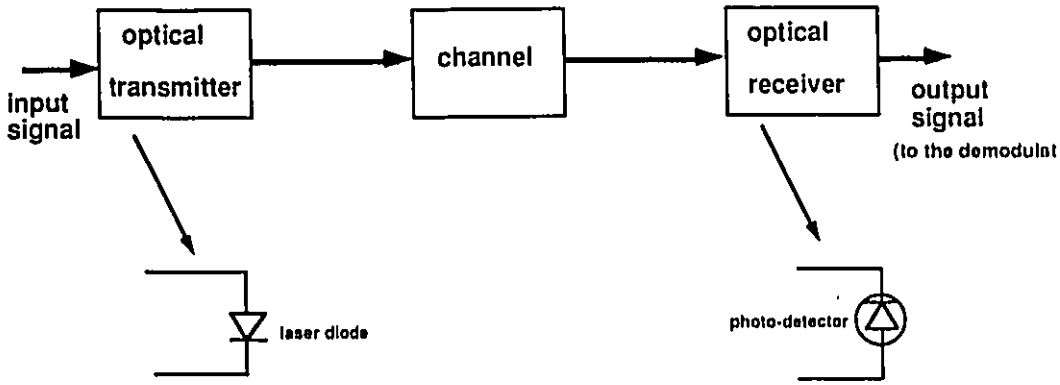

Figure 2.1. Optical transmitter-receiver system

2.1 Literature Survey

Subcarrier multiplexing (SCM) is an efficient technique in multiple-access lightwave systems particularly cable-television (CATV) applications. There are some impairments in SCM system; the relative intensity noise (RIN) of the transmitting laser, the thermal and electronic noise of the receiver, shot noise of receiving photodiode and nonlinear distortion (NLD) within the transmitting laser which is caused by the light-current (L/I) characteristics of the laser. Nonlinear distortion at the transmitter limits the power per signaling channel. In other words, each signal has to be kept at a limited power level before transmission. This is done by limiting the optical modulation depth. Linearization of the L/I curve would eliminate this impairment. However, the optical power cannot be negative, so clipping can occur at the zero-power level, as shown in Fig.2.2. Solution to this is to have a limit on the maximum allowable number of channels capable of maintaining a specified CNR for a given laser power level. To achieve a certain amount of CNR, the optical modulation depth per carrier should be less than $\frac{1}{N}$, where N is the number of carriers. However, this is too conservative, hence some NLD is accepted when modulation index is larger than this value. Consequently, the combination of this minimum distortion and the shot noise, leads to a fundamental limit on the maximum allowable number of channels while a given value of CNR is maintained [2].

In a directly modulated semiconductor injection laser the major distortion that is of concern is third-order intermodulation distortion. Third order products of two frequencies ω_1 and ω_2 are $2\omega_1 - \omega_2$ and $2\omega_2 - \omega_1$, which may be frequencies within the transmission channel and are considered distortion. Lau and Yariv [5] have studied the IM products of a semiconductor laser and their dependence on different parameters such as optical modulation depth, signal frequencies, laser bias level, etc.

Their observations were that:

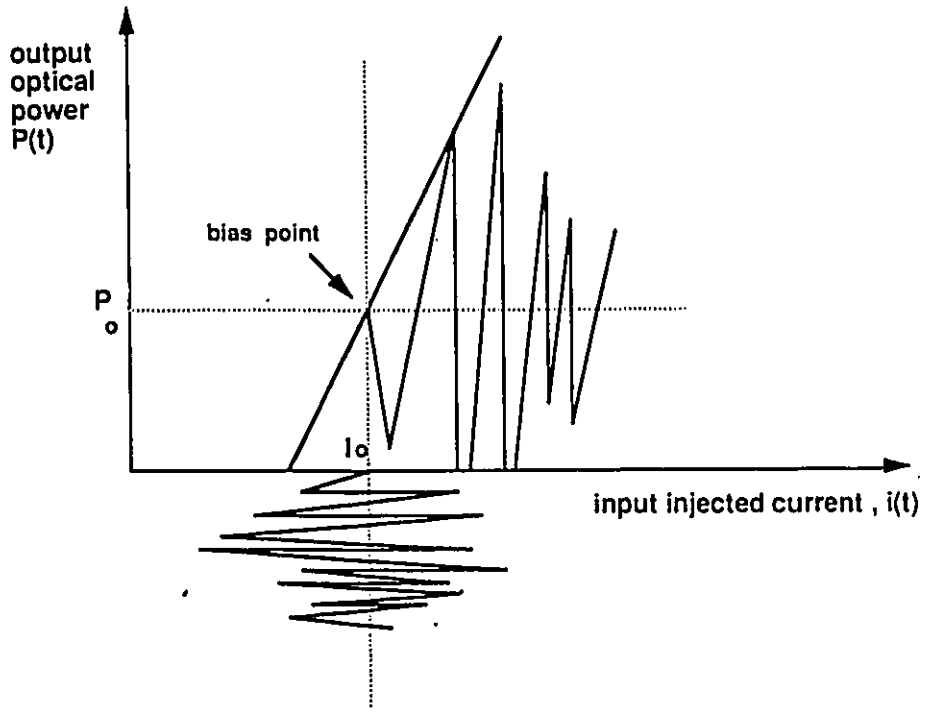

Figure 2.2. Zero-level clipping at the output power

(1) At low modulation frequencies, all tested lasers showed low intermodulation products of below -60 dB level, even at optical modulation depths around 100 percent. Here, low frequencies are about a few hundred MHz.

(2) The second harmonics of the modulation signals increase roughly as the square of the OMD, while the IM products increase as the cube of the OMD.

(3) The ratio of the IM product amplitude to the signal amplitude increases at a rate of 40dB/decade as frequency increases [5].

A theoretical analysis of intermodulation and harmonic distortion in semiconductor lasers was carried out by Darcie, et.al.[6]. They extended the analysis of Lau and Yariv [5] to incorporate additional distortion terms and damping due to gain compression. They expressed the magnitudes of second-order harmonic distortion, third-order harmonic distortion and intermodulation distortion relative to the optical carrier density by:

$$\frac{2HD}{C} = OMD\frac{{f_1}^2}{{f_r}^2 g(2f_1)} \tag{2.1}$$

$$\frac{3HD}{C} = \frac{3}{2}(OMD)^2\frac{(\frac{f_1}{f_r})^4 + \frac{1}{2}(\frac{f_1}{f_r})^2}{g(2f_1)g(3f_1)} \tag{2.2}$$

and

$$\frac{IMD}{C} = \frac{1}{2}(OMD)^2\frac{(\frac{f_1}{f_r})^4 - \frac{1}{2}(\frac{f_1}{f_r})^2 + \frac{2\pi {f_1}^3 \tau_p}{{f_r}^2}}{g(2f_1)g(f_1)} \tag{2.3}$$

and $g(f)$ is the inverse of the small signal frequency response of the device which is given by

$$g(f) = [\{(\frac{f_1}{f_r})^2 - 1\}^2 + (\frac{2\pi\epsilon f_1}{g_o})^2]^{\frac{1}{2}} \tag{2.4}$$

here ϵ is a gain compression damping coefficient, τ_p is the average photon lifetime and g_o is the gain slope. Here C is the carrier power.

Way [7] estimated the large-signal nonlinear distortion from a directly-modulated single-mode GaAlAs laser diode by using a large-signal equivalent circuit model. A large-signal circuit model of a complete laser diode was first introduced and modified by Tucker [8],[9]. Way [7] verified his large-signal circuit model for predicting the nonlinear distortions in large-signal intensity modulation. He used various types of large microwave signals to directly modulate the laser diode and for all cases the simulation results matched well with the measurements [7].

Another model based on the equivalent electrical circuit of lasers was presented by Lin et.al. [10]. They also reported measurements of the second harmonic distortion in InGaAsP lasers.

Analysis of nonlinearities of laser diodes should be considered without predistortion first in order to have a reference for the performance enhancement achievable by predistortion. Experimental results on harmonic distortion were obtained for various laser structures [11]. These agree with results obtained by using the rate equations for a precise description of distortion in the lasers.

Volterra kernels of semiconductor lasers were derived by Czylwik [3] for the first time. He analyzed the nonlinear distortions by using Volterra series obtained from the rate equations of the semiconductor laser. We will discuss the Volterra series expansion of the rate equations in detail in Chapter 3.

The optimum design of Subcarrier Multiplexing Lightwave systems requires a lin-

earized optical transmitter. An optical predistortion linearizer of directly modulated DFB lasers was used by Childs et.al.[12]. Composite-second-order (CSO) and Composite-triple-beat (CTB) are measurements of the worst case sum of the second and the third order distortion products produced over the entire video band. The predistortion circuit consists of a nonlinear device that generates distortion products equal in amplitude but opposite in phase with the distortion products produced in the device under test which can be either a DFB laser or a Mach-Zehnder modulator coupled to a high-power optical source. A predistortion technique was described that reduces the dominant distortion of a DFB laser and external modulator by 12 and 14 dB, allowing a relatively large increase in the modulation index. The dominant distortion of a DFB laser is CSO and of an external modulator is CTB.

A block diagram of the predistortion linearizer that was used is shown in Fig.2.3.

Reduction of distortion can be done by feedforward techniques. The distortion is assessed by detecting the output of the modulator in a loop which contains a detector and after amplification the linear term is subtracted out. Another modulator driven by the extracted distortion signal provides a signal which is added to the original signal and the distortion component is cancelled. A distortion suppression ratio of more than 15 dB over the range of 50-300 MHz and more than 25 dB in the range of 300-500 MHz was achieved [13]. Another method in feedforward compensation is almost the same but with some difference in coupling of the primary and the secondary beams. A part of the optical signal from the primary laser is picked up and sent directly onto a photodiode. The resulting electric signal is compared with the original modulation, in order to generate an error signal which is sent to a secondary laser. But the optical beam from the secondary laser is not coupled immediately into the primary beam. The alternative configuration is to transmit the primary and secondary signals separately, either on two different fibers, or as WDM signals on the same fiber. A relative adjustment of the

phase between the two signals would then be performed in each receiver before the final subtraction. This method is more suitable for a distributed access transmission because the difference between the central wavelengths of the two lasers, the primary and the secondary would propagate at different speeds along the transmission fiber. They would come more and more dephased relative to each other during their propagation. This method showed a reduction of 54 dB in the third order intermodulation distortion with a 0.8 modulation index and for 3 TV-channels.

Treating a laser as a nonlinear device with memory was verified by Way [14]. A frequency-dependent and a frequency-independent nonlinear characteristics for high-speed laser diode was experimentally demonstrated [14]. For an operating condition, with a modulation depth below sixty percent, the RF bandwidth over which the laser diode can be considered to be memoryless is generally very narrow. For higher modulation depths, of above seventy-five percent the effect of LD memory is not significant. The conclusion was that the phenomon of frequency-dependent nonlinearity is a reason to treat LD as a nonlinear device with memory. If the nonlinear distortion has to be predicted for wideband signal transmission, alternatives such as circuit modelling or Volterra series expansion must be used.

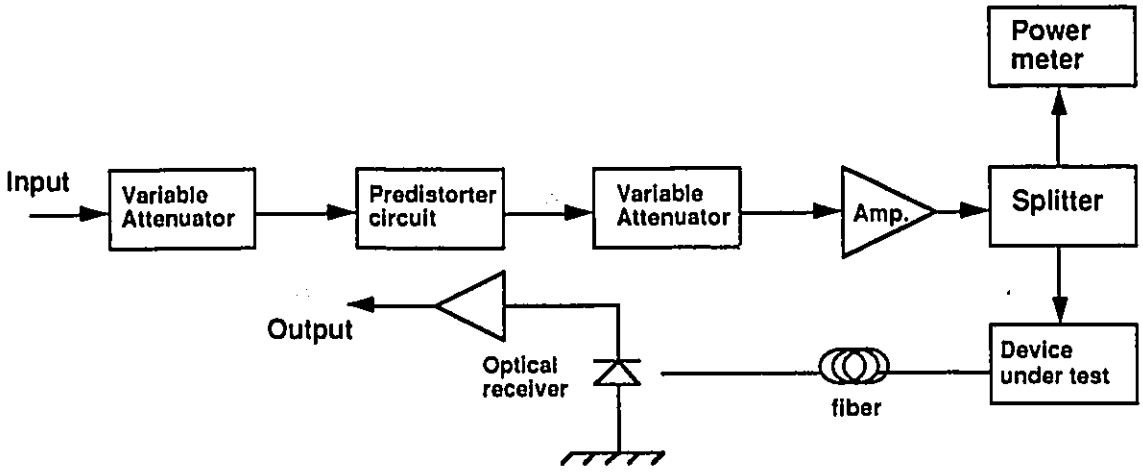

Figure 2.3. Block diagram of predistortion linearizer [13].

Chapter 3

Semiconductor Lasers

3.1 Basics

Semiconductor lasers work on the basis of interaction between the light and matter. In semiconductor materials two energy states are considered for the atoms. Suppose the higher energy state is E_h and the lower one is E_l. If a photon of energy equal to the difference between these energy states; $E_h - E_l$, is incident on the material an electron in state E_l may absorb it and makes a transition to the state E_h. Alternatively, when the atom is in a higher state which is state E_h, it can make a transition to the lower energy state E_l and emit a photon at a frequency f for which $E_h - E_l = hf$, where $h = 6.626 \times 10^{-34}$ Js is the Planck's constant. The emission process occurs in two ways:

(1) Spontaneous emission in which the atom returns to the lower energy state in a random manner.

(2) Stimulated emission, when a photon with an energy equal to the $E_h - E_l$ interacts with the atom in the upper energy state and causes it to return to the lower state with the creation of a second photon. The emitted photon has the same energy and the same frequency as that of the stimulating one. So the result is a coherent light with a narrow linewidth. On the other hand, the light associated with the stimulating photon and the emitted one is in phase and has the same polarization. Therefore, coherent radiation is obtained.

Stimulated emission does not happen when the atom is in thermal equilibrium. In

this state, the density of the electrons in the lower energy level E_l is more than the density of the electrons in the upper energy level E_h. The light amplification or *lasing condition* happens when the injected current is larger than a threshold value, I_{th}. This phenomenon is called *population inversion* and is accomplished by injecting electrons into the material. As the name suggests, in this state the density of the electrons in the upper energy state E_h is larger than the density of the electrons in the lower energy state E_l. Fig.3.1. shows the changes of the optical output power in terms of the injected current into a semiconductor laser.

3.2 Laser structure

To maintain the lasing condition in amplified coherent emission, mirrors are placed at the two ends of the amplifying medium. The optical cavity in this way is playing the role of an oscillator as it provides a positive feedback for the photons by reflection on the mirrors at either end of the cavity. The basic structure is shown in Fig.3.2. [15].

3.3 Laser Modes

The optical radiation within the resonance cavity sets up a pattern of electric and magnetic field lines called the modes of the cavity. These can conveniently be separated into two independent sets of transverse electric (TE) and transverse magnetic (TM) modes. According to the laser diode structure shown in Fig.3.3., modes can be described in terms of longtitudinal and lateral sizes of the resonator cavity.

Lasers can operate in two different types:

(1) Single-mode

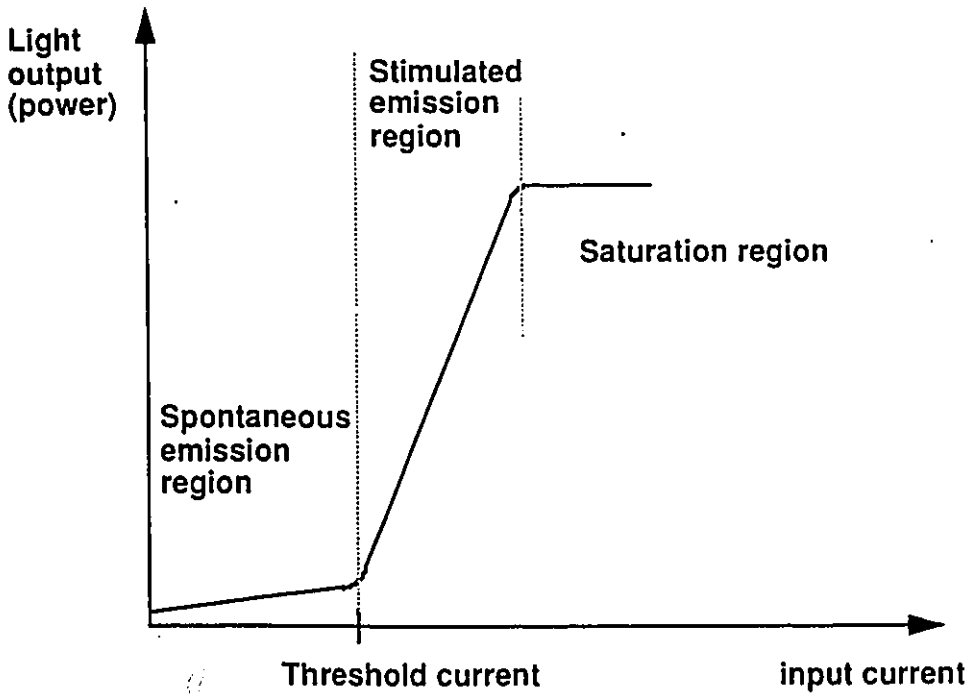

Figure 3.1. Light-current characteristic of a semiconductor laser.

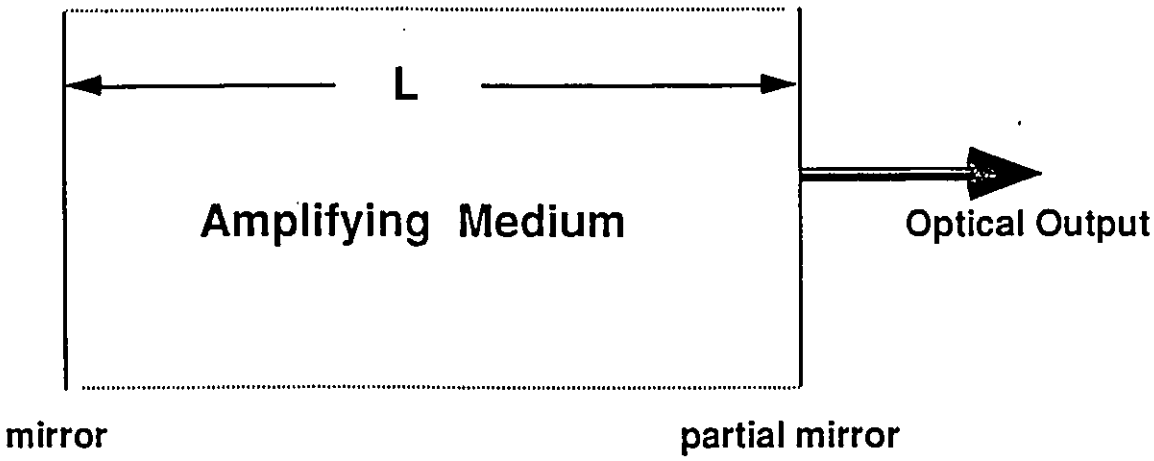

Figure 3.2. Basic structure of laser.

(2) Multi-mode

The output spectrum for a broad area injection laser consists of a series of wavelength peaks corresponding to the different longitudinal modes within the structure. For single mode operation, the optical output from a laser must contain only a single longitudinal and a single transverse mode.

3.4 Laser Nonlinearity

There are two principal light sources used for fiber optic communications applications. These are injection laser diodes (ILDs) or semiconductor laser diodes and light-emitting diodes (LEDs). A major difference between LEDs and laser diodes is that the optical output from an LED is incoherent, whereas that from a laser diode is coherent. In a coherent light source, the optical energy (in the form of emitted photons) is produced in an optical resonator cavity. A light source is a coherent source when it is highly monochromatic and directional. In the laser diodes the optical energy released from the cavity has spatial and temporal coherence which means that it is highly monochromatic and the output beam is very directional. Since in a LED there is not any optical resonator cavity, there is not any wavelength selectivity and the output light of an LED is not coherent. The output radiation of an LED has a broad spectral width, so it is not appropriate for broadband analog applications. Laser diodes have coherent optical outputs and are appropriate for broadband analog applications especially when a number of subcarriers has to be imposed on a specified wavelength to be transmitted through a fiber. Both of these light sources; LEDs and lasers exhibit nonlinearity distortions at their outputs. Light emitting diodes; LEDs, have nonlinear distortions due to effects depending on the carrier injection level, radiative recombination and other mechanisms. In certain laser diodes, there can be nonlinearities in the curve for optical power output versus diode current as shown in Fig.3.4.

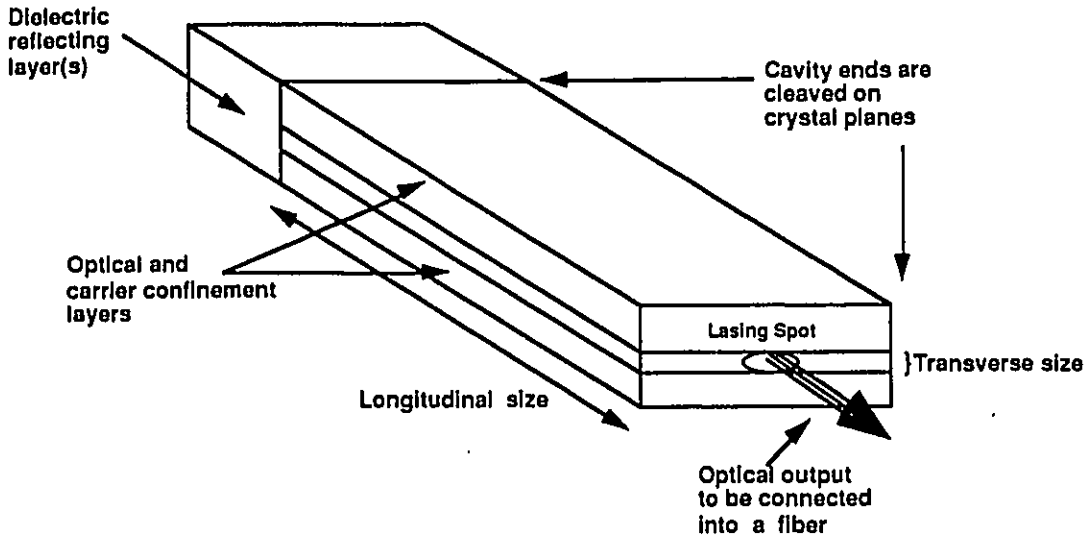

Figure 3.3. Fabry-perot resonator cavity for a laser diode.

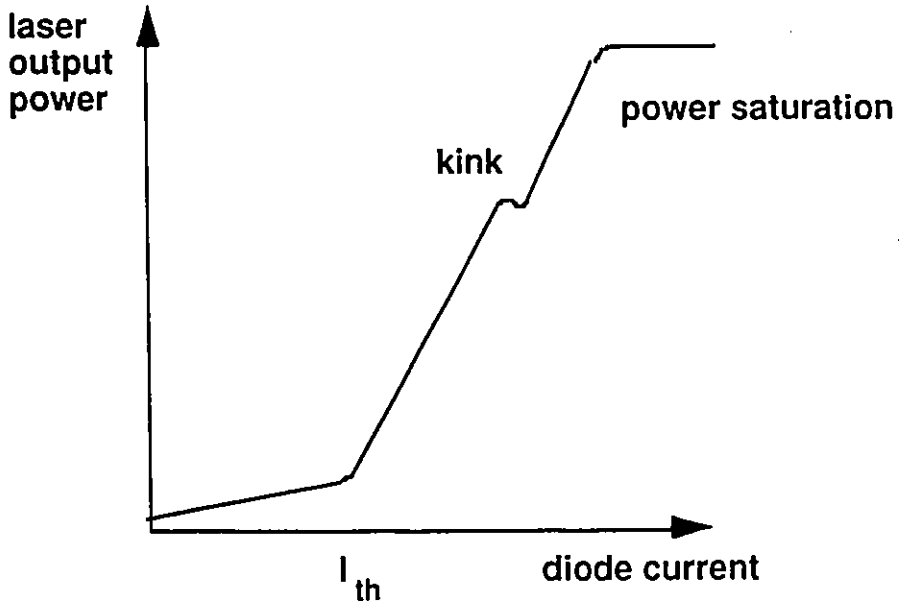

Figure 3.4. Characteristic of an extremely nonlinear laser.

These nonlinearities are the results of inhomogeneities in the active region of the device. Power switching between the dominant lateral modes in the laser cause them, as well. These are generally referred to as *kinks*. In modern laser diodes using the described structure with some additional features, these kinks are not formed. However, power saturation can occur at high output levels because of active-layer heating.

Laser diodes are appropriate optical sources for wide-band analog applications provided a method is implemented to compensate for nonlinearities of the device. In an analog system, the time-varying electric analog signal $s(t)$ is used to intensity modulate an optical source about a bias current point I_B , as shown in Fig.3.5. The optical output power can be expressed by eq.(3.1) [15]:

$$P(t) = P_B[1 + ms(t)] \tag{3.1}$$

in which P_B is the optical power output when there is no signal ($s(t) = 0$) and m is the modulation depth ($m = \frac{\Delta I}{I_B - I_{th}}$).

The parameter ΔI is the variation of current around the bias point. As we explained before, to prevent distortions in the output signal, the modulation must be confined to the linear region of the input-output curve. If ΔI is greater than $I_B - I_{th}$ (m greater than 100 percent), the lower portion of the signal is cut-off and zero-level clipping occurs which is a severe distortion. Typical m values for analog applications are in the range of 0.25 to 0.50. It should be noted that here we are referring to the total modulation depth in subcarrier multiplexing case which is $m_t = m_i\sqrt{N}$, since this total modulation depth is the modulating factor in intensity modulation of the laser and its effect on each subcarrier is given by $m_i = \frac{m_t}{\sqrt{N}}$. In analog applications any device nonlinearity creates frequency components in the output signal that are not present in the input signal. The important nonlinear effects are harmonic and intermodulation distortions of the signal.

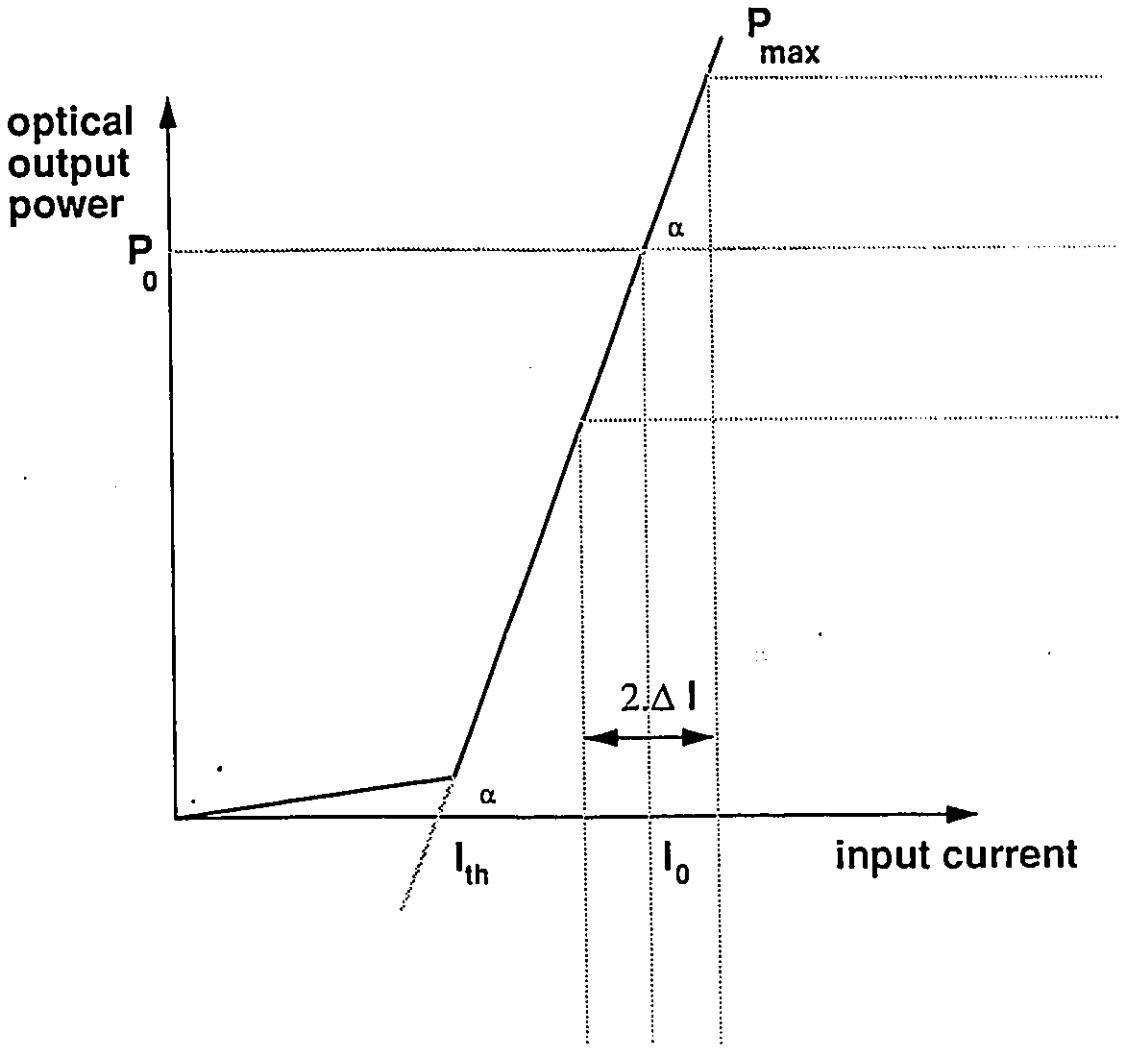

Figure 3.5. Input current modulates the output power.

If the input to a nonlinear device is $x(t) = A\cos\omega t$, the output will be:

$$y(t) = A_o + A_1\cos\omega t + A_2\cos 2\omega t + A_3\cos 3\omega t + ... \tag{3.2}$$

The output signal consists of a component at the input frequency, usually referred to as fundamental component, plus other components at zero frequency, at the second harmonic frequency 2ω, at the third harmonic frequency 3ω and higher harmonic frequencies. The presence of components with frequencies that are multiples of the input frequency is referred as harmonic distortion. The amount of $n^{th} - order$ distortion or n^{th}-harmonic distortion in decibels is:

$$n^{th} - order \quad harmonic \quad distortion = 20\log\frac{A_n}{A_1} \tag{3.3}$$

Another important nonlinear effect that should be determined is intermodulation distortion. To determine the intermodulation distortion, the modulating signal of a nonlinear device or the input signal to the device is chosen to be the sum of two cosine waves or two tones:

$$x(t) = A_1\cos\omega_1 t + A_2\cos\omega_2 t \tag{3.4}$$

The output signal will then be of the form

$$y(t) = \sum_{m,n} B_{mn}\cos(m\omega_1 + n\omega_2)t \tag{3.5}$$

where m and n are positive and negative integers ($n = 0, \pm 1, \pm 2, ...$). This signal includes all the harmonics of ω_1 and ω_2 plus cross-product terms such as $\omega_2 - \omega_1$, $\omega_2 + \omega_1, \omega_2 -$

$2\omega_1, \omega_2 + 2\omega_1$ and so on. The sum and difference frequencies give rise to intermodulation distortion. The sum of the absolute values of the coefficients m and n gives us the order of the intermodulation distortion. For example, the second-order intermodulation products are at frequencies $\omega_1 \pm \omega_2$, the third-order intermodulation products are at $\omega_1 \pm 2\omega_2$ and $2\omega_1 \pm \omega_2$; and so on. In general, the odd-order intermodulation products with $m = n \pm 1$ are the major sources of problem, since they may fall within the bandwidth of the channel. In practice, the third-order terms are significantly more important than higher-order terms which are significantly smaller. All other intermodulation products can be eliminated with appropriate bandpass filters in the receiver.

The amount of intermodulation distortion depends on optical modulation depth. For modulation depths around 0.5, total harmonic distortion in laser diodes are in the range of 30-40 dB below the output at the modulation frequency. Second and third order harmonic distortions as a function of fundamental frequency are shown in Fig.3.6 and 3.7. The intermodulation curves almost follow the same characteristics as harmonic distortions. The curves showing the second and third order intermodulation are in Fig.3.8 and 3.9.

Intermodulation distortions change with bias current. Intermodulation distortion is high when bias current is near threshold. As the bias is increased relatively lower intermodulation distortion is obsereved. However, for much higher bias currents, distortion increases , since the operating point is near the laser saturation region. There is a bias current that gives the minimum distortion and this is half a way from the threshold current and the current for which the power saturation starts. For this amount of bias current, the optimum bias point and consequently less distortion are obtained. We considered this value for the bias current in other parts of our work.

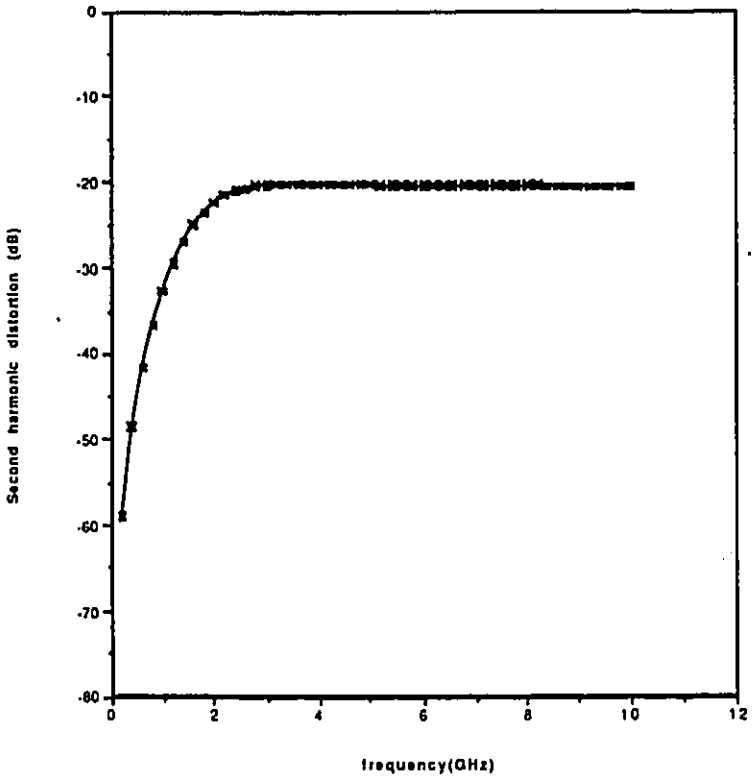

Figure 3.6. Second harmonic distortion versus carrier frequency.

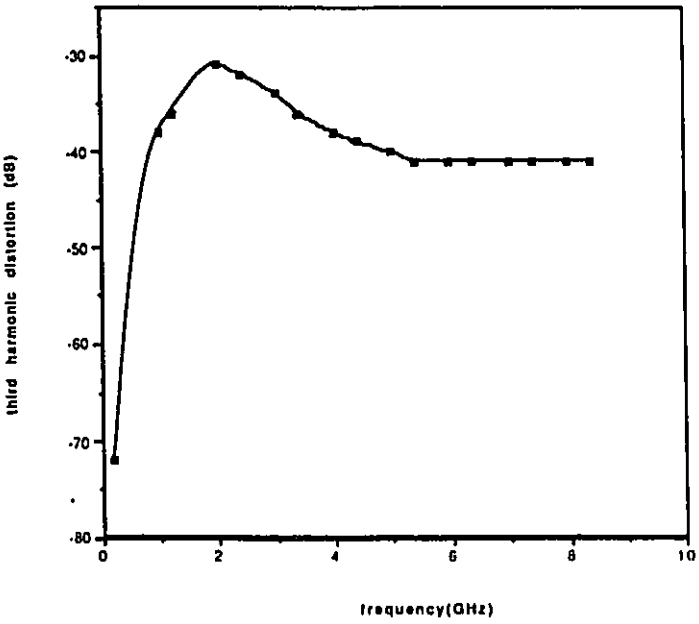

Figure 3.7. Third harmonic distortion versus carrier frequency.

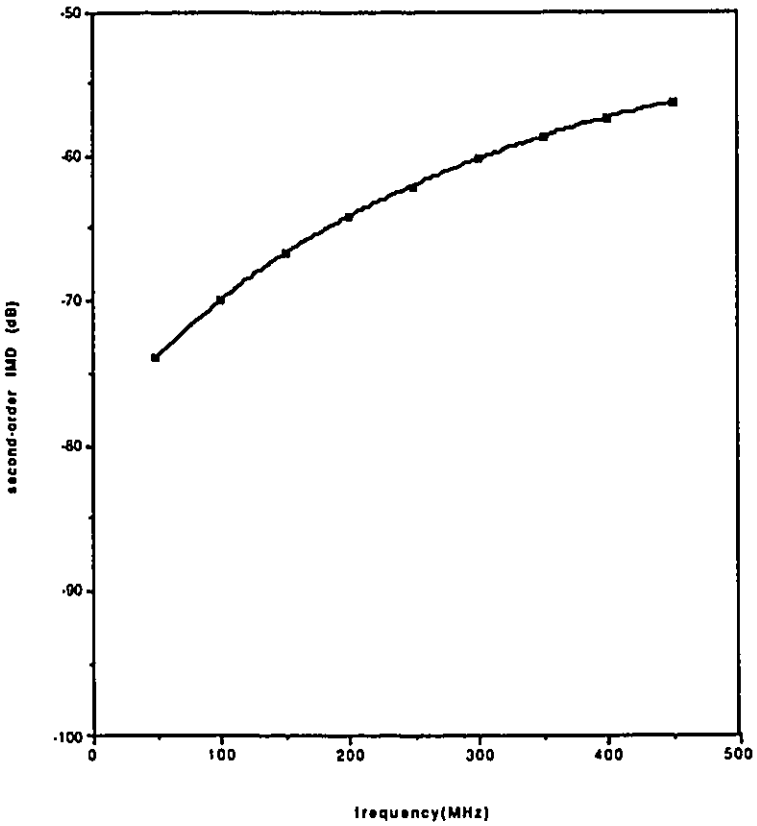

Figure 3.8. Second-order IMD versus frequency.

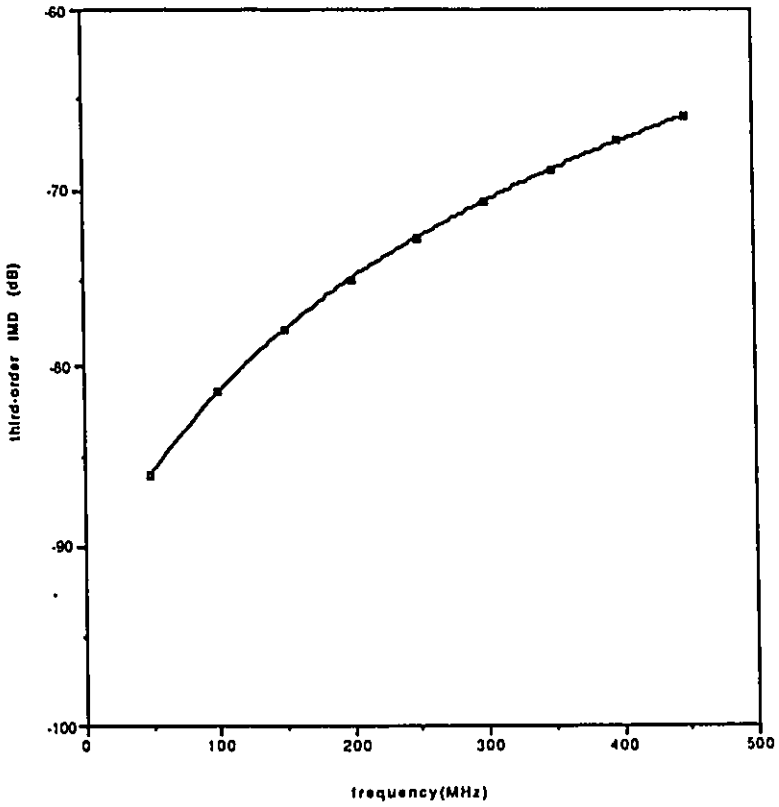

Figure 3.9. Third-order IMD versus frequency.

3.5 Dynamic Response of Semiconductor Laser

Semiconductor injection lasers exhibit a complex dynamic behaviour. The dynamic behaviour of a semiconductor injection laser is expressed by the rate equations. There are quantum-mechanical rate equations for the electrons density and photons density which give information about the time development of the photon amplitude, frequency, phase and also about the statistical properties related to quantum fluctuations. In many cases, where only the time dependence of the mean photon number is of interest and an interaction of modes with a very narrow wavelength spacing does not occur, the analysis can be performed by the much simpler classical rate equations for the electron density in the active layer and the photon density. There are cases which the photon numbers in the modes are of concern but for single-mode semiconductor lasers information about photons density in the operation mode is adequate. We proceed with the assumption of having a single-mode laser and its associated rate equations [16].

Dynamic response of a laser diode is expressed by the rate equations which are two coupled equations relating the density of the injected electrons to the density of the emitted photons [16].

$$\frac{dN}{dt} = \frac{I_o}{V} - \frac{N}{\tau_s} - g(N - N_o)(1 - \epsilon S)S \qquad (3.6.a)$$

$$\frac{dS}{dt} = \Gamma g(N - N_o)(1 - \epsilon S)S - \frac{S}{\tau_{ph}} + \Gamma\beta\frac{N}{\tau_s} \qquad (3.6.b)$$

The parameters of the equations have been described in Chapter 1.

This set of equations express the transient behaviour of a semiconductor laser. Rate equations are appropriate when the following assumptions are valid:

(1) Laser is operating in a single-mode state and the injected current is above threshold. In the multimode case, the inhomogeneous distribution of the electron and photon densities must be taken into account.

(2) The population inversion is homogeneous in an ideal cavity.

(3) The gain coefficient is a linear function of the injected carrier density N where N is greater than a minimal value N_o, or in other words, laser is above the threshold state. Parameter ϵ , which is called the optical-field-dependent gain compression was taken into account by Tucker [17] who first introduced a large signal model for the rate equations. Typical values of the parameters are shown in Table 3.1. These values are for Ortel SL-620 laser [7].

The derivative of N with respect to time; $\frac{dN}{dt}$, is the rate of change of carrier density. This value is related to the rate of carrier injection into the active region which is the ratio of the bias current to the volume of the active region. The second term; $-\frac{N}{\tau_s}$, describes the decrease in the carrier due to spontaneous emission and the last term expresses carrier decrease due to stimulated emission which gives rise to the nonlinear effects of the laser diode because it is a product of the values related to the input and output. Rate of change of photon density is given by $\frac{dS}{dt}$. The product term which is the first term on the right hand side of second equation is the rate increase due to stimulated photon emission. Similar to the equation for carrier density, the second term;$-\frac{S}{\tau_{ph}}$, gives the rate of loss of photon by radiation and absorption. Last term is the increase of photon density due to spontaneous emission which occurs in the lasing mode with probability of β.

Parameter	Description	Values	Units
I_{th}	Threshold current	21	mA
V	Volume of active region times electronic charge	1.44E-35	m^3-coulomb
τ_{ph}	Photon lifetime	2	ps
τ_s	Electron lifetime	3.72	ns
N_o	Transparent carrier density	4.6E24	m^{-3}
g	Optical gain coefficient	1E-12	$s^{-1}m^3$
Γ	Optical confinement factor	0.646	-
β	Spontaneous emission factor	0.001	-
ϵ	gain compression factor	2.6E-23	m^3

Table 3.1. Laser parameters

Each of the parameters in the rate equations have their own contribution and effect in a stimulated emission state. For example, Γ , which is the ratio of the volume of the active region to the model volume and is called optical confinement factor is a parameter that is less than unity meaning that all the emitted photons are not confined to the active region. N_o is a threshold value for carrier density, below this threshold g is negative, i.e., does not correspond to a stimulated state. In order for the optical gain ; g , to be positive, the carrier density; N, should be larger than N_o. The value for N_o is related to the threshold current of the laser. An approximation of N_o is:

$$N_o = \frac{I_o \tau_s}{V} \tag{3.7}$$

The expression of threshold current of the laser can be derived by solving the rate equations in a static state of the laser with bias points of (I_B, S_B). In this case the derivative terms $\frac{d}{dt}$ are set to zero.

$$0 = \frac{I_o}{V} - \frac{N}{\tau_s} - g(N - N_o)(1 - \epsilon S)S \tag{3.8}$$

$$0 = \Gamma g(N - N_o)(1 - \epsilon S)S - \frac{S}{\tau_{ph}} + \Gamma\beta\frac{N}{\tau_s} \tag{3.9}$$

Threshold current is given by the intersection of the two approximately straight lines of the light/current characteristics of the laser for the currents less than I_{th} and currents greater than I_{th}. This analytical solution yields :

$$I_{th} = \frac{V}{\tau_{sp}}(\frac{1}{g\tau_{ph}} + N_o) \tag{3.10}$$

This expression for I_{th} has been used in our simulation programs.

3.6 Volterra Series

The output of a linear system; $y(t)$, is obtained by the well-known convolution integral of the impulse response of the system and the input:

$$y(t) = \int_{-\infty}^{+\infty} h(\tau)x(t - \tau)d\tau \tag{3.11}$$

If a system is nonlinear, the relation between the output and the input can be expressed in a Volterra series form as [18]:

$$y(t) = \int_{-\infty}^{+\infty} h_1(\tau_1)x(t - \tau_1)d\tau_1 + \int_{-\infty}^{+\infty}\int_{-\infty}^{+\infty} h_2(\tau_1, \tau_2)x(t - \tau_1)x(t - \tau_2)d\tau_1 d\tau_2$$

$$+ ... + \int_{-\infty}^{+\infty} ... \int_{-\infty}^{+\infty} h_n(\tau_1, \tau_2, ..., \tau_n)x(t - \tau_1)x(t - \tau_2)...x(t - \tau_n)d\tau_1 d\tau_2 ... d\tau_n \tag{3.12}$$

for an integer n.

The functions $h_n(\tau_1, \tau_2, ..., \tau_n)$ are called the Volterra kernels of the system. Another way of expressing the series is by Volterra operators denoted by $\mathcal{H}_n[x(t)]$ where:

$$\mathcal{H}_n[x(t)] = \int_{-\infty}^{+\infty} ... \int_{-\infty}^{+\infty} h_n(\tau_1, \tau_2, ..., \tau_n) x(t-\tau_1) x(t-\tau_2) ... x(t-\tau_n) d\tau_1 d\tau_2 ... d\tau_n \quad (3.13)$$

The Volterra series is a power series with memory and the integrals of it are forms of convolution integrals. Many physical systems exhibit a nonlinear behaviour modelled by a nonlinear differential equation expressed as:

$$y(t) = \mathcal{H}[x(t)] = \mathcal{H}_1[x(t)] + \mathcal{H}_r[x(t)] \quad (3.14)$$

where $\mathcal{H}_1$ is the first order Volterra operator of the system and $\mathcal{H}_r$ represents the remaining terms of Volterra series representation of the system. $\mathcal{H}_r[x(t)]$ is obtained by expanding the nonlinear terms in the differential equation in a Taylor series expansion. Also, the Volterra transfer functions for frequency domain analysis can be derived from the equation by the same approach. After the nonlinear term is expanded in its Taylor series, a single frequency tone; $e^{j\omega_o t}$, is applied as an input to the system and the coefficients of $e^{j\omega_o t}$ form the first order Volterra transfer function of the system. A second order Volterra transfer function is derived by applying the sum of the two single frequency tones as inputs to the system and taking into account the coefficient of the tone with the frequency which is the sum of the two applied frequencies. This results in intermodulation distortion for second order systems. The same approach is applicable to obtaining Volterra transfer functions of higher order.

Volterra series can be applied in order to find the inverse of a nonlinear system. The p^{th} order inverse of a given nonlinear system H is defined as a system that when

connected in tandem with H results in another system for which the first order Volterra kernel is a unit impulse and the second to the p^{th} order kernels are zero.

Some nonlinear systems can be represented in terms of a limited number of Volterra operators. If Q is the system operator then:

$$Q[x(t)] = \sum_{n=1}^{k} Q_n[x(t)] \tag{3.15}$$

in which Q_n is the n^{th}-order Volterra operator of the system Q and k is an integer. Therefore, one of the applications of the p^{th}-order inverse is in linearization of nonlinear systems.

Practical applications are usually for the systems that are *weakly* nonlinear so that only a few Volterra kernels need be taken into account. Semiconductor lasers without kinks or jumps fulfill this condition and a well-behaved semiconductor laser exhibits very little nonlinear distortion when it is modulated around an operating point well above the threshold current. Therefore, only Volterra kernels of low order must be taken into account. Experimental results have shown that a series expansion containing the kernels h_1, h_2 and h_3 are enough to predict the behaviour of the laser and intermodulation distortion at its output [3]. In our work, the frequency domain transform of the kernels are used.

A laser characteristic is expressed by a pair of nonlinear differential equations known as rate equations. This set of equations presents the light-current characteristics for a semiconductor laser. Also, the combination of these equations gives a nonlinear differential equation relating the input current to the output photon density. The Volterra transfer functions of the laser are derived by first expanding the nonlinear terms of this equation in Taylor series around the bias point and then applying an appropriate input.

Fourier transform of the Volterra kernels of the system are derived by applying tones as input to the system. In each case, coefficients of a tone with a specified frequency form the desirable transfer function of the particular order. For a first order function, the coefficients of the tone whose frequency is equal to the applied frequency are considered. The second order function is the sum of all the coefficients of the tone which has a frequency equal to the sum of the two input frequencies [18].

3.7 Volterra model of laser diode and predistortion block

The stimulated emission term in the rate equations formed by the product of the photon and electron densities causes the laser nonlinearity. The system has memory because the output and the input are related by differential equations. Before proceeding with the Volterra series expansion of the rate equations, first the coupled rate equations are combined in one equation expressing the input current in terms of the output photons. By solving the second equation for N we can combine two equations in one, relating the input current to the optical output. The steps are as follows [3]:

$$\frac{dS}{dt} = \Gamma g(N - N_o)(1 - \epsilon S)S - \frac{S}{\tau_{ph}} + \Gamma\beta\frac{N}{\tau_s} \tag{3.16}$$

$$\frac{dS}{dt} = [\Gamma g(1 - \epsilon S)S + \frac{\Gamma\beta}{\tau_s}]N - \Gamma g(1 - \epsilon S)SN_o - \frac{S}{\tau_{ph}} \tag{3.17}$$

$$N = [\frac{dS}{dt} + \frac{S}{\tau_{ph}} + \Gamma g(1 - \epsilon S)SN_o]\frac{1}{\Gamma g(1 - \epsilon S)S + \frac{\Gamma\beta}{\tau_s}} \tag{3.18}$$

By substitution of N from above computations in the first equation:

$$\frac{I_o}{V} = \frac{N_o}{\tau_s} + [\frac{1}{\tau_s} + g(1-\epsilon S)S]\frac{\frac{dS}{dt} + \frac{S}{\tau_{ph}} - \frac{\Gamma\beta N_o}{\tau_s}}{\Gamma g(1-\epsilon S)S + \frac{\Gamma\beta}{\tau_s}}$$

$$+\frac{d}{dt}\{[\frac{dS}{dt} + \frac{S}{\tau_{ph}} - \frac{\Gamma\beta N_o}{\tau_s}]/[\Gamma g(1-\epsilon S)S + \frac{\Gamma\beta}{\tau_s}]\} \tag{3.19}$$

Since this equation is a nonlinear differential equation, a closed form solution has not been found for it. Also, for the memory in the system, a Volterra-series approach for solving it is an appropriate approach. The Volterra transfer functions for this equation can be derived by the expansion of the nonlinear term into a Taylor series [4].

Assuming a bias point (I_b, S_b), the input current and the optical output can be written as:

$$I_b + i(t) = I_o$$

$$S_b + s(t) = S$$

Substituting $S = S_b + s(t)$ and $I_o = I_b + i(t)$ in eq.3.19 results in :

$$\frac{I_b + i(t)}{V} = \frac{N_o}{\tau_s} + [\frac{1}{\Gamma} + \frac{1}{\tau_s}(\frac{1}{A} - \frac{B}{A^2}s + Hs^2 + Ms^3)]$$
$$[\frac{dS}{dt} + \frac{S_b + s}{\tau_{ph}} - \frac{M\beta N_o}{\tau_s}]$$
$$+\frac{d}{dt}\{[\frac{dS}{dt} + \frac{S_b + s}{\tau_{ph}} - \frac{M\beta N}{\tau_s}][\frac{1}{A} - \frac{B}{A^2}s + Hs^2 + Ms^3]\} \tag{3.20}$$

The above expressions will simplify to:

$$i(t) = \alpha + \{ds(t) + cs'(t) + fs''(t)\}$$

$$-\{ls(t)^2 + ms(t)s'(t) + ns(t)s''(t) + ns'(t)^2\} \times$$

$$\times\{rs(t)^3 + \sigma s(t)^2 s'(t) + ...\} \tag{3.21}$$

The constants $d, e, f, l, ...$ are expressed in terms of laser parameters in Appendix C. Volterra transfer functions for laser input-output characteristics are derived from eq.3.23. Since this equation gives the input current in terms of the output, we first derive the *backward* Volterra transfer functions for the system which treats $s(t)$ as their inputs and then *forward* Volterra transfer functions are derived which treat $i(t)$ as the input of the system. In this way, both models for the laser and its inverse system are achieved. Suppose $s(t) = e^{j\omega t}$, substitution in eq.3.21 results in:

$$i(t) = \alpha + \{de^{j\omega t} + e(j\omega)e^{j\omega t} + f(jw)^2 e^{j\omega t}\} - le^{2j\omega t} + ... \tag{3.22}$$

Taking the coefficients of $e^{j\omega t}$ we have $B_1(\omega)$ which is the first order Volterra transfer function:

$$B_1(\omega) = d + je\omega - f\omega^2 \tag{3.23}$$

To derive second order Volterra transfer function $q(t) = e^{j\omega_1 t} + e^{j\omega_2 t}$ is substituted in eq.3.21 and the coefficients of $e^{j(\omega_1+\omega_2)t}$ form $B_2(\omega_1, \omega_2)$:

$$B_2(\omega_1, \omega_2) = -2l - jm(\omega_1 + \omega_2) + n(\omega_1 + \omega_2)^2 \tag{3.24}$$

In a similar way, third order Volterra transfer function is derived, i.e., substitution of $s(t) = e^{j\omega_1 t} + e^{j\omega_2 t} + e^{j\omega_3 t}$ in eq. (3.3) and taking the coefficients of the term $e^{j(\omega_1+\omega_2+\omega_3)t}$:

$$B_3(\omega_1, \omega_2, \omega_3) = 6r - 2g(\omega_1 + \omega_2 + \omega_3)^2 + 2j\sigma(\omega_1 + \omega_2 + \omega_3) \tag{3.25}$$

Now, suppose we want to interpret the inverse functions of B_1, B_2 and B_3 ; say F_1, F_2 and F_3, respectively. Each block in Fig.3.10 corresponds to a Volterra operator. The first order operators as B_1 and F_1 are similar to linear system transfer function. If a sum of two tones $e^{j\omega_1 t} + e^{j\omega_2 t}$ is applied as input to the second order operators B_2 and F_2 , the outputs include terms as $e^{j\omega_1 t}, e^{j\omega_2 t}$ and $e^{j(\omega_1+\omega_2)t}$. Output of the third order operators include terms of $e^{j(2\omega_1+\omega_2)t}$ and $e^{j(2\omega_2+\omega_1)t}$ which correspond to third order intermodulation distortion. We will first proceed for time domain description of the output of a Volterra system and obtain the transfer functions of the block diagram shown in Fig.3.10.

Assume that a p_{th}-order Volterra system acts like an operator on its input and denote this operator with $\mathcal{H}_p$, where:

$$\mathcal{H}_p[a(t)] = \int_{-\infty}^{+\infty} ... \int_{-\infty}^{+\infty} h_p(\tau_1, \tau_2, ..., \tau_p) x(t_1 - \tau_1) x(t_2 - \tau_2) \\ ...x(t_p - \tau_p) d\tau_1 d\tau_2 ... d\tau_p \tag{3.26}$$

So the operation of second and third order Volterra systems with an input equal to the sum of two tones $e^{j\omega_1 t} + e^{j\omega_2 t}$ is:

$$\mathcal{H}_2[a(t)] = \int_{-\infty}^{+\infty} \int_{-\infty}^{+\infty} h_2(u_1, u_2)(e^{j\omega_1(t-u_1)} + e^{j\omega_2(t-u_2)}) \\ (e^{j\omega_1(t-u_2)} + e^{j\omega_2(t-u_2)}) du_1 du_2$$

$$= 2H_2(\omega_1, \omega_2) e^{j(\omega_1+\omega_2)t} + H_2(\omega_1, \omega_1) e^{2j\omega_1 t} + H_2(\omega_2, \omega_2) e^{2j\omega_2 t} \tag{3.27}$$

and the third-order system:

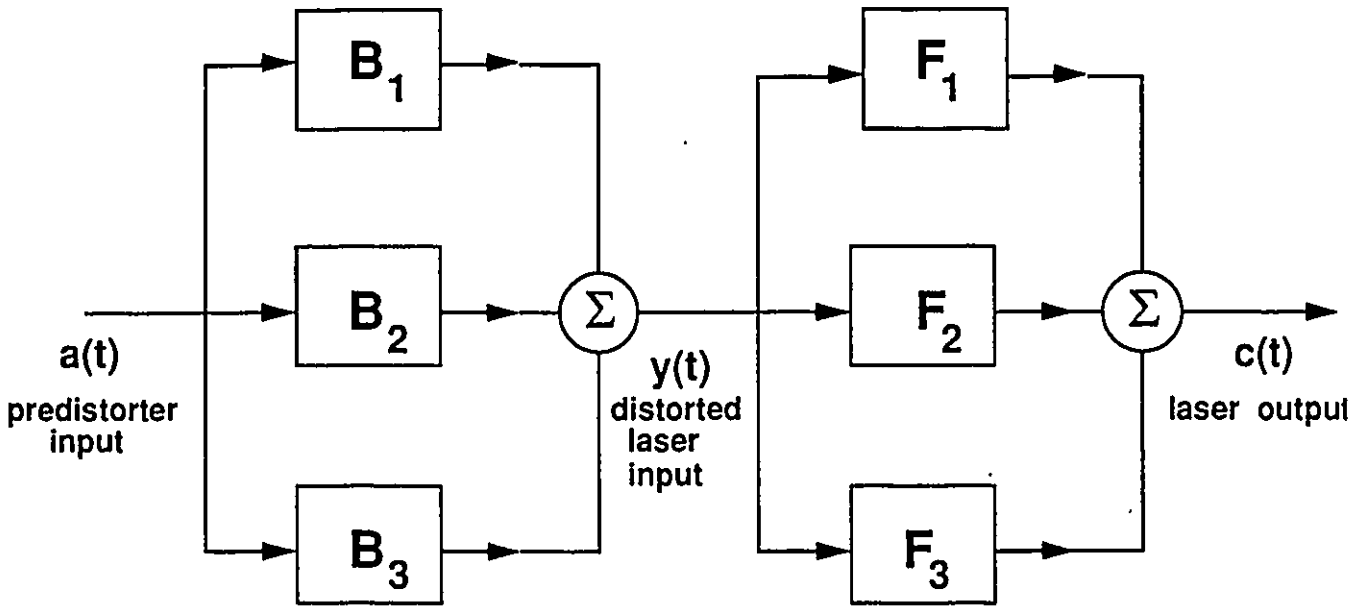

Figure 3.10. Block diagram presentation of laser diode and its inverse system modelled as Volterra series.

$$\mathcal{H}_3[a(t)] = \int_{-\infty}^{+\infty}\int_{-\infty}^{+\infty}\int_{-\infty}^{+\infty} h_3(u_1,u_2,u_3)a(t-u_1)a(t-u_2)a(t-u_3)du_1du_2du_3$$

$$= H_3(\omega_1,\omega_1,\omega_1)e^{j\omega_1 t} + H_3(\omega_2,\omega_2,\omega_2)e^{3j\omega_2 t}$$

$$+H_3(\omega_1,\omega_1,\omega_2)e^{j(2\omega_1+\omega_2)t} + H_3(\omega_1,\omega_2,\omega_2)e^{j(2\omega_2+\omega_1)t} \tag{3.28}$$

The two sets of transfer functions in Fig.3.10 correspond to inverse systems. The first order functions have a simple relation; like linear systems:

$$B_1(\omega) = \frac{1}{F_1(\omega)} \tag{3.29}$$

The second-order function, $F_2(\omega_1,\omega_2)$ is obtained by applying an input equal to $e^{j\omega_1 t} + e^{j\omega_2 t}$ to the system and then cancelling the terms of $e^{j(\omega_1+\omega_2)t}$ which correspond to the operation of the second order system.

$$a(t) = e^{j\omega_1 t} + e^{j\omega_2 t} \tag{3.30}$$

$$\mathcal{B}_1[a(t)] = B_1(\omega_1)e^{j\omega_1 t} + B_1 e^{j\omega_2 t} \tag{3.31}$$

So the output of an overall second order system would be:

$$y(t) = B_1(\omega_1)e^{j\omega_1 t} + B_1(\omega_2)e^{j\omega_2 t} + B_2(\omega_1,\omega_2)e^{j(\omega_1+\omega_2)t} \tag{3.32}$$

Now, this is considered as an input to another second order system, say $\mathcal{F}_2[y(t)]$. The final output is:

$$c(t) = F_1(\omega_1)B_1(\omega_1)e^{j\omega_1 t} + F_1(\omega_2)B_1(\omega_2)e^{j\omega_2 t}$$

$$F_1(\omega_1+\omega_2)B_2(\omega_1,\omega_2)e^{j(\omega_1+\omega_2)t} + F_2(\omega_1,\omega_2)B_1(\omega_1)B_1(\omega_2)e^{j(\omega_1+\omega_2)t}$$

$$+F_2(\omega_1,\omega_1+\omega_2)B_1(\omega_1)B_2(\omega_1,\omega_2)e^{j(2\omega_1+\omega_2)t}$$

$$+F_2(\omega_2,\omega_1+\omega_2)B_1(\omega_2)B_2(\omega_1,\omega_2)e^{j(\omega_1+2\omega_2)t} \qquad (3.33)$$

The coefficients of $e^{j(\omega_1+\omega_2)t}$ should be zero in order that the overall sytem acts like a linear system; $F_2(\omega_1,\omega_2)$ should be:

$$F_2(\omega_1,\omega_2) = \frac{-B_2(\omega_1,\omega_2)}{B_1(\omega_1)B_2(\omega_2)B_1(\omega_1+\omega_2)} \qquad (3.34)$$

Consider the systems shown in Fig.3.10. In a similar way, F_3 is determined. The input in this case consists of three tones, $e^{j\omega_1 t} + e^{j\omega_2 t} + e^{j\omega_3 t}$. The output of the first system is:

$$y(t) = B_1(\omega_1)e^{j\omega_1 t} + B_1(\omega_2)e^{j\omega_2 t} + B_1(\omega_3)e^{j\omega_3 t}$$

$$+B_2(\omega_1,\omega_2)e^{j(\omega_1+\omega_2)t} + B_2(\omega_1,\omega_3)e^{j(\omega_1+\omega_3)t}$$

$$+B_2(\omega_2,\omega_3)e^{j(\omega_2+\omega_3)t} + B_3(\omega_1,\omega_2,\omega_3)e^{j(\omega_1+\omega_2+\omega_3)t} \qquad (3.35)$$

This is an input to the cascade system. The coefficient of the term $e^{j(\omega_1+\omega_2+\omega_3)t}$ in the final output should be zero and this way $F_3(\omega_1,\omega_2,\omega_3)$ can be expressed as:

$$F_3(\omega_1,\omega_2,\omega_3) = \frac{-1}{B_1(\omega_1+\omega_2+\omega_3)B_1(\omega_1)B_1(\omega_2)B_1(\omega_3)}[B_3(\omega_1,\omega_2,\omega_3) -$$

$$\frac{B_2(\omega_2,\omega_3)B_2(\omega_1,\omega_2+\omega_3)}{B_1(\omega_2+\omega_3)} - \frac{B_2(\omega_1,\omega_3)B_2(\omega_2,\omega_1+\omega_3)}{B_1(\omega_1+\omega_3)} +$$

$$(-\frac{B_2(\omega_1,\omega_2)B_2(\omega_3,\omega_1+\omega_2)}{B_1(\omega_1+\omega_2)})] \tag{3.36}$$

Now that the transfer functions of the system are determined, the performance of the system for input tones can be evaluated by means of the operators and the transfer functions.

We obtained B transfer functions of the laser. Since the Volterra model for laser is represented by the inverse transfer functions of B, in this way Volterra models for both laser and its inverse system have been derived.

Chapter 4

Performance Analysis

In the previous chapter we introduced the Volterra series model for the laser diode and its predistortion block. The predistortion block serves as the inverse system for the laser diode. The cascade of this block and the laser diode block exhibits a much lower nonlinear distortion level. Nonlinearity measurements can be done by measuring the harmonic distortion and intermodulation distortion levels at the final output.

4.1 Harmonic Distortion Analysis

Performance of the two systems in cascade for harmonic distortion can be evaluated by applying a single frequency tone to the input. Since the cascade blocks are inverse of each other, the overall system performs almost as a linear system and the level of harmonic distortion at the output is very small. To proceed with the analysis, a frequency domain approach is used. If $y(t)$ is the output of operator $\mathcal{H}_p$ in equation (3.7), the frequency domain description of this output is:

$$Y_p(\omega) = \frac{1}{(2\pi)^{p-1}} \int_{-\infty}^{+\infty} \int_{-\infty}^{+\infty} \dots \int_{-\infty}^{+\infty} H_p(\omega - \omega_1 - \omega_2 \dots - \omega_p, \omega_1, \omega_2, \dots, \omega_p)$$

$$A(\omega - \omega_1 - \omega_2 - \dots - \omega_p) A(\omega_1) A(\omega_2) \dots A(\omega_p) d\omega_1 d\omega_2 \dots d\omega_p \qquad (4.1)$$

Recalling Fig.3.10 from previous chapter, the frequency domain description of the output $y(t)$ is:

$$Y(\omega) = B_1(\omega)A(\omega) + \frac{1}{2\pi}\int_{-\infty}^{+\infty} B_2(\omega-\omega_1,\omega_1)A(\omega-\omega_1)A(\omega_1)d\omega_1$$

$$+\frac{1}{(2\pi)^2}\int_{-\infty}^{+\infty}\int_{-\infty}^{+\infty} B_3(\omega-\omega_1-\omega_2,\omega_1,\omega_2)A(\omega-\omega_1-\omega_2)A(\omega_1)A(\omega_2)d\omega_1 d\omega_2 \quad (4.2)$$

If $a(t)$ is $e^{j\omega_o t}$ then by the fact that $A(\omega) = \delta(\omega-\omega_o)$ we get:

$$Y(\omega) = B_1(\omega_o)\delta(\omega-\omega_o) + \frac{1}{2\pi}\int_{-\infty}^{+\infty} B_2(\omega-\omega_1,\omega_1)\delta(\omega-\omega_1-\omega_o)\delta(\omega_1-\omega_o)d\omega_1$$

$$+\frac{1}{(2\pi)^2}\int_{-\infty}^{+\infty}\int_{-\infty}^{+\infty} B_3(\omega-\omega_1-\omega_2,\omega_1,\omega_2)\delta(\omega-\omega_1-\omega_2-\omega_o)\delta(\omega_1-\omega_o)\delta(\omega_2-\omega_o)d\omega_1 d\omega_2 \quad (4.3)$$

and;

$$Y(\omega) = B_1(\omega_o)\delta(\omega-\omega_o)+\frac{1}{2\pi}B_2(\omega_o,\omega_o)\delta(\omega-2\omega_o)+\frac{1}{(2\pi)^2}B_3(\omega_o,\omega_o,\omega_o)\delta(\omega-3\omega_o) \quad (4.4)$$

Now, $y(t)$ is an input to the second system with Volterra transfer functions as F, so in eq. (4.2) $A(\omega)$ and $B(\omega)$ are substituted by $Y(\omega)$ and $F(\omega)$, respectively. The frequency domain description of the final output is $C(\omega)$ which consists of terms of $\delta(\omega-n\omega_o)$ with $n = 1,2,...,9$. A detailed computation of this output can be found in Appendix A. The coefficients of δ-functions in $C(\omega)$ are:

$\delta(\omega-\omega_o)$:

$$F_1(\omega_o)B_1(\omega_o) = 1 \quad (4.5)$$

$\delta(\omega-2\omega_o)$:

$$\frac{1}{2\pi}[F_1(2\omega_o)B_2(\omega_o,\omega_o) + F_2(\omega_o,\omega_o){B_1}^2(\omega_o)] \quad (4.6)$$

$\delta(\omega - 3\omega_o)$:

$$\frac{1}{(2\pi)^2}[F_1(3\omega_o)B_3(\omega_o,\omega_o,\omega_o)$$
$$+F_2(2\omega_o,\omega_o)B_2(\omega_o,\omega_o)B_1(\omega_o)$$
$$+F_2(\omega_o,2\omega_o)B_1(\omega_o)B_2(\omega_o,\omega_o)$$
$$+F_3(\omega_o,\omega_o,\omega_o){B_1}^3(\omega_o)] \tag{4.7}$$

$\delta(\omega - 4\omega_o)$:

$$\frac{1}{(2\pi)^3}[B_1(\omega_o)B_3(\omega_o,\omega_o,\omega_o)F_2(3\omega_o,\omega_o)$$
$$+F_2(2\omega_o,2\omega_o)B_2(\omega_o,\omega_o)B_2(\omega_o,\omega_o)$$
$$+F_3(2\omega_o,\omega_o,\omega_o){B_1}^2(\omega_o)B_2(\omega_o,\omega_o)$$
$$+F_3(\omega_o,2\omega_o,\omega_o){B_1}^2(\omega_o)B_2(\omega_o,\omega_o)$$
$$+F_3(\omega_o,\omega_o,2\omega_o){B_1}^2(\omega_o)B_2(\omega_o,\omega_o)] \tag{4.8}$$

$\delta(\omega - 5\omega_o)$:

$$\frac{1}{(2\pi)^4}[F_3(3\omega_o,\omega_o,\omega_o){B_1}^2(\omega_o)B_3(\omega_o,\omega_o,\omega_o)$$
$$+F_3(2\omega_o,2\omega_o,\omega_o)B_1(\omega_o){B_2}^2(\omega_o,\omega_o)$$
$$+F_3(\omega_o,3\omega_o,\omega_o){B_1}^2(\omega_o)B_3(\omega_o,\omega_o,\omega_o)$$
$$+F_3(2\omega_o,\omega_o,2\omega_o)B_1(\omega_o){B_2}^2(\omega_o,\omega_o)$$
$$+F_3(\omega_o,2\omega_o,2\omega_o){B_2}^2(\omega_o,\omega_o)B_1(\omega_o)$$
$$+F_3(\omega_o,\omega_o,3\omega_o){B_1}^2(\omega_o)B_3(\omega_o,\omega_o,\omega_o)] \tag{4.9}$$

$\delta(\omega - 6\omega_o)$:

$$\frac{1}{(2\pi)^5}[F_3(3\omega_o,2\omega_o,\omega_o)B_1(\omega_o)B_2(\omega_o,\omega_o)B_3(\omega_o,\omega_o,\omega_o)$$

$$+F_3(2\omega_o, 3\omega_o, \omega_o)B_1(\omega_o)B_2(\omega_o, \omega_o)B_3(\omega_o, \omega_o, \omega_o)$$

$$+F_3(3\omega_o, \omega_o, 2\omega_o)B_1(\omega_o)B_2(\omega_o, \omega_o)B_3(\omega_o, \omega_o, \omega_o)$$

$$+F_3(2\omega_o, 2\omega_o, 2\omega_o){B_2}^3(\omega_o, \omega_o)$$

$$+F_3(\omega_o, 3\omega_o, 2\omega_o)B_2(\omega_o, \omega_o)B_3(\omega_o, \omega_o, \omega_o)$$

$$+F_3(2\omega_o, \omega_o, 3\omega_o)B_1(\omega_o)B_2(\omega_o, \omega_o)B_3(\omega_o, \omega_o, \omega_o)$$

$$+F_3(\omega_o, 2\omega_o, 3\omega_o)B_1(\omega_o)B_2(\omega_o, \omega_o)B_3(\omega_o, \omega_o, \omega_o)] \quad (4.10)$$

$\delta(\omega - 7\omega_o)$:

$$\frac{1}{(2\pi)^6}[F_3(3\omega_o, 3\omega_o, \omega_o)B_1(\omega_o){B_3}^2(\omega_o, \omega_o, \omega_o)$$

$$+F_3(3\omega_o, 2\omega_o, 2\omega_o){B_2}^2(\omega_o, \omega_o)B_3(\omega_o, \omega_o, \omega_o)$$

$$+F_3(2\omega_o, 3\omega_o, 2\omega_o)B_3(\omega_o, \omega_o, \omega_o){B_2}^2(\omega_o, \omega_o)B_1(\omega_o)$$

$$+F_3(3\omega_o, \omega_o, 3\omega_o)B_1(\omega_o){B_3}^2(\omega_o, \omega_o, \omega_o)$$

$$+F_3(2\omega_o, 2\omega_o, 3\omega_o)B_3(\omega_o, \omega_o, \omega_o){B_2}^2(\omega_o, \omega_o)$$

$$+F_3(\omega_o, 3\omega_o, 3\omega_o){B_3}^2(\omega_o, \omega_o, \omega_o)B_1(\omega_o)] \quad (4.11)$$

$\delta(\omega - 8\omega_o)$:

$$\frac{1}{(2\pi)^7}[F_3(3\omega_o, 3\omega_o, 2\omega_o)B_2(\omega_o, \omega_o){B_3}^2(\omega_o, \omega_o, \omega_o)$$

$$+F_3(3\omega_o, 2\omega_o, 3\omega_o)B_2(\omega_o, \omega_o){B_3}^2(\omega_o, \omega_o, \omega_o)$$

$$+F_3(2\omega_o, 3\omega_o, 3\omega_o)B_2(\omega_o){B_3}^2(\omega_o, \omega_o, \omega_o)] \quad (4.12)$$

$\delta(\omega - 9\omega_o)$:

$$\frac{1}{(2\pi)^8}F_3(3\omega_o, 3\omega_o, 3\omega_o){B_3}^3(\omega_o, \omega_o, \omega_o) \quad (4.13)$$

The ratio of the coefficients of the harmonics to the fundamental frequency is a measure of the linearization. When the ratio is small enough, it shows that effects of nonlinearity are small. The results of the simulating program are discussed in chapter 6.

When dealing with nonlinearities, also of great concern is the analysis of intermodulation products. In a multichannel FDM (Frequency Division Multiplex) carrier system intermodulation noise is an undesired effect since it can distort the signalling channels. This effect arises due to nonlinear mixing that takes place among different carriers in the system. Some studies on intermodulation noise have approached the problem of analyzing the intermodulation distortion in a pure theoretical manner. In these works first are considered the interaction of a small number of discrete tones. The results are then extended to a very large number of tones to simulate the condition of the system during the heavy traffic periods. This approach is highly numerically intensive.

4.2 Intermodulation Distortion Analysis

In practice, the measurement of intermodulation noise in a multiplexed system is done by loading the input of the system with a bandlimited white noise, thus simulating the actual load of the system during the peak hours. Fig. 4.1 shows the frequency spectrum of the input signal in this case. The bandwidth is chosen to be between the lowest subcarrier f_l and the highest subcarrier f_h. If we assume that the transmitted power of each subcarrier is P_i then $S_a(f) = \frac{NP_i}{2df}$. Here, df is the available bandwidth for transmission or the bandwidth that subcarriers occupy. The transmitted power of each subcarrier is $I_m^2/2$ per ohm resistor where I_m is the peak amplitude of the current. Optical modulation depth can be defined as the ratio of the peak transmitted light power to

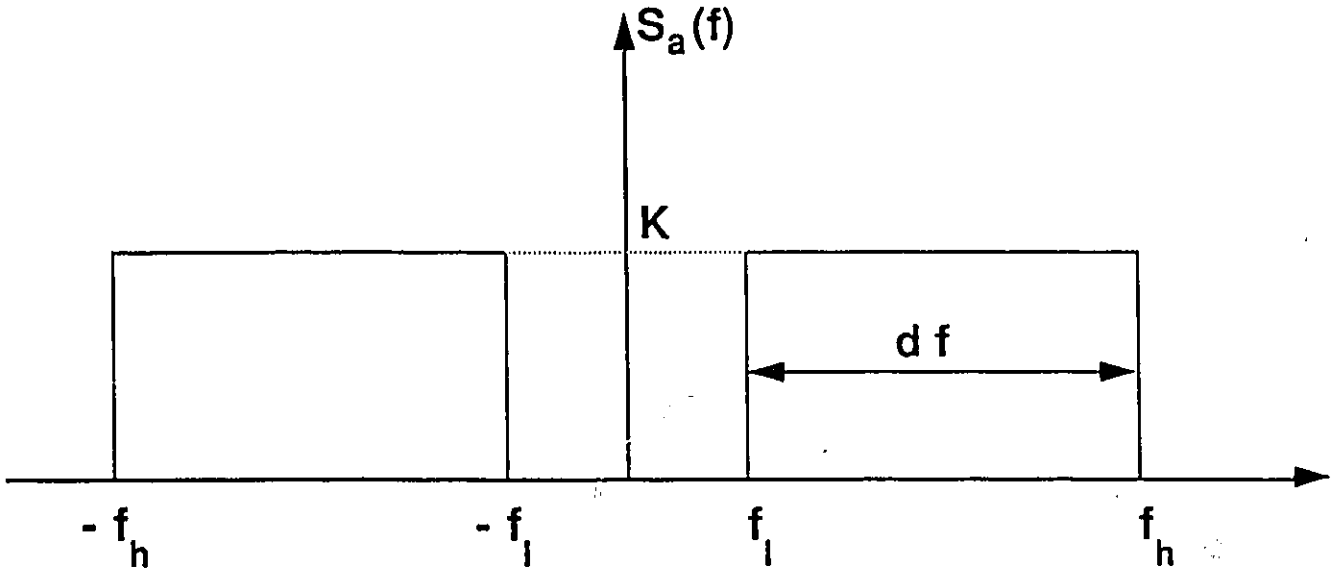

Figure 4.1. Frequency spectrum of the subcarriers.

the average transmitted light power. Recalling Fig. 3.5 we have [1],[15]:

$$\tan\alpha = \frac{P_{max} - P_0}{\Delta I} = \frac{P_0}{I_0 - I_{th}}$$
$$= \frac{P_{max} - P_0}{P_0} = \frac{\Delta I}{I_0 - I_{th}} \tag{4.14}$$

On the other hand, $m = \frac{\Delta I}{I_0 - I_{th}}$ so, $m = \frac{P_{max} - P_0}{P_0}$. Using this definition I_m is expressed as:

$$I_m = \frac{m(I_0 - I_{th})}{R} \tag{4.15}$$

where R is the slope of the light-current characteristic of the semiconductor laser that is well approximated by $|F_1(0)|$. Since $P_i = \frac{I_m^2}{2}$,the frequency spectrum of the input is:

$$S_a(\omega) = \frac{Nm^2(I_0 - I_{th})^2}{4R.df} \tag{4.16}$$

This is the value of K in Fig. 4.1.

At the output, the intermodulation noise is measured in a narrowband (referred to as a frequency notch) from which the noise has been excluded. In this procedure the frequency domain description of the system is used. The first step in this process is to find the frequency spectrum of the second and the third order intermodulation noise at the output. The frequency spectrum of any signal is the Fourier transform of its autocorrelation function. The autocorrelation of the output signal when the system is represented by Volterra kernels of first, second and third order is derived directly by finding the expectation of $y(t).y(t-\tau)$. The resulting power spectrum for the first system is [19]:

$$S_y(\omega) =< a(t)^2 > \delta(\omega) + S_a(\omega)|B_1(\omega) + \frac{1}{2}\int_{-\infty}^{+\infty} S_a(\lambda)B_3(\omega,\lambda,-\lambda)d\lambda|^2$$

$$+\frac{1}{2!}\int_{-\infty}^{+\infty} S_a(\lambda)S_a(\omega-\lambda)|B_2(\lambda,\omega-\lambda)|^2 d\lambda$$

$$+\frac{1}{3!}\int_{-\infty}^{+\infty} S_a(\lambda)S_a(\gamma)s_a(\omega-\lambda-\gamma)|B_3(\lambda,\gamma,\omega-\lambda-\gamma)|^2 d\lambda d\gamma \qquad (4.17)$$

In a similar way, the power spectrum of the final output is derived as:

$$S_c(\omega) =< c(t)^2 > \delta(\omega) + S_y(\omega)|F_1(\omega) + \frac{1}{2}\int_{-\infty}^{+\infty} S_y(\lambda)F_3(\omega,\lambda,-\lambda)d\lambda|^2$$

$$+\frac{1}{2!}\int_{-\infty}^{+\infty} S_y(\lambda)S_y(\omega-\lambda)|F_2(\lambda,\omega-\lambda)|^2 d\lambda$$

$$+\frac{1}{3!}\int_{-\infty}^{+\infty} S_y(\lambda)S_y(\gamma)S_y(\omega-\lambda-\gamma)|F_3(\lambda,\gamma,\omega-\lambda-\gamma)|^2 d\lambda d\gamma \qquad (4.18)$$

We present the details of the steps to obtain this expression in Appendix B. The δ-function terms of $S_y(\omega)$ and $S_c(\omega)$ are zero frequency components and are removed at both outputs by highpass filtering. However, the major sources of distortion are the third and fourth terms which correspond to the second and third-order intermodulation distortion, respectively.

Equation (4.17) can be written in a way that makes the analysis simpler. Recalling equations (3.5) and (3.6) from previous chapter and substituting them in eq.(4.17) results in:

$$S_y(\omega) =< a(t)^2 > \delta(\omega) + S_a(\omega)|B_1(\omega) + \frac{1}{2}(6r - 2g\omega^2 + 2j\sigma\omega)\int_{-\infty}^{+\infty} S_a(\lambda)d\lambda|^2$$

$$+\frac{1}{2!}[(-2l + n\omega^2)^2 + m^2\omega^2]\int_{-\infty}^{+\infty} S_a(\lambda)S_a(\omega - \lambda)d\lambda$$

$$+\frac{1}{3!}[(6r - 2g\omega^2)^2 + 4\sigma^2\omega^2]\int_{-\infty}^{+\infty}\int_{-\infty}^{+\infty} S_a(\lambda)S_a(\gamma)S_a(\omega - \lambda - \gamma)d\lambda d\gamma \qquad (4.19)$$

If we call the fundamental component S_{y_1} and the second and the third-order intermodulation products S_{y_2} and S_{y_3} , then:

$$S_{y_1}(\omega) = S_a(\omega)|B_1(\omega) + \frac{1}{2}(6r - 2g\omega^2 + 2j\sigma\omega)\int_{-\infty}^{+\infty} S_a(\lambda)d\lambda|^2 \qquad (4.20)$$

$$S_{y_2}(\omega) \propto \int_{-\infty}^{+\infty} S_a(\lambda)S_a(\omega - \lambda)d\lambda = S_a(\omega) * S_a(\omega) \qquad (4.21)$$

$$S_{y_3}(\omega) \propto \int_{-\infty}^{+\infty} S_a(\lambda)S_a(\gamma)S_a(\omega - \lambda - \gamma)d\lambda d\gamma = S_a(\omega) * S_a(\omega) * S_a(\omega) \qquad (4.22)$$

So the second and the third-order intermodulation terms can be expresssed by single and double convolution of fundamental terms, repectively. We showed the intermodulation products of the laser without any predistortion block in Fig. 3.9 and Fig. 3.10. The predistortion block acts as an inverse block for the laser. The total operation of the system is linear. Therefore, intermodulation distortion must be very small compared to the fundamental carrier component, once the laser is linearized. The results in this case, where the inverse predistortion block has been used prior to the system are shown in Fig. 4.2 and 4.3. As the figures indicate, the second order intermodulation distortion is at least 70 dB lower than the case for the system without predistortion. For the

third order intermodulation distortion this amount is about 20 dB. We computed the integral of the expression for frequency spectrum by numerical methods using Simpson Integration Rule. We have obtained the results corresponding to the different values of optical modulation index. The modulation index considered in this part of the analysis and in the simulation program is the optical modulation depth per carrier. As shown in Fig. 4.4 and 4.5, variation of the optical modulation depth causes vertical shifts in the curves. The smaller optical modulation depths yield smaller intermodulation distortion, as expected, because the effective amplitude of the applied signal is smaller. The reason is that with a smaller modulation index a smaller portion of the light/current characteristic of the laser is utilized, i.e., the range which is less nonlinear. Fig. 4.6 shows variations of intermodulation distortion as a function of different values of bias current when the predistortion block is used prior to the laser. As can be seen from the corresponding curve, nonlinear effects depend on the laser bias current. The optimum bias current is at the midpoint between the threshold current and the saturation region. The optical modulation depth remains a constant in this case. The selected value is 0.04 per carrier.

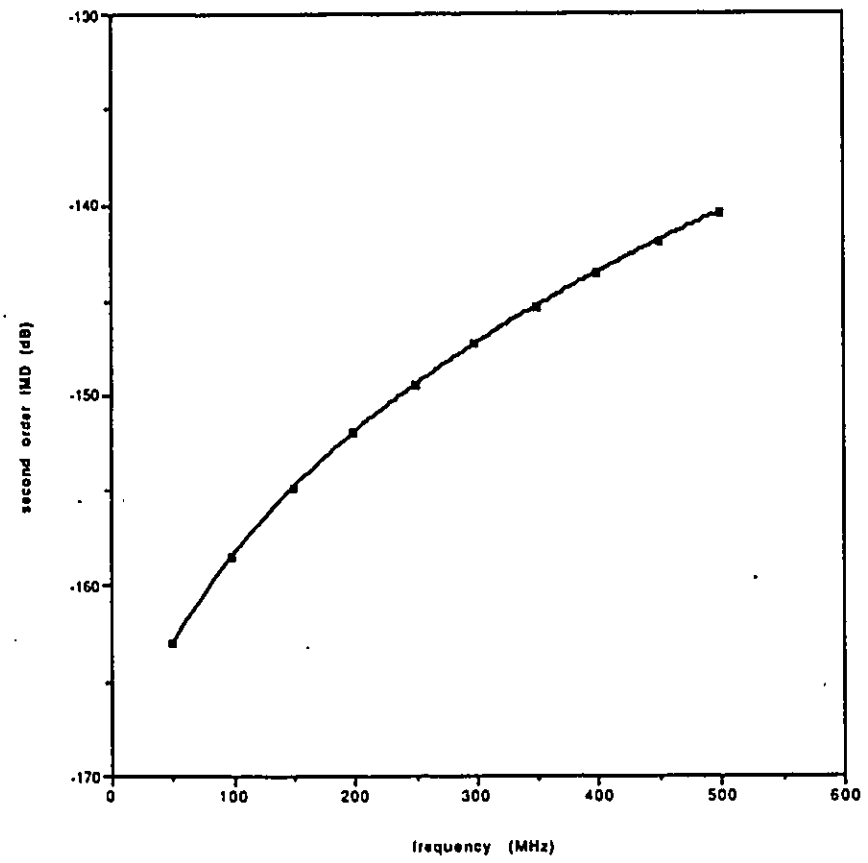

Figure 4.2. Second-order IMD at the output when predistortion is used.

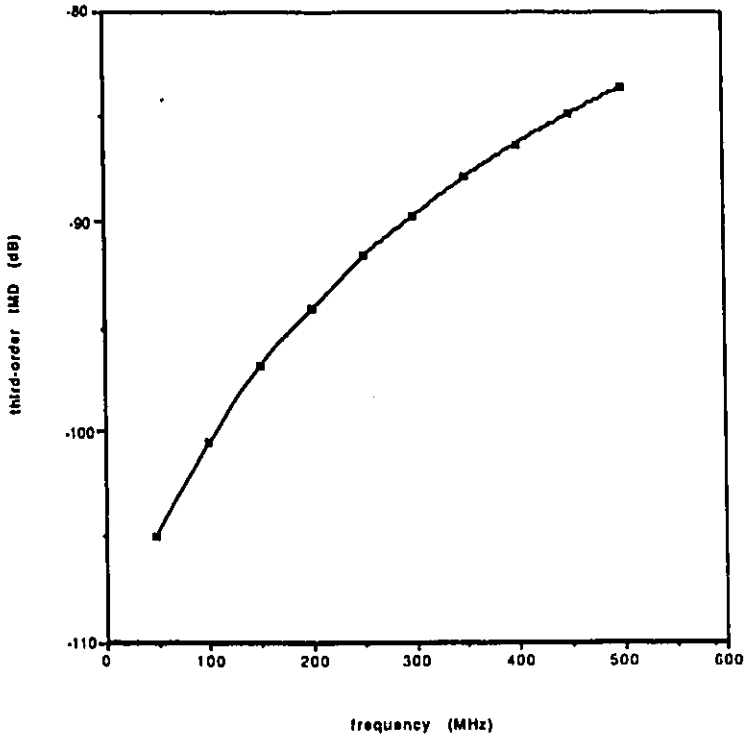

Figure 4.3. Third-order IMD at the output when predistortion is used.

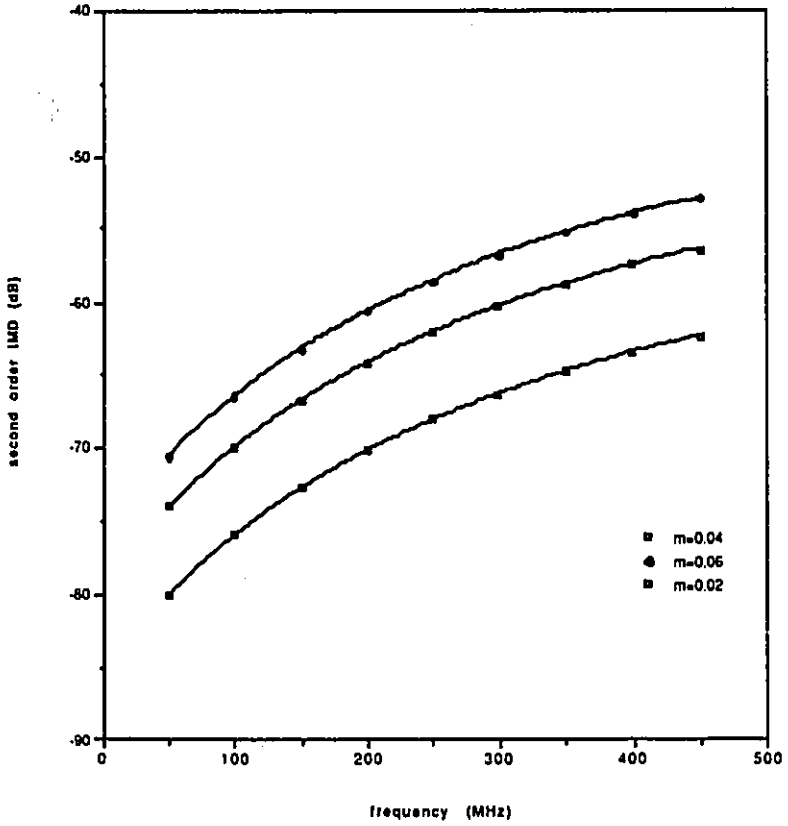

Figure 4.4. Second-order IMD without predistortion for different modulation depth values, m.

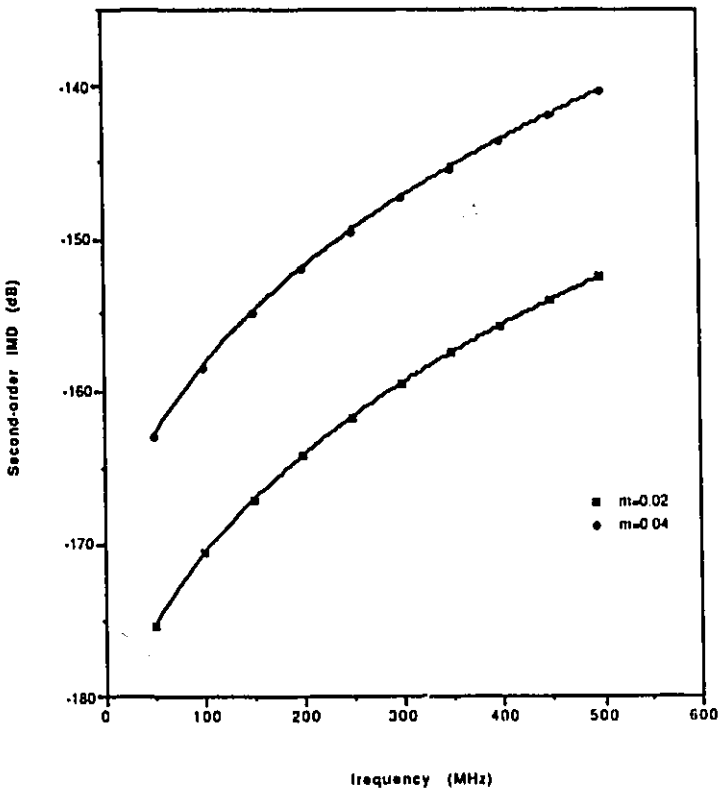

Figure 4.5. Second-order IMD with predistortion for different modulation depth values, m.

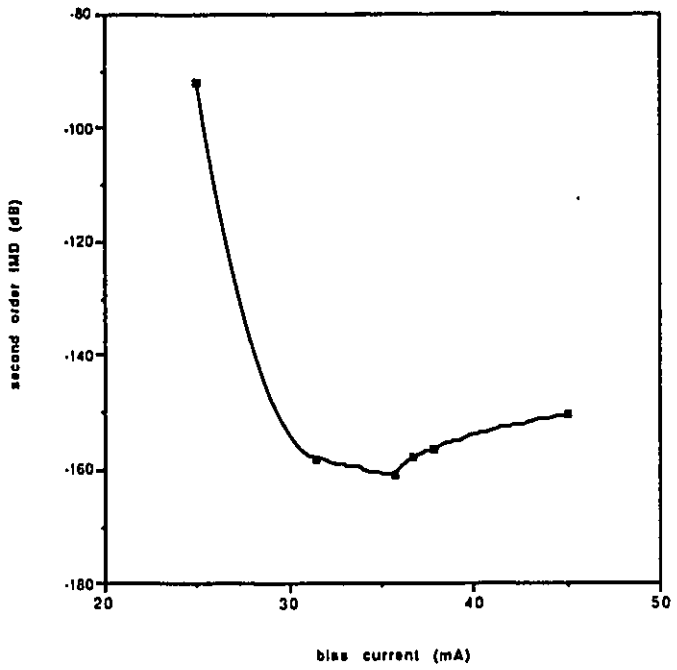

Figure 4.6. Second-order IMD versus bias current of the laser.

Chapter 5
Realization of Volterra systems

Volterra systems of low-order are implemented by decomposiotion of the system Volterra function into lower-order functions of linear type [18]. Combination of these linear systems by multiplication and addition techniques delivers the function for Volterra system. This can be viewed as a method to implement systems modelled in Volterra functions. We describe the procedure for a second-order system. We denote the kernel of this system by $h_2(\tau_1, \tau_2)$. This kernel has a Laplace transform denoted by $H_2(s_1, s_2)$:

$$H_2(s_1, s_2) = \int_{-\infty}^{+\infty} \int_{-\infty}^{+\infty} h_2(\tau_1, \tau_2) e^{-(s_1\tau_1 + s_2\tau_2)} d\tau_1 d\tau_2 \tag{5.1}$$

Here, $s_i = \sigma_i + j\omega_i$ so that the Fourier transforms we discussed are obtained by $\sigma_i = 0$. We write $H_2(s_1, s_2)$ in the form of multiplication of linear systems Laplace transforms.

$$H_2(s_1, s_2) = H_a(s_1) H_b(s_2) H_c(s_1 + s_2) \tag{5.2}$$

in which

$$H(s) = \int_{-\infty}^{+\infty} h(t) e^{-st} dt \tag{5.3}$$

So $H_a(s)$, $H_b(s)$ and $H_c(s)$ are the system functions of the linear systems with impulse responses $h_a(t)$, $h_b(t)$ and $h_c(t)$, respectively. This can be viewed in a schematic form shown in Fig. 5.1. The linear system with the unit impulse response $h_a(t)$ has the input

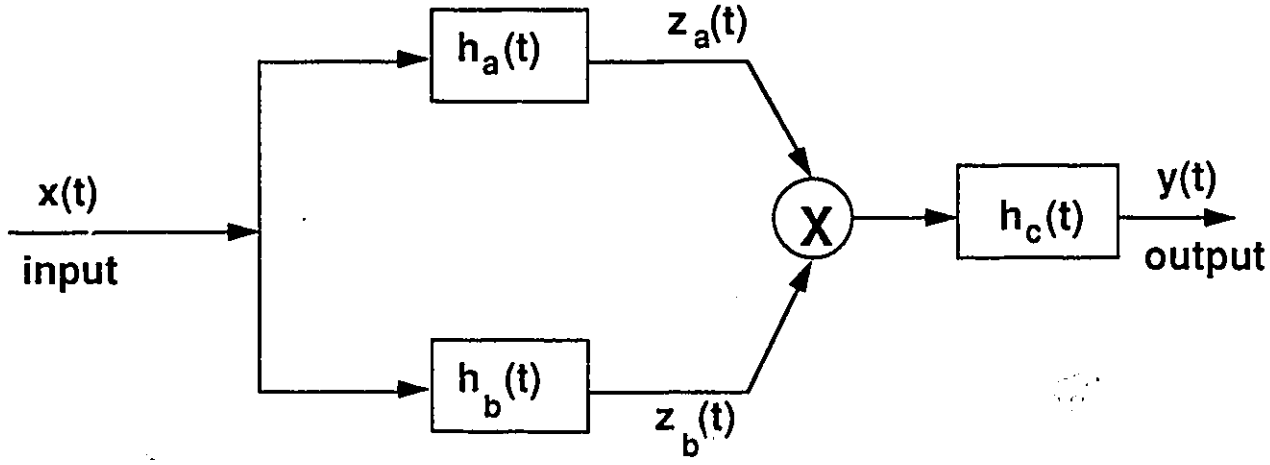

Figure 5.1. Realization of a second -order Volterra system.

$x(t)$ and its output is $z_a(t)$; the linear system with the unit impluse response $h_b(t)$ has the same input but with an output $z_b(t)$. The product $z_a(t)z_b(t)$ is the input of the linear system with the unit impulse response $h_c(t)$ for which the output is $y(t)$, so that:

$$y(t) = \int_{-\infty}^{+\infty} h_c(t) z_a(t-\sigma) z_b(t-\sigma) d\sigma \tag{5.4}$$

$$= \int_{-\infty}^{+\infty} \int_{-\infty}^{+\infty} \int_{-\infty}^{+\infty} h_c(\sigma) h_a(\sigma_1) h_b(\sigma_2) x(t-\sigma-\sigma_1) x(t-\sigma-\sigma_2) d\sigma_1 d\sigma_2 d\sigma \tag{5.5}$$

If we want to express $y(t)$ in the functional form of the Volterra operator $\mathcal{H}_2$, we substitute $\tau_1 = \sigma + \sigma_1$ and $\tau_2 = \sigma + \sigma_2$ in eq. (5.5):

$$y(t) = \int_{-\infty}^{+\infty} \int_{-\infty}^{+\infty} \int_{-\infty}^{+\infty} h_c(\sigma) h_a(\tau_1 - \sigma) h_b(\tau_2 - \sigma) x(t-\tau_1) x(t-\tau_2) d\sigma d\tau_1 d\tau_2$$

$$= \int_{-\infty}^{+\infty} \int_{-\infty}^{+\infty} h_2(\tau_1, \tau_2) x(t-\tau_1) x(t-\tau_2) d\tau_1 d\tau_2 \tag{5.6}$$

in which

$$h_2(\tau_1, \tau_2) = \int_{-\infty}^{+\infty} h_c(\sigma) h_a(\tau_1 - \sigma) h_b(\tau_2 - \sigma) d\sigma \tag{5.7}$$

is the kernel of the basic second-order system. A more convenient form for this discussion is the Laplace transform of the second-order kernel, that is:

$$H_2(s_1, s_2) = \int_{-\infty}^{+\infty} \int_{-\infty}^{+\infty} k_2(\tau_1, \tau_2) e^{-(s_1\tau_1 + s_2\tau_2)} d\tau_1 d\tau_2 \tag{5.8}$$

in which $s_1 = \alpha_1 + j\omega_1$ and $s_2 = \alpha_2 + j\omega_2$. The two-dimensional Fourier transform, $H_2(j\omega_1, j\omega_2)$ of the second-order kernel is obtained when $\alpha_1 = \alpha_2 = 0$ in eq.(5.8). The kernel transform of the basic second-order system is obtained by substituting eq.(5.7) into eq. (5.8):

$$H_2(s_1, s_2) = \int_{-\infty}^{+\infty} \int_{-\infty}^{+\infty} \int_{-\infty}^{+\infty} h_c(\sigma) h_a(\tau_1 - \sigma) h_b(\tau_2 - \sigma) e^{-(s_1 2\tau_1 + s_2 \tau_2)} d\sigma d\tau_1 d\tau_2 \quad (5.9)$$

If we change variables, $\tau_1 - \sigma = \gamma_1$ and $\tau_2 - \sigma = \gamma_2$, we obtain:

$$H_2(s_1, s_2) = \int_{-\infty}^{+\infty} \int_{-\infty}^{+\infty} \int_{-\infty}^{+\infty} h_a(\gamma_1) h_b(\gamma_2) h_c(\sigma) e^{-(s_1\gamma_1 - s_2\gamma_2)} e^{-(s_1+s_2)\sigma} d\sigma d\gamma_1 d\gamma_2$$

$$= \int_{-\infty}^{+\infty} h_a(\beta_1) e^{-s_1\beta_1} d\beta_1 . \int_{-\infty}^{+\infty} h_b(\beta_2) e^{-s_2\beta_2} d\beta_2$$

$$. \int_{-\infty}^{+\infty} h_c(\sigma) e^{-(s_1+s_2)\sigma} d\sigma$$

$$= H_a(s_1).H_b(s_2).H_c(s_1 + s_2) \quad (5.10)$$

so that $H_a(s_1)H_b(s_2)$ and $H_c(s_1 + s_2)$ are the system functions of the linear systems with impulse responses $h_a(t)$, $h_b(t)$ and $h_c(t)$, respectively. The transfer function $H(s)$ of a linear time invariant system can be written in the form:

$$H(s) = \frac{P(s)}{Q(s)} \quad (5.11)$$

Then zeros of $P(s)$ are the zeros of $H(s)$ and zeros of $Q(s)$ are the poles of $H(s)$. We can write the kernel transform of $h_2(\tau_1, \tau_2)$ as

$$H_2(s_1, s_2) = \frac{P_a(s_1)P_b(s_2)P_c(s_1 + s_2)}{Q_a(s_1)Q_b(s_2)Q_c(s_1 + s_2)} \tag{5.12}$$

In this way, the poles and zeros of the linear systems of Fig. 5.1 gives us some idea about the stability of the second-order Volterra system and whether it is realizable. This method is extendable to higher-order Volterra systems. For higher-order Volterra systems the number of multipliers and linear systems blocks are more than those of a second-order system. For third-order systems the same method is applied. The basic third-order system can be obtained with only two multipliers. This configuration is shown in Fig. 5.2. In this figure, $x(t)$ is the common input to the system H_2, a basic second-order system and the corresponding output is $z_a(t)$. Another linear system with impulse response $h_b(t)$, has $x(t)$ as the input and $z_b(t)$ as the output. The product of $z_a(t)z_b(t)$ is the input of the linear system with impulse response $h_c(t)$ for which the output is $y_3(t)$. If we denote the kernel of this third-order system by $h_3(\tau_1, \tau_2, \tau_3)$ then the kernel Laplace transform is:

$$H_3(s_1, s_2, s_3) = \int_{-\infty}^{+\infty} \int_{-\infty}^{+\infty} \int_{-\infty}^{+\infty} h_3(\tau_1, \tau_2, \tau_3) e^{-(s_1\tau_1 + s_2\tau_2 + s_3\tau_3)} d\tau_1 d\tau_2 d\tau_3 \tag{5.13}$$

On the other hand, we want that the basic third-order system gives us the same output as the system shown in Fig. 5.2. The output $y_3(t)$ expressed in terms of third-order kernel $h_3(\tau_1, \tau_2, \tau_3)$ is:

$$y_3(t) = \int_{-\infty}^{+\infty} \int_{-\infty}^{+\infty} \int_{-\infty}^{+\infty} h_3(\tau_1, \tau_2, \tau_3) x(t - \tau_1) x(t - \tau_2) x(t - \tau_3) d\tau_1 d\tau_2 d\tau_3 \tag{5.14}$$

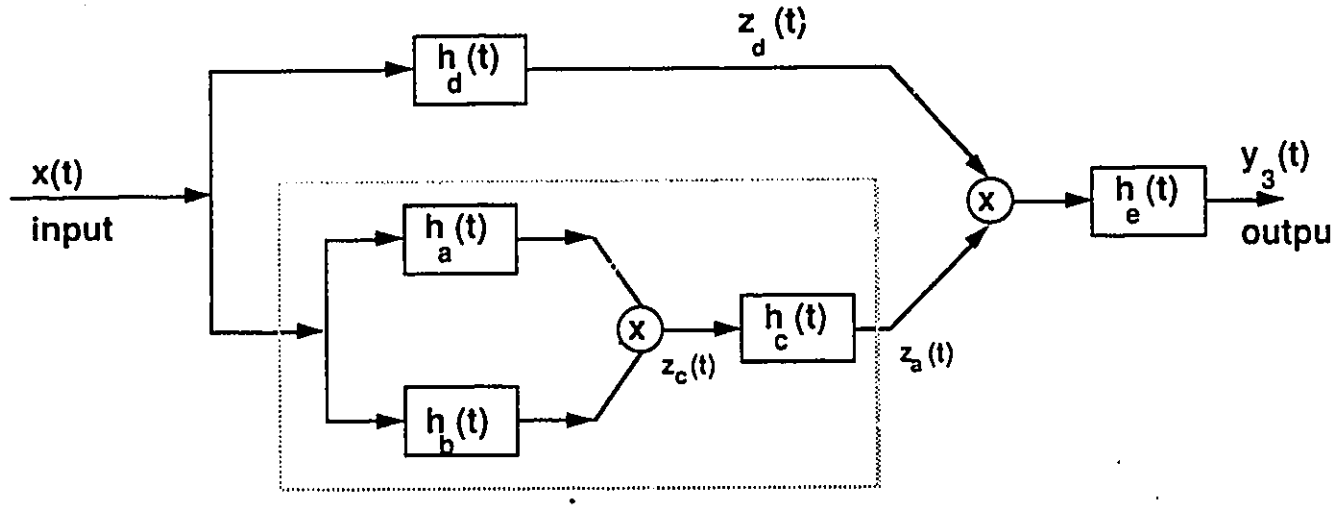

Figure 5.2. Realization of a third-order Volterra system.

This output is equal to:

$$y_3(t) = \int_{-\infty}^{+\infty} h_c(\tau_3) z_b(t-\tau_3) z_a(t-\tau_3) d\tau_3$$

$$= \int_{-\infty}^{+\infty} h_c(\tau_3) \left[\int_{-\infty}^{+\infty} h_d(\tau_2) x(t-\tau_3-\tau_2) d\tau_2 \right] z_a(t-\tau_3) d\tau_3 \qquad (5.15)$$

The output $z_a(t-\tau_3)$ is:

$$z_a(t-\tau_3) = \int_{-\infty}^{+\infty} z_c(t-\tau_3-\tau_1) h_a(\tau_1) d\tau_1 \qquad (5.16)$$

The output $z_c(t-\tau_3-\tau_1)$ is:

$$z_c(t-\tau_3-\tau_1) = \int_{-\infty}^{+\infty} x(\lambda) h_a(t-\tau_3-\tau_1-\lambda) d\lambda$$

$$\cdot \int_{-\infty}^{+\infty} x(\gamma) h_b(t-\tau_3-\tau_1-\gamma) d\gamma \qquad (5.17)$$

By changing the variables and substituting the integral form of each output in eq.(5.15) and taking the Laplace transform, we have :

$$H_3(s_1, s_2, s_3) = H_a(s_1) H_b(s_2) H_c(s_1+s_2) H_d(s_3) H_e(s_1+s_2+s_3) \qquad (5.18)$$

So, for a basic third-order system the condition for implementation is that its kernel Laplace transform can be written in the form of eq.(5.18). In other words, if a third-order system has a kernel Laplace transform in the form of eq.(5.18), then it is equivalent to the combination of linear systems shown in Fig. 5.2.

Now, we describe the synthesis method for our Volterra kernels which represent the inverse system of the laser. The kernel Fourier transforms in the case of inverse system are:

$$B_3(\omega_1,\omega_2,\omega_3) = 6r + j2\sigma(\omega_1+\omega_2+\omega_3) - 2g(\omega_1+\omega_2+\omega_3)^2 \tag{5.19}$$

as the third-order Volterra function and

$$B_2(\omega_1,\omega_2) = -2l - jm(\omega_1+\omega_2) + n(\omega_1+\omega_2)^2 \tag{5.20}$$

and

$$B_1(\omega) = d + je\omega - f\omega^2 \tag{5.21}$$

as the second-order and the first-order Volterra functions, respectively. The above Fourier transforms can be viewed as substitution of $\alpha = 0$ in $s = \alpha + j\omega$ in the system Laplace transforms. So if we replace $s = \alpha + j\omega$ instead of $j\omega$ in the above expressions, we obtain the kernels Laplace transform for the system:

$$B_3(s_1,s_2,s_3) = 6r + 2\sigma(s_1+s_2+s_3) + 2g(s_1+s_2+s_3)^2 \tag{5.22}$$

$$B_2(s_1,s_2) = -2l + m(s_1+s_2) - n(s_1+s_2)^2 \tag{5.23}$$

$$B_1(s) = d + es + fs^2 \tag{5.24}$$

As can be seen, the kernels Laplace transform are in the forms developed in eq. (5.18). So in this case they are realized by linear systems and multipliers. According to Fig. 5.2 for $B_3(s_1, s_2, s_3)$ there is just one linear system with a unit impulse response $b_e(t)$, because B_3 is simply a function of $s_1 + s_2 + s_3$. So according to Fig. 5.2, the unit impulse responses of $b_a(t)$, $b_b(t)$, $b_c(t)$ and $b_d(t)$ are simply δ-functions and we can remove the corresponding blocks and simplify the figure to Fig. 5.3. As shown in Fig. 5.3, $b_e(t)$ is a linear system which its Laplace transform is obtained by substitution of $s_1 + s_2 + s_3$ by s in $B_3(s_1 + s_2 + s_3)$:

$$B_e(s) = 6r + 2gs^2 + 2\sigma s \tag{5.25}$$

This corresponds to an amplifier with a gain of $6r$, that is added to two differentiator system. Fig. 5.4 shows the block diagram for $B_e(s)$.

Now, we consider the implementation of the second-order Volterra system. The kernel Fourier transform of the second-order system was obtained as:

$$B_2(\omega_1, \omega_2) = -2l - jm(\omega_1 + \omega_2) + n(\omega_1 + \omega_2)^2 \tag{5.26}$$

Similar to the method that we used for $B_3(\omega_1, \omega_2, \omega_3)$ to obtain $B_3(s_1, s_2, s_3)$, the kernel Fourier transform is in fact its Laplace transform but with $s = \alpha + j\omega$ and $\alpha = 0$. Therefore the kernel Laplace transform of the second-order system is its Fourier transform but with $s = \alpha + j\omega$ and $\alpha = 0$ ($s = j\omega$). The kernel Fourier transform for second-order system is:

$$B_2(s_1, s_2) = -2l - m(s_1 + s_2) - n(s_1 + s_2)^2 \tag{5.27}$$

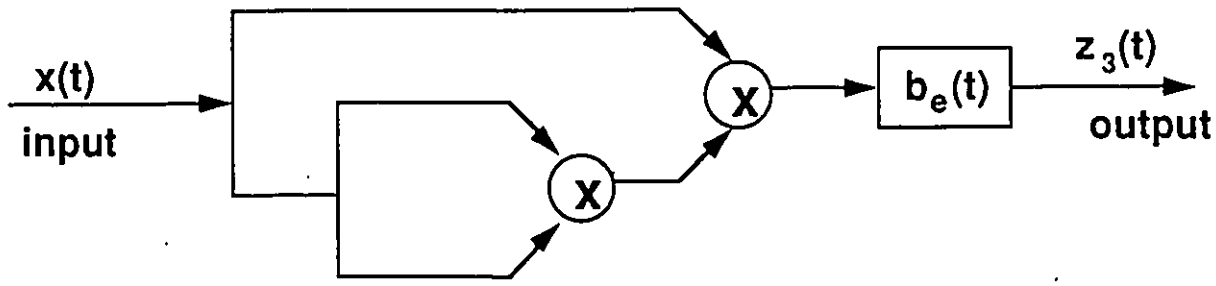

Figure 5.3. Realization of the third-order Volterra system of the predistortion block.

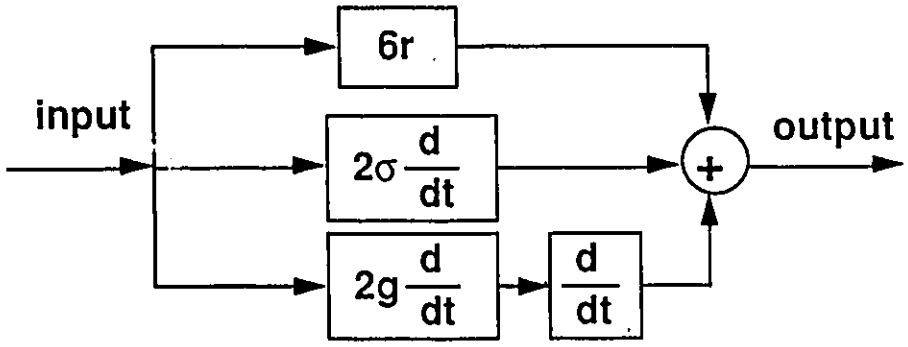

Figure 5.4. Block diagram of $B_e(s)$ for predistortion block.

For synthesis of $B_2(s_1, s_2)$ we write its equivalent expression in terms of linear systems Laplace transform as:

$$B_2(s_1, s_2) = B_a(s_1)B_b(s_2)B_c(s_1 + s_2) \tag{5.28}$$

Since $B_2(s_1, s_2)$ is just an expression of $(s_1 + s_2)$ we assume $B_a(s_1)$ and $B_b(s_2)$ are equal to unity. Their corresponding impulse responses are δ-functions. Fig. 5.5 shows the block diagram of $B_2(s_1, s_2)$ synthesized by a multiplier and a linear system with impulse response $b_c(t)$. The Laplace transform of $b_c(t)$ is $B_2(s_1, s_2)$ with $s = s_1 + s_2$:

$$B_c(s) = -2l - ms - ns^2 \tag{5.29}$$

Fig. 5.6 shows the block diagram representation of $B_c(s)$.

Finally, we consider synthesis of B_1. In fact, any first order Volterra system is a linear system because its output is the convolution integral of its input and the first-order Volterra kernel. Fig. 5.7 shows the block diagram representation of $B_1(s)$. Note that again $B_1(s)$ is obtained when we substitute $j\omega$ with s in $B_1(\omega)$. Therefore, $B_1(s)$ is:

$$B_1(s) = d + es + fs^2 \tag{5.30}$$

Now, that we showed the implementation method for the Volterra transfer functions of the predistortion block we can combine them by adders and obtain the block diagram of the whole block. Fig. 5.8 shows the block diagram of the predistortion system. The input current to the laser passes through this predistortion block before it is applied to the laser. The output of the predistortion block is denoted as $\hat{i}(t)$ in Fig. 5.8. This current; $\hat{i}(t)$, is then applied to the laser as an input. Since predistortion block is formed

by the inverse Volterra transfer functions of the laser, the overall system or the cascade of these blocks is a system which is the linearized laser system. In other words, it has a much lower nonlinear distortion noise than laser itself. We discussed the performance of the two systems in cascade in previous sections and showed the results for harmonic and intermodulation distortion noises in the corresponding graphs. We discuss the results with more details in Chapter 6.

For implementation of any system with a given Laplace transform its pole-zero root locus must be checked to be in a region of the s-plane that realization of the system is possible. If a system has a pole in the right-hand side of the s-plane it is not stable and so it cannot be implemented. Recalling the kernels Laplace transforms of the predistortion block and their corresponding realization with linear systems and multipliers, it is possible to implement these systems since they do not have any poles and their expressions in s-plane are polynomials in s. So they just have zeros and this is consistent with their real implementation. Also, they are causal systems. According to the block diagrams of equivalent linear systems of Volterra kernels shown in Fig. 5.3, 5.5 and 5.7 when the input to the system is zero the output is zero and there is no output until a nonzero input is applied. So the systems are causal and hence realizable.

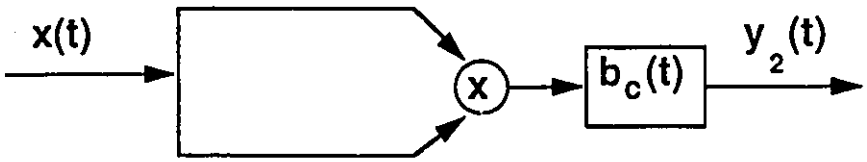

Figure 5.5. Realization of the second-order Volterra system of the predistortion block.

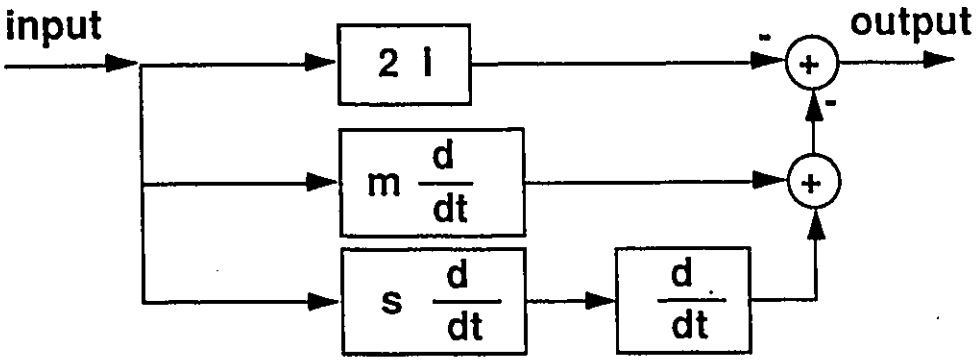

Figure 5.6. Block diagram of $B_c(s)$ for predistortion block.

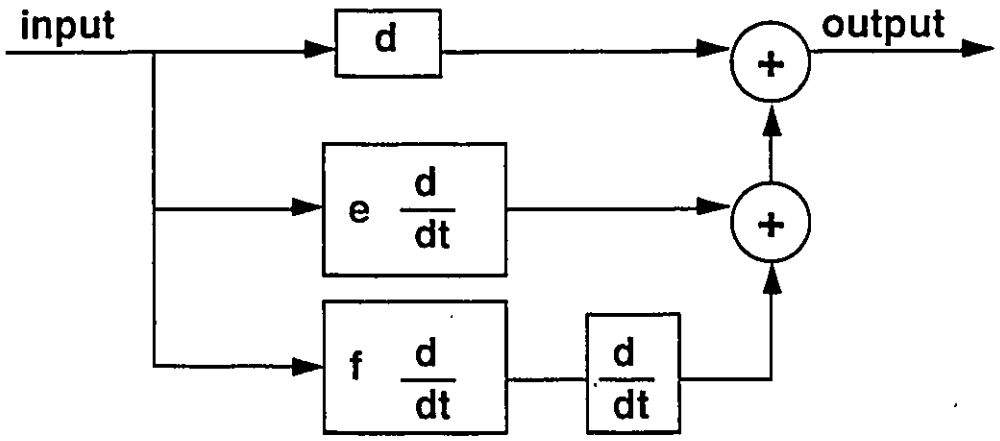

Figure 5.7. Block diagram of $B_1(s)$ for predistortion block.

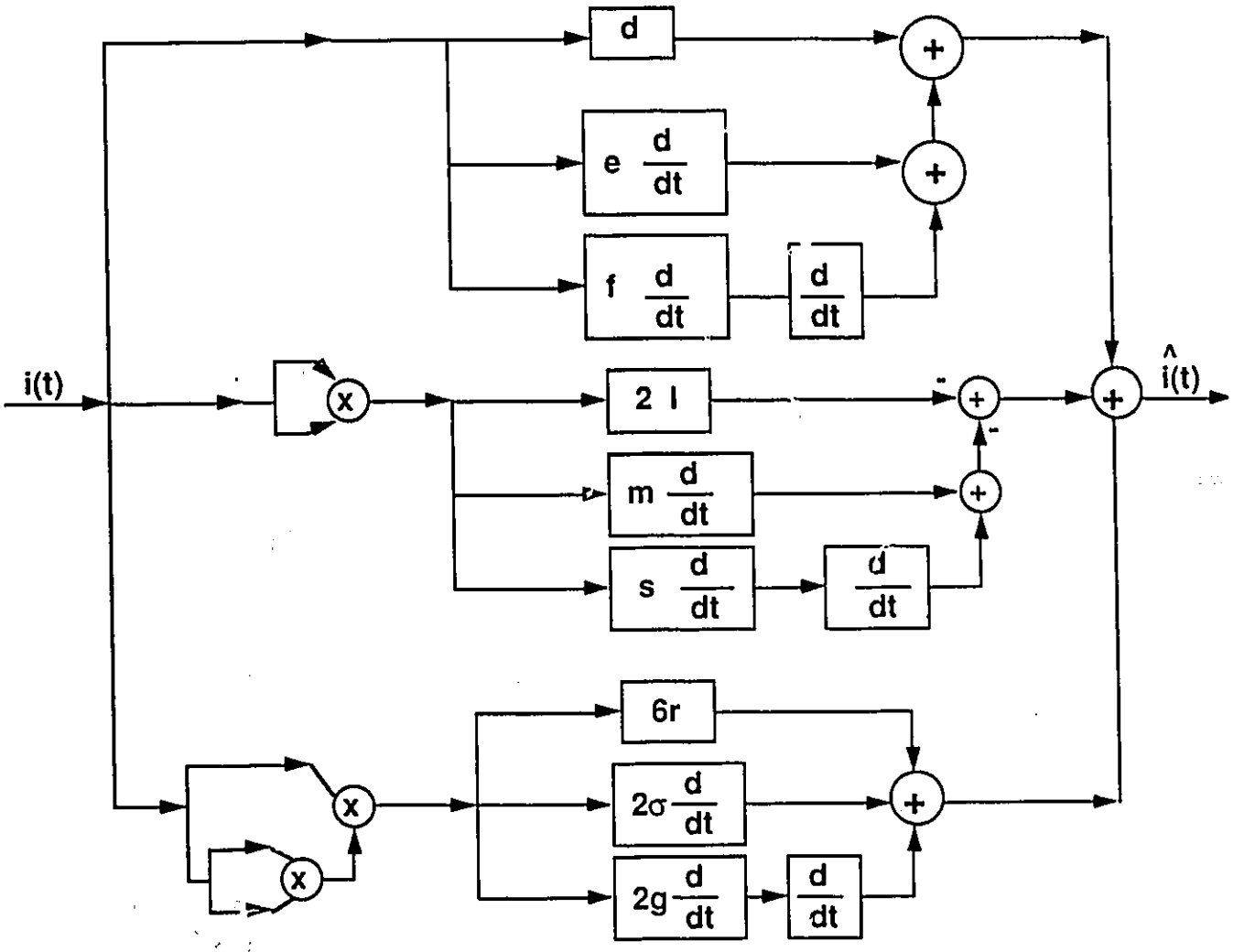

Figure 5.8. Realization of predistortion block.

Chapter 6
Numerical Results

6.1 Results for cascade system:

In chapter 3, we discussed the performance of the predistortion block and laser when they are working in cascade. We gave the methods for analysis of the performance for harmonic distortion and intermodulation distortion. Harmonic distortion is analyzed by applying a single-frequency tone; $e^{j\omega_0 t}$, as the input to the system and evaluating the total output of the two system in cascade. We did the detailed calculations of this part in Appendix A and the final results are in chapter 3. The ratio of the amplitude of the second harmonic $e^{2j\omega_0 t}$, to the amplitude of the fundamental frequency, $e^{j\omega_0 t}$, gives the amount of the second-order harmonic distortion. A similar ratio is defined for the third-order and higher-order harmonic distortions. According to the total output of the system which is composed of the sum of the coefficients of all the δ-functions given in chapter 3 , i_{th}-order harmonic distortion is the coefficient of $\delta(\omega - i\omega_0)$ because the coefficient of $\delta(\omega - \omega_0)$, the fundamental frequency, is equal to unity. We calculated all of these ratios and the results showed that the amount of harmonic distortions are negligible when the predistortion is used prior to the laser diode. The corresponding diagrams are in Fig. 6.1. For intermodulation distortion analysis another approach was used. Definition of intermodulation distortion implies the use of an input which consists of two single-frequency tones with frequencies ω_1 and ω_2. Some terms in the output have frequencies that are a combination of ω_1 and ω_2. For example, the frequencies $m\omega_1 + n\omega_2$, for integers m and n. The sum of absolute values of m and n gives us the order of intermodulation. Second-order intermodulation distortion frequency is $\omega_1 \pm \omega_2$ and the third-order corresponds to $\pm\omega_1 \pm 2\omega_2$ and $\pm 2\omega_1 \pm \omega_2$ frequencies. If we want

to determine the amount of second and third-order IMD at the output by applying an input such as $e^{j\omega_1 t} + e^{j\omega_2 t}$ to the system and then evaluating the final output, we must accomplish complicated and tedious computations. Thus, we use another method that in fact is a frequency domain analysis. The frequency spectrum of all the subcarriers can be considered as a flat spectrum with a particular bandwidth, as shown in Fig. 4.1. In this figure, f_h is the highest frequency subcarrier and f_l is the lowest frequency subcarrier. For measuring the amount of intermodulation distortion in the output, the frequency contents of the spectrum is extracted from a very narrow bandwidth or a notch frequency and then the amount of IMD noise is measured in the narrow frequency band. This method is used in practice and is an appropriate method for theoretical analysis, as well. We have described the steps in finding the output of the laser and its inverse system, when the input frequency spectrum is as Fig. 4.1, in Appendix B. In fact we obtained the frequency spectrum of the output when the predistortion module and the laser are connected in tandem. Second-order IMD is reduced by a minimum of 70 dB when predistortion is employed. Reduction of third-order IMD is by about 20 dB. Higher-order IMD products are negligible. So the total IMD is reduced to:

$$10 \log \left[\frac{1}{(IMD)_2} + \frac{1}{(IMD)_3} \right]^{-1} = 20 \quad dB \tag{6.1}$$

Results for harmonic distortion shows that the performance of the two systems, predistortion and laser, in cascade is free of harmonic distortion noise. In other words, since the predistortion inverts laser nonlinear characteristic, the output of the two system in cascade is almost free of harmonic distortion noise and the overall characteristic exhibits minor nonlinearity effects. We mentioned in previous chapters that bias current is an important factor in system performance. With a large bias current, even a small input signal saturates laser output. With a small bias current the probability that the input signal goes below threshold current and zero-level clipping occurs is high. A

bias current at the midpoint of saturation region and threshold current has the optimum performance conditions. We obtain the amount of second-order intermodulation for different bias currents. Results are shown in Fig. 4.6. As shown in this figure, a bias current about the midpoint between the threshold current and the saturation region gives the minimum distortion. The corresponding curves are for optical modulation depths of 0.04 per carrier. If the optical modulation depth is increased, the amount of distortion noise or nonlinearity noise increases at the output. When the modulation index is decreased, there is less distortion noise at the output. We have obtained the amount of second-order intermodulation distortion noise for various optical modulation depths in Fig. 4.4 and 4.5. According to Fig. 4.1, the frequency spectrum of the input signal, when it is composed of a number of equally-spaced subcarriers in the available bandwidth is a flat spectrum. The constant K or the height of the spectrum is determined by the transmitted power. We assume that subcarriers have equal transmitted power so K can be expressed in terms of transmitted power. In this way, $K = N \times$transmitted power in each subcarrier, with N =number of subcarriers. If we denote the peak amplitude of the input current of each subcarrier by I_m, then $\frac{I_m^2}{2}$ is the power of each subcarrier per ohm resistor. Current I_m is proportional to the optical modulation depth. Therefore, K is proportional to m^2. Changes of m yields vertical shifts in the curves for intermodulation distortion, as shown in Fig. 4.4 and 4.5. In practice, the total optical modulation depth which is $m_t = m_i\sqrt{N}$ is in the range of 0.25-0.50 or 25-50 percent [15]. The modulation depth per carrier, m_i, for a system with 75 subcarriers is typically 0.04. Most of our results have been obtained assuming this value of modulation depth.

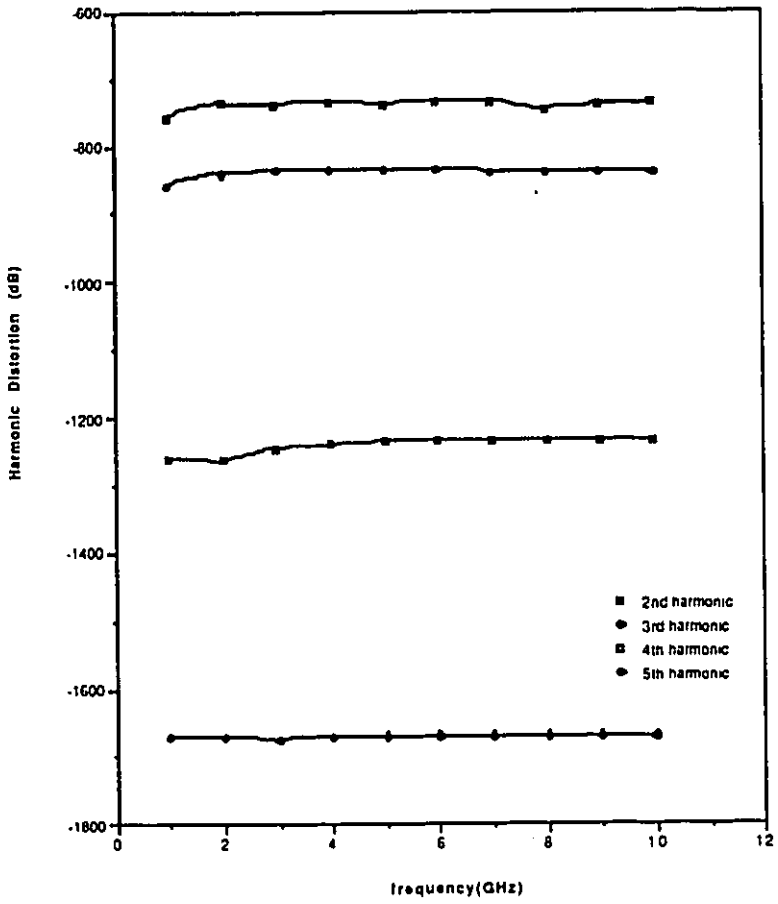

Figure 6.1. Harmonic distortion when predistortion is used.

6.2 CNR calculations:

For transmitting multiple signals over the same channel, a subcarrier modulation technique can be used. The information signals are first modulated onto the RF subcarriers. These carriers are then combined and the resulting electrical signal is used to modulate the optical carrier. A limiting factor in these systems is the noise arising from harmonic and intermodulation distortions. Fig. 6.2 shows the basic elements of an analog link. Optical sources in this figure could be a Light Emitting Diode (LED) or a laser diode. Bias point of the optical sources is usually chosen approximately at the midpoint of the linear region of the input-output characteristic. For this bias point less distortion exists. Baseband signal modulates an electrical subcarrier prior to intensity modulation of the source. In CATV transmission systems a subcarrier can be modulated in formats as Amplitude Modulation with Vestigial Sidebands (AM-VSB), Frequency Modulation (FM), 4-level Quadrature Amplitude Modulation (4-QAM) and High-Definition Television (HDTV), where the latter has different types. Nonlinearities in the optical source include distortions, intermodulation products and relative intensity noise (RIN) in the laser. Primary concern in a receiver is its sensitivity and bandwidth. Major receiver noise sources are quantum noise in the photodiode and thermal amplifier noises in the receiver front-end [15].

Carrier-to-noise Ratio

In performance analysis of analog systems, the ratio of the rms carrier power to rms noise power at the output of the optical receiver is usually calculated and is referred to as carrier-to-noise ratio (CNR):

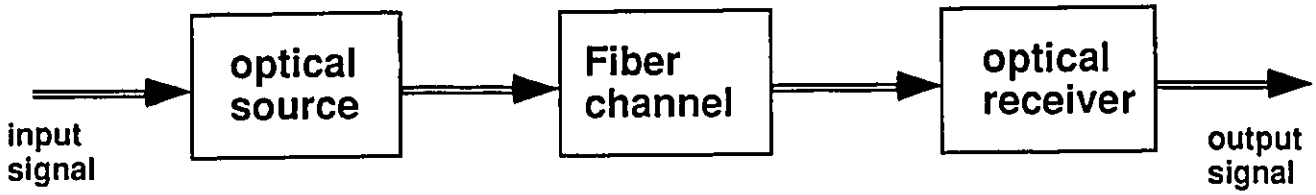

Figure 6.2. Basic elements of an optical link.

$$CNR = \frac{carrier\ \ power}{source\ \ noise\ +\ \ receiver\ \ noise} \tag{6.2}$$

For nonlinear multiplexed carrier systems, intermodulation noise is considered, as well. Carrier power C at the output of the receiver, in units of $(Ampere)^2$, is:

$$C = \frac{1}{2}(mI_o)^2 \tag{6.3}$$

where I_o is the total received photocurrent and m is the optical modulation depth per channel [20]. Noise sources in a fiber optic link that are of concern in carrier-to-noise ratio calculations, consist of shot noise and thermal noise at the receiver and relative intensity noise (RIN) at the transmitter laser. Quantum or shot noise is the result of quantum detection of light and the random processes involved in the conversion of photons to electrons in a photodetector. The mean-squared shot noise; $\bar{I}^2_{sh}$, for an ideal square law detector is expressed by [15]:

$$\bar{I}^2_{sh} = 2eI_dB \tag{6.4}$$

where e is an electron charge, B is the equivalent noise bandwidth and I_d is the photodetected current.

In any electronic receiver system, there is agitations of electrons leading to a Gaussian thermal noise, e.g., noise generated in a pre-amplifier resistor. Thermal noise power is given by:

$$P_{th} = n^2B \tag{6.5}$$

where n is the contribution of the preamplifier to the thermal noise power and is the effective thermal noise current (typically 10 $\frac{pA}{\sqrt{Hz}}$), B is the equivalent thermal noise bandwidth set by the receiver front-end circuits. Relative Intensity Noise consists of noise intrinsic to the laser such as quantum effects in electron-to-photon conversion and extrinsic effects that may be caused by reflections and dispersion. Laser RIN is measured in dB/Hz and is defined by

$$RIN = \frac{< (\Delta P_L)^2 >}{\bar{P}_L^2} \tag{6.6}$$

where $< (\Delta P_L)^2 >$ is the mean-squared intensity fluctuation of the laser output and $\bar{P}_L^2$ is the average laser light intensity. Overall carrier-to-noise ratio (CNR) of the system can be calculated by a different method if we consider the CNR for each of the noise sources separately and then finding the total CNR. In fact in this method the inverse of the corresponding CNRs are added, and the result is the inverse of the total CNR of the system. This is applied by assuming the contributing noise sources are Gaussian in nature, as we can assume so in our case. Therefore, their total contribution can be arrived at on a power addition basis.

Noise considerations:

In an analog transmission link and for different methods of modulation, a carrier-to-noise ratio (CNR) of some specified value is required for the quality of the signal at the receiver to be acceptable. We showed the basic elements of an analog link in Fig. 6.2. In analog applications, first; a bias point on the source characteristic curve is set. The analog signal can then be transmitted using a modulation technique. The simplest form for optical fiber transmission uses intensity modulation. Intensity modulation of optical output of the source is accomplished by varying the current

around the bias point in proportion to the message signal level. Message signal by itself can be a modulated version of the original baseband signal. This is more efficient than the method of sending the baseband signal directly to modulate the optical output of the source [15]. Baseband signal is translated onto an electrical subcarrier prior to intensity modulation of the source. This is done using AM-VSB, FM or any other appropriate modulation technique. Whatever modulation technique used, nonlinearities of the optical source must be considered carefully. These include harmonic distortions, intermodulation products and relative intensity noise (RIN) in the laser. Frequency dependence of the amplitude, phase and group delay in the fiber must be taken into account as well. Thus the fiber must have a flat amplitude and group-delay response within the passband required to send the signal free of nonlinear distortion. In addition, it is better to choose a single-mode fiber because of lack of modal-disperssion. Fiber attenuation is also important because carrier-to-noise performance of the system changes as a function of the received optical power. As was described in the previous sections, mean-squared shot noise or quantum noise of the photodetector is given by:

$$\bar{I}_{sh}^2 = 2eI_oB \tag{6.7}$$

where I_o is the photodetector current, e is the electron charge and B is the noise equivalent bandwidth. So $\bar{I}_{sh}^2$ gives the amount of shot noise power per resistor ohm. Signal power for one channel, per ohm of load resistor at the output is:

$$C = \frac{1}{2}m^2{I_o}^2 \tag{6.8}$$

where I_o is the total received photocurrent and m is the optical modulation depth per channel [20]. So CNR for shot noise is the ratio of the carrier power to the shot noise power:

$$(CNR)_{shot-noise} = \frac{m^2 I_o}{4eB} \tag{6.9}$$

Thermal noise is caused by the preamplifier resistor and its power is given by:

$$(P_n)_{thermal} = n^2 B \tag{6.10}$$

where n is the effective input current noise, typically 10 $pA/\sqrt{Hz}$. Again, B is the noise equivalent bandwidth of the receiver. Carrier-to-noise ratio for thermal noise is expressed as:

$$(CNR)_{thermal} = \frac{{I_o}^2 m^2}{2n^2 B} \tag{6.11}$$

Noise power due to relative intensity noise (RIN) was described before. It can be written as

$$\begin{aligned}(P_n)_{RIN} &= B.RIN.(\mathcal{R}_o P)^2 \\ &= B.RIN.{I_o}^2\end{aligned} \tag{6.12}$$

where RIN is the ratio of the mean-squared intensity fluctuations of the laser output to the average laser light intensity, $\mathcal{R}_o$ is the photodetector responsivity and P is the received optical power. Overall carrier-to-noise ratio for the system is the contribution of all of the above carrier-to-noise ratios [20]:

$$(CNR)_{total} = \frac{(I_o m)^2}{2B[{I_n}^2 + {I_o}^2\{RIN + \frac{2e}{I_o}\}]} \tag{6.13}$$

This expression for CNR can be converted to [26]:

$$\frac{1}{(CNR)_{total}} = \frac{1}{(CNR)_{shot-noise}} + \frac{1}{(CNR)_{R.I.N}} + \frac{1}{(CNR)_{thermal-noise}} \qquad (6.14)$$

Any other carrier-to-noise allocation such as that for clipping or intermodulation distortion can be added to the above expression in the same powerwise manner in order to find the total system carrier-to-noise ratio.

For example, if the ratio of the second order intermodulation distortion to the carrier is; $(CNR)_{IMD2}$, then just the term $\frac{1}{(CNR)_{IMD2}}$ is added to the right hand side in equation (6.14) and similarly for the third order products a term as $\frac{1}{(CNR)_{IMD3}}$ is added to the sum. According to equation (4.19), the second order intermodulation product in frequency domain has a power spectrum equal to:

$$\frac{1}{2!}[(-2l + n\omega^2)^2 + m^2\omega^2] \int_{-\infty}^{+\infty} S_a(\lambda) S_a(\omega - \lambda) d\lambda \qquad (6.15)$$

For each value of ω this integral is computed by numerical methods with enough accuracy. The fundamental frequency power spectrum is the former term:

$$S_a(\omega)|B_1(\omega) + \frac{1}{2}(6r - 2g\omega^2 + 2j\sigma\omega) \int_{-\infty}^{+\infty} S_a(\lambda) d\lambda|^2 \qquad (6.16)$$

In this way, the ratio of second order intermodulation distortion to the carrier or fundamental part is the ratio of the above two terms. So we can substitute this ratio instead of $(CNR)_{IMD2}$ in the expression for carrier-to-noise ratio.

The amount of CNR and whether it meets the required carrier-to-noise ratio or not, determines the number of subcarriers that can be transmitted in a given bandwidth.

Another parameter that determines this number is the optical modulation depth per carrier. A large number of subcarriers is like a large number of small signal inputs that combine and form a large input signal. Since the resultant signal is large, the effects of nonlinearity in laser characteristic are more pronounced than the case for a small signal input. In some cases even zero-level clipping occurs in the optical output because it cannot be negative. If the number of subcarriers is limited because of a small optical modulation depth, the nonlinearity effects are reduced [2].

The effective optical modulation depth for the total signal is:

$$m = \sqrt{\sum_{i=1}^{N} m_i^2} \tag{6.17}$$

where N is the number of subcarriers and m_i is the optical modulation depth per carrier. If we assume that m_i is the same for all carriers, then the effective optical modulation depth is simplified to:

$$m = m_i\sqrt{N} \tag{6.18}$$

The definition of optical modulation depth is the ratio of peak current amplitude to the bias current or in terms of bias current

$$m = \frac{I_{peak} - I_{bias}}{I_{bias} - I_{threshold}} \tag{6.19}$$

If m is large, then $I_{peak} - I_{bias}$ can be larger than $I_{bias} - I_{threshold}$. For values of the current which are less than $I_{threshold}$, according to laser input-output characteristics, there is no optical power at the output, hence, zero-level clipping occurs. Also, if $I_{peak} - I_{bias}$ is larger than $I_{bias} - I_{threshold}$, then zero-level clipping occurs. This has

been shown in Fig. 1.3 and 1.4. So optical modulation depth is an extremely important factor in the system design. In practice, bias current is usually about 1.5-2 times of threshold current. In this way, the modulating current can extend over a larger range. The total optical modulation depth is considered in the range 0.25-0.50 which is a practically achievable range. So if we assume equal modulation indices for all the carriers then:

$$m_i = \frac{m}{\sqrt{N}} \tag{6.20}$$

which gives m_i in the range of 0.03-0.07 for 75 subcarriers (N=75). The standard desired subcarrier number in CATV transmission is N=75. From the expression of optical modulation depth it can be seen that a limit on the number of subcarriers prevents zero-level crossings. When N is not large, m is in the range in which $I_{peak} - I_{bias}$ is less than $I_{bias} - I_{threshold}$ and so zero-level clipping does not occur in the output. This is the maximum limit on the number of subcarriers. Another limit is determined by evaluating the system performance in terms of requirements for CNR and the system noise margin. For any system with a given modulation scheme there is a requirement on the value of CNR at the receiver input. Different noise sources determine the total system noise level as explained at the beginning of this section. Nonlinear distortion can approximately be taken into account in the CNR evaluations by treating it as a noise-like phenomenon. For large values of number of subcarriers, noise level is more than that which has been assumed for the system and so CNR will not meet the basic requirement for the analog link. On the other hand, reduction of noise level allows more margin for CNR. In a case where CNR is more than the required CNR, the difference can be traded with an increamental increase in the number of subcarriers.

In CATV systems that use subcarrier multiplexing, different modulation schemes are

being considered for transmission of video signals. These schemes are AM-VSB, FM, 4-level QAM and various HDTV formats. For each scheme, there are some parameters to be considered in system design. These are the utilized bandwidth, the spacing between the adjacent channels, noise equivalent bandwidth, required carrier-to-noise ratio and transmission system design margin. The quality of the signal at the receiver determines the optimum value for these parameters. The transmitted power, fiber loss and received power at the photodetector are used to evaluate the signal quality at the receiver.

In any analog communication system, the quality of the received signal is highly dependent on the signal-to-noise ratio at the receiver. Carrier-to-noise ratio at the receiver input and the type of modulation set the signal-to-noise ratio (SNR) at the demodulator output. For example, in FM systems the CNR at the input to the subcarrier FM demodulator is [21]:

$$CNR = \frac{R^2 {A_c}^2/2}{2B_m N_o} \tag{6.21}$$

Here, R is the responsivity of the photoreceiver given in $A^2/Watt$, A_c is the amplitude of the carrier, B_m is the bandwidth and N_o is the electronic amplifier noise figure. The SNR at the subcarrier demodulator output is [21]:

$$SNR = 6\beta^2(\beta^2+1)\frac{P_a R^2 {A_c}^2/2}{2B_m N_o} \tag{6.22}$$

where in eq.(6.22) P_a is the normalized power of the message signal so that $P_a \leq 1$ and β is the frequency deviation ratio defined by:

$$\beta = \frac{peak\ \ frequency\ \ deviation}{highest\ \ frequency\ \ component\ \ in\ \ the\ \ message\ \ signal} = \frac{f_d}{W} \tag{6.23}$$

So the relation between CNR and SNR is:

$$SNR = 6\beta^2[\beta^2 + 1]P_a.CNR \tag{6.24}$$

If we assume the highest value for P_a (which is $P_a = 1$), then the expression is simplified to:

$$SNR = 6\beta^2[\beta^2 + 1].CNR \tag{6.25}$$

Therefore, in FM systems signal-to-noise ratio is enhanced by $6\beta^2[\beta^2 + 1]$ since β in FM modulation is chosen to be greater than 1. This relation has been experimentally verified with 60 frequency-modulated (FM) video channels multiplexed and transmitted over 18 kilometers of single-mode fiber [22].

The SNR is proportional to CNR and so is the received signal quality, for signals as AM-VSB, 4-level QAM and HDTV. In link designs for subcarrier multiplexed systems there are some factors that must be considered before proceeding with other design steps.

First the transmission bandwidth must be considered. Overall system bandwidth depends on the fiber, photodetector and transmitter laser. One of the parameters affecting the laser bandwidth is its bias current. In fact, the modulation response is dependent on the intrinsic laser parameters, such as ϵ, β, Γ, and g. Bias current determines the steady-state condition of electron and photon densities, N_o and S_o. So bias current affects the laser transfer characteristics. Transfer function is a term in linear systems theory. Laser is a nonlinear system. However, for evaluation of its bandwidth, first the laser rate equations are linearized. Then linear system theory can be used to calculate an approximate laser modulation bandwidth. Linearization is done about a bias point.

Bias point of a laser is found by replacing the derivative terms in rate equations by zero. This is the condition for steady-state operation. Recalling the original rate equations:

$$\frac{dN}{dt} = \frac{I_o}{V} - \frac{N}{\tau_s} - g(N - N_o)(1 - \epsilon S)S \qquad (6.26.a)$$

$$\frac{dS}{dt} = \Gamma g(N - N_o)(1 - \epsilon S)S - \frac{S}{\tau_{ph}} + \Gamma\beta\frac{N}{\tau_s} \qquad (6.26.b)$$

Assume the variations around the bias point are small. So carrier density, photon density and input current can be expressed as:

$$N = N_b + n$$

$$S = S_b + s$$

$$I_o = I_b + i$$

where N_b, S_b and I_b correspond to the laser bias point. Substitution of the above expressions in rate equations gives a linearized form of these equations around the bias point:

$$\frac{dn}{dt} = [-g_o(1 - \epsilon S_b)S_b - \frac{1}{\tau_n}]n$$
$$-g_o(N_b - N_o)(1 - 2\epsilon S_b)s + \frac{i}{V} \qquad (6.27.a)$$

$$\frac{ds}{dt} = [\Gamma g_o(1 - \epsilon S_b)S_b + \Gamma\beta\frac{1}{\tau_n}]n$$
$$+[\Gamma g_o(N_b - N_o)(1 - 2\epsilon S_b) - \frac{1}{\tau_p}]s \qquad (6.27.b)$$

Fourier transform of these equations gives the transfer function of the laser. If we refer to the transfer function as the ratio of the output photon density to the input laser bias current then:

$$\frac{S(\omega)}{\mathcal{I}(\omega)} = \frac{\Gamma g_o(1-\epsilon S_b)S_b + \Gamma\beta\frac{1}{\tau_n}}{V'} \cdot \frac{1}{-\omega^2 + \alpha\beta - \Gamma\theta + j\omega(-\alpha-\beta)} \tag{6.28}$$

where

$$\alpha = -g_o(1-\epsilon S_b)S_b - \frac{1}{\tau_n}$$

$$\beta = \Gamma g_o(N_b - N_o)(1-2\epsilon S_b) - \frac{1}{\tau_p}$$

$$\Gamma = -g_o(N_b - N_o)(1-2\epsilon S_b)$$

$$\theta = \Gamma g_o(1-\epsilon S_b)S_b + \Gamma\beta\frac{1}{\tau_n}$$

Since the expression in the denominator is a second order expression of ω, same method of analysis that is used for second order linear systems can be used here. The response is dependent on the coefficients α, β, γ and θ which are expressions of laser intrinsic parameters. So bandwidth of the laser is determined by these parameters. For example, for an Ortel SL-620 laser with a gain compression factor of $\epsilon = 2.6 \times 10^{-23}$, the laser modulation band is 6 GHz. It should be noted that the laser bandwidth affects both the R.I.N and nonlinear distortions.

Another important parameter is the optical modulation index that must be determined. For different levels of optical modulation index there are different levels of input

signal resulting in different levels of nonlinear distortions, clipping distortions, thermal and shot noise. Therefore, the total CNR depends on the optical modulation index. Simulations of subcarrier multiplexing systems have shown that the CNR variations versus optical modulation index peaks for some value of optical modulation depth and for other values is less than the peak [23]. For each system, with a specified modulation format, there is a requirement on the CNR to be met by the system designer in order to receive signals with the desired quality. The required CNR has been obtained by considering the transmitted power, various system losses such as coupling loss due to fibers, receiver photodetector responsivity and the system noise margin. For example, for an AM-VSB system the utilized bandwidth for transmission is 50-500 MHz. The noise equivalent bandwidth according to [24] is 4 MHz. With a channel spacing of 6 MHz, 75 subcarriers are accomodated in the specified bandwidth. The required CNR is 40 dB and the system margin is 12 dB. Similar parameters are defined for other systems with modulation schemes such as FM, 4-level QAM and HDTV.

For each system there is a dominant noise term, playing a major role in setting the total noise level. The dominant noise is not necessarily the nonlinear distortion noise. For systems that nonlinear distortion dominates, use of predistortion shows an enhancement in the per carrier total CNR. To be compatible with the present NTSC/TV transmission standard, assume it is desired to have an AM-VSB system. For 75 subcarriers, the per carrier required CNR is 40 dB which is not met according to our evaluations, as shown in Table 6.1. For the AM-VSB system, the dominant noise is caused by zero-level clipping, hence predistortion does not affect the total CNR. Reducing the number of subcarriers to 20 causes a decrease in the nonlinear distortion noise level and hence the required CNR is met. This can be observed in Table 6.2. For an FM modulation scheme, as shown in Table 6.3, with an optical modulation depth of 0.02, before the use of predistortion, CNR value is less than the requirement. With predistortion, a higher

level of CNR that is even more than the system requirement is achievable. Therefore, predistortion enables us to use a FM modulation scheme with a modulation depth 0.02 with 75 subcarriers. We have considered the effect of predistortion block for other cases as 4-level QAM and HDTV (Zenith). The results are shown in Tables 6.4 and 6.5.

Modulation Scheme	OMD m	per carrier required CNR (dB)	achievable CNR without predistortion (dB)	achievable CNR with predistortion (dB)
AM-VSB	0.02	40	30	31.72
	0.04	40	35.68	37.687
	0.06	40	30	34
	0.08	40	20	22.96

OMD=Optical Modulation Depth

Number of accommodated subcarriers within the available bandwidth=75

Table 6.1: CNR results for AM-VSB modulation scheme.

Carrier-to-noise ratios with no predistortion have been obtained by the following computer simulation [23]:

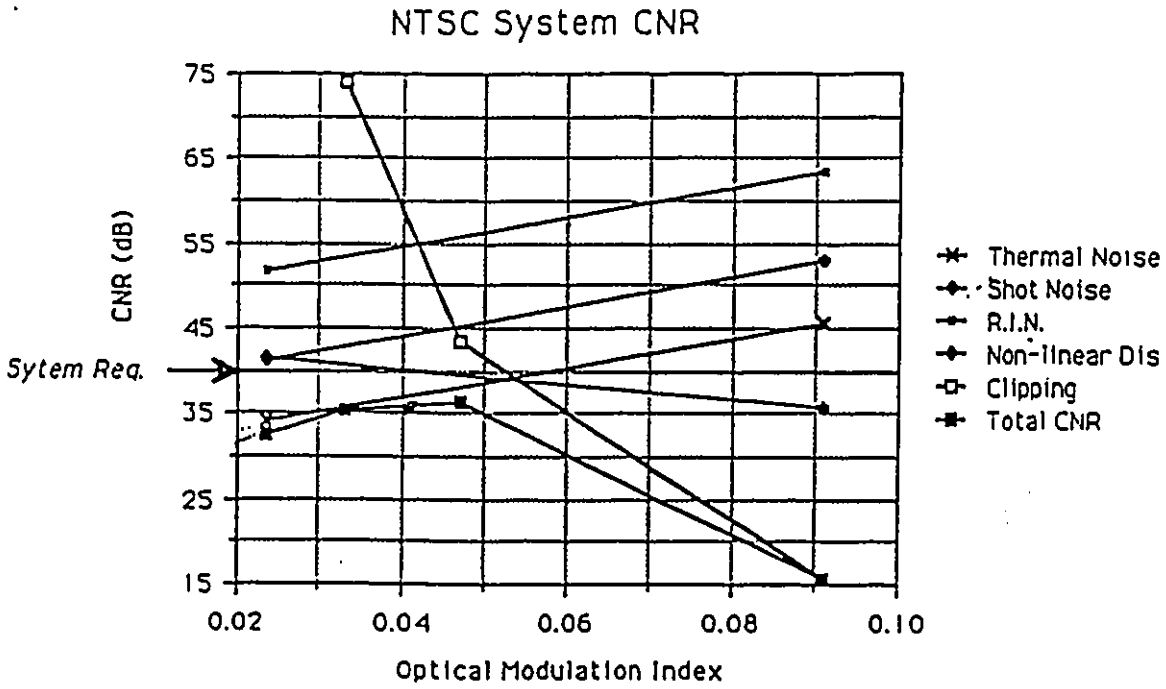

Modulation Scheme	OMD m	per carrier required CNR(dB)	achievable CNR without predistortion (dB)	achievable CNR with predistortion (dB)
AM-VSB**	0.04	40	36.9	37.72
	0.06	40	39	41.12 *
	0.08	40	40.16	43.74

* CNR requirement is met by using the predistortion block prior to the laser.

OMD=Optical Modulation Depth

**Number of accommodated subcarriers within the available bandwidth=20

Table 6.2: CNR results for AM-VSB modulation scheme.

Carrier-to-noise ratios with no predistortion have been obtained by the following computer simulation [23]:

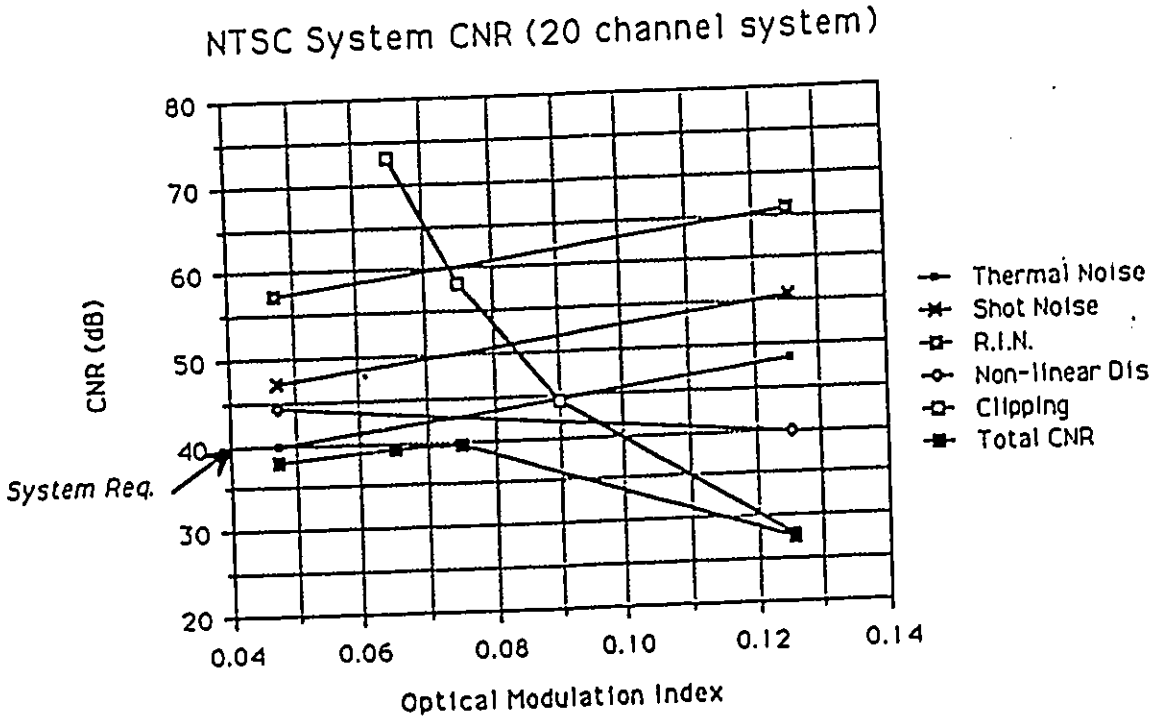

Modulation Scheme	OMD m	per carrier required CNR (dB)	achievable CNR without predistortion (dB)	achievable CNR with predistortion (dB)
FM	0.01	16.5	12	12.6
	0.02	16.5	11.75	18 *
	0.03	16.5	7.7	19.49 *

* CNR requirement is met by using the predistortion block prior to the laser.

OMD=Optical Modulation Depth

Number of accommodated subcarriers within the available bandwidth=75

Table 6.3: CNR results for FM modulation scheme.

Carrier-to-noise ratios with no predistortion have been obtained by the following computer simulation [23]:

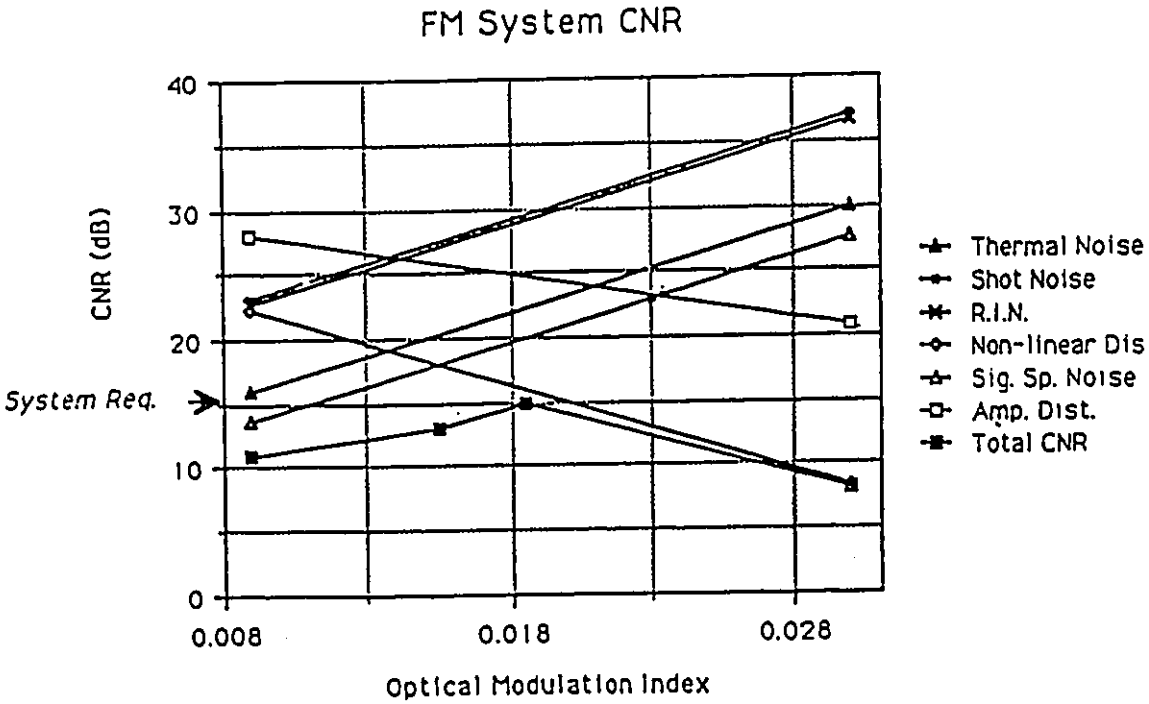

Modulation Scheme	OMD m	per carrier required CNR (dB)	achievable CNR without predistortion (dB)	achievable CNR with predistortion (dB)
4-level QAM	0.02	15.6	12.1	12.42
	0.04	15.6	15.98	16.87
	0.06	15.6	15	18.3 *
	0.08	15.6	15.2	16.5 *

* CNR requirement is met by using the predistortion block prior to the laser.

OMD=Optical Modulation Depth

Number of accommodated subcarriers within the available bandwidth=75

Table 6.4: CNR results for 4-level QAM modulation scheme.

Carrier-to-noise ratios with no predistortion have been obtained by the following computer simulation [23]:

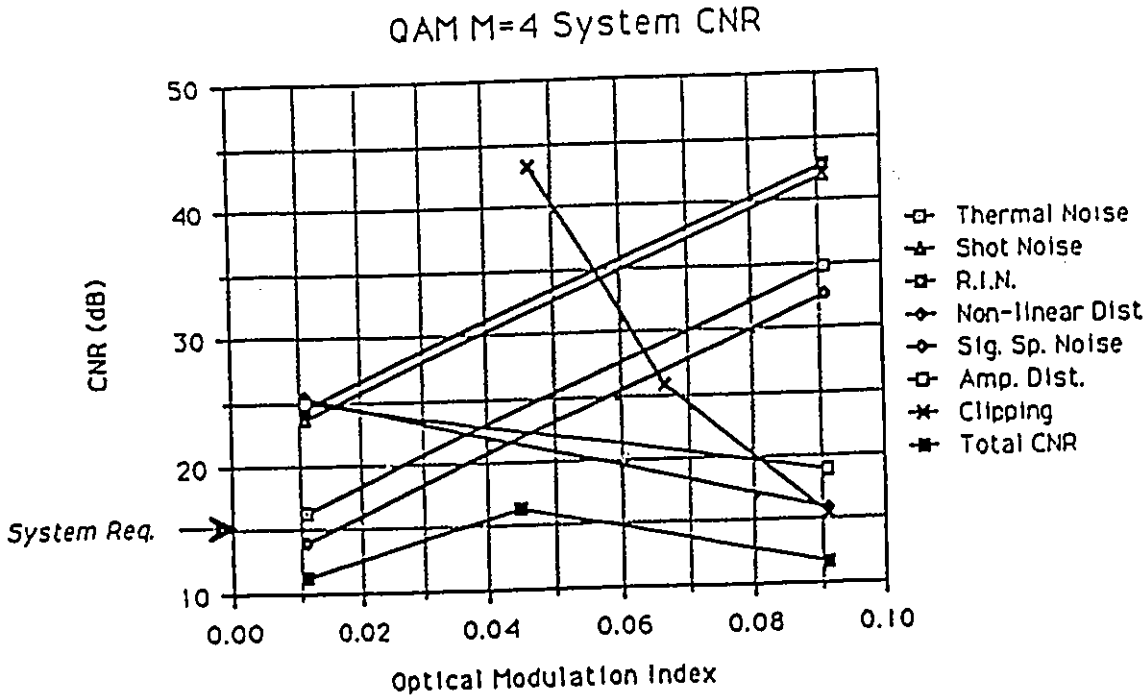

Modulation Scheme	OMD m	per carrier required CNR (dB)	achievable CNR without predistortion (dB)	achievable CNR with predistortion (dB)
HDTV	0.02	18	12.4	12.47
	0.04	18	17.8	18.48 *
	0.06	18	17	21.657 *
	0.08	18	17.6	18.68 *

* CNR requirement is met by using the predistortion block prior to the laser.

OMD=Optical Modulation Depth

Number of accommodated subcarriers within the available bandwidth=75

Table 6.5: CNR results for HDTV (Zenith) modulation scheme.

Carrier-to-noise ratios with no predistortion have been obtained by the following computer simulation [23]:

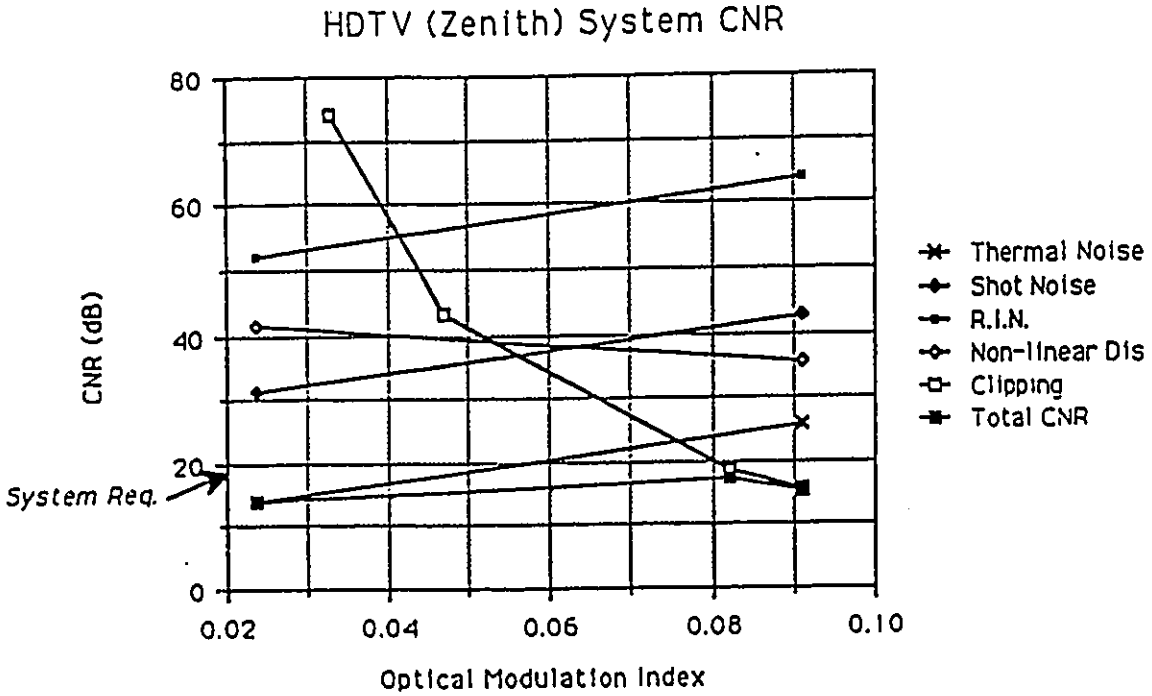

Chapter 7
Conclusions

Subcarrier multiplexing is an efficient use of the available fiber bandwidth in video transmission. Video signals modulate equally-spaced subcarriers. Sum of the subcarriers is applied as an input to the transmission system. The transmission system includes a semiconductor laser. Laser diodes exhibit a nonlinear characteristic which degrades the system performance in terms of the carrier-to-noise ratio and capacity. We proposed a technique for compensating the nonlinearity in a laser characteristic by using a predistortion block prior to the laser diode. The characteristic of this block inverts that of the laser, so the overall system causes a significantly lower nonlinear noise level. We evaluated the performance of the linearized system by harmonic distortion and intermodulation distortion analyses. The corresponding results were presented in chapter 4. As seen from the curves of IMD versus bias current, there is an optimum bias current for which the amount of the IMD noise is lower than for other cases. This point is at the midpoint between the threshold current and the saturation region of the source laser. Dependence of nonlinear noise on the optical modulation depth is another aspect. Larger modulation depths cause more nonlinear noise. The modulation depth for operation of the system is determined by the number of channels and the power budget. We considered optical modulation depths of 0.04 per carrier for 75 subcarriers systems which deliver an efficient optical modulation depth of about 0.32 for the total modulating current. We suggest a method for realization of the predistortion system in chapter 5.

The proposed model is based on the expansion of nonlinear terms around a bias point. Therefore, the model is dependent on the operating condition of the laser. Effects

of leakage currents and effects outside the active region have not been considered [32]. Harmonic distortion is eliminated at the output and intermodulation distortions levels are decreased, significantly. We used the system with the predistortion block with different modulation schemes as AM-VSB, FM, 4-level QAM and HDTV (Zenith). Cancellation of nonlinear distortion greatly enhances the system performance for cases where nonlinear noise is dominant or considerable compared to other sources of noise in the system. For example, for an FM system, as shown in Table 4.3, the CNR of the system improves when predistortion is used. Here the nonlinear distortion level is comparable to other noise levels of the system. In the case of amplitude modulated signals and 4-level QAM signals which contains envelope zero-crossings corresponding to 180 degrees phase jumps of the modulated carrier, clipping noise dominates. This noise is not reduced by the predistorter, hence, the predistortion does not greatly improve the overall system performance for signals with temporal variations in the modulation envelope. Therefore, predistortion works efficiently for FM type signals. For future research, clipping is a very important problem and methods that can deal with clipping must be found. In evaluating the system performance, the noise sources are considered to be independent from each other, as they are. This assumption enables us to obtain the total noise power of the system by adding the power of each noise source. This assumption is valid as long as noise sources are considered independent Gaussian sources which approximately are in our case. However, for clipping noise some other asymptotic distribution have been found [28]. We have assumed direct intensity modulation of the laser. For cases that the system requirements are not met, other alternative methods may result in an acceptable performance. For direct intensity modulation, linearization of the laser diode characteristic results in reduction of nonlinear noise level and hence, an increase in the carrier-to-noise ratio.

References

1. M. Kavehrad and E. Savov,"Fiber-optic transmission of microwave 64-QAM signals", IEEE J. on Selected Areas in Commun., Vol. 8 , No. 7, pp. 1320-1326, Sept. 1990.

2. A. A. M. Saleh,"Fundamental limit on number of channels in subcarrier-multiplexed lightwave CATV system", Electronics Lett., Vol. 25, No. 12, pp. 776-777, June 1989.

3. A. Czylwik,"Nonlinear system modelling of semiconductor lasers based on Volterra series", J. of Optical Commun., No. 3, pp. 104-114, July 1986.

4. T. K. Biswas and W. F. McGee,"Analytical predictions of the intermodulation noise of semiconductor laser diode", Canadian Conference on Electrical and Computer Engineering, Ottawa, Sept. 1990.

5. K. Y. Lau and A. Yariv,"Intermodulation distortion in a directly modulated semiconductor injection laser", Appl. Phys., Lett. 45, No. 10, pp. 1034-1036, Nov. 1984.

6. T. E. Darcie, R. S. Tucker and G. J. Sullivan,"Intermodulation and harmonic distortion in InGaAsP lasers", Electronics Lett., Vol. 21, No. 16, pp. 665-666, Aug. 1986.

7. W. I. Way,"Large signal nonlinear distortion prediction for a single-mode laser diode under microwave intensity modulation", J. of Lightwave Technol., Vol. LT-5, No. 3, March 1987.

8. R. S. Tucker and I. P. Kaminow,"High-frequency characteristics of directly mod-

ulated in GaAsP ridge waveguide and buried heterostructure lasers", J. Lightwave Technol., Vol. LT-2, pp.385-393, Aug. 1984.

9. R. S. Tucker,"Large-signal circuit model for simulation of injection laser modulation dynamics", Proc. of IEEE, Vol. 128, pt-I, pp. 180-184, Oct. 1981.

10. M. S. Lin, S. J. Wang and N. K. Dutta,"Frequency dependence of the harmonic distortion in InGaAsP distributed feedback lasers", Proc. of OFC., 1990.

11. K. Stubkjaer and M. Danielson,"Nonlinearities of GaAlAs lasers-Harmonic distortion" IEEE J. of Quantum Electronics, Vol. QE-16, No. 5, May 1980.

12. R. B. Childs, T. A. Tatlock and V. A. O'Byrne,"AM-Video distribution system with 64-way passive optical splitting", IEEE Photonics Technol. Lett., Vol. 4, No. 1, pp. 86-88, Jan. 1992.

13. R. M. Ridder and K. Korotky,"Feedforward compensation of integrated optic modulator distortion", Proc. of OFC., 1990.

14. W. I. Way,"Frequency-dependent and frequency-independent nonlinear characteristics of a high-speed laser diode", IEEE MTT-S Digest, pp. 991-994, 1988.

15. G. Keiser, *Optical fiber communications*, New York: McGraw-Hill Inc. 1983.

16. H. Kressel and J. K. Bulter, *Semiconductor lasers and heterojunction LED's*, New York: Academic Press, 1977.

17. R. S. Tucker, D. J. Pope,"Circuit modelling of the effect of diffusion on damping in a narrow-stripe semiconductor laser", IEEE J. Quantum Electron., Vol. QE-19, No. 7, pp. 1179-1183, July 1983.

18. M. Schetzen, *The Volterra and Wiener theories of nonlinear systems*, New York: Wiley, 1980.

19. E. Bedrosian and S. O. Rice,"The output properties of Volterra systems (nonlinear systems with memory) driven by harmonic and gaussian inputs", Proc. of IEEE, Vol. 59, No. 12, Dec. 1971.

20. T. E. Darcie and G. E. Bodeep,"Lightwave multichannel analog AM video distribution systems", Proc. of ICC. 1989, pp. 32.4.1-32.4.4.

21. J. M. Senior, *Optical fiber communications*, London: Prentice-Hall International, Inc. 1985.

22. R. Olshansky and V. A. Lanzisera,"60-channel FM video subcarrier multiplexed optical communication system", Electronics Letters, Vol. 23, No. 22, pp. 1196-1197, October 1987.

23. P. Neusy and W. McGee,"Effects of laser nonlinearities on TV distribution using subcarrier multiplexing", Canadian Conference on Electrical and Computer Engineering, Montreal, PQ, Sept. 1989, pp. 883-836.

24. T. E. Darcie, M. E. Dixon, B. L. Kasper and C. A. Burrus,"Lightwave system using microwave subcarrier multiplexing", Electron. Lett., Vol. 22, pp. 774-775, 1986.

25. T. E. Darcie, J. Lipson, C. B. Roxlo and C. J. Mcgrath,"Fiber optic device technology for broadband analog video systems", IEEE LCS magazine, No. 2, pp. 46-52, Feb. 1990.

26. R. Olshansky,"Optimal design of subcarrier multiplexed lightwave systems employing linearized external modulators", J. of Lightwave Tech., Vol. 10, No. 3, March 1992.

27. T. E. Darcie,"Subcarrier multiplexing for multiple-access lightwave networks", J. of lightwave Technol., Vol. LT-5, No. 8, pp. 1103-1110, Aug. 1987.

28. J. E. Mazo,"Asymptotic distortion spectrum of clipped, dc-biased, Gaussian noise", IEEE Trans. on Commun., Vol. 40, No. 8, Aug. 1992.

29. J. C. Fuenzalida, O. Shimbo and W. L. Cook,"Time-domain analysis of intermodulation effects caused by nonlinear amplifiers", COMSAT Technical Rev., Vol. 3, No. 1, pp. 89-141, Spring 1973.

30. A. Takemoto, H. Watanabe, Y. Nakajima, Y. Sakakibara, S. Kakimoto, H. Namazaki,"Low harmonic distortion distributed feedback laser diode and module for CATV systems", Proc. of OFC., 1990.

31. S. Benedetto, E. Biglieri, R. Daffara,"Modelling and performance evaluation of nonlinear satellite links-A Volterra series approach", IEEE Trans. on Aerospace and Electronic systems, Vol. AES-15, No. 4, pp. 494-506, July 1979.

32. R. Olshansky, et.al.,"Subcarrier Multiplexed Lightwave System for Broadband Distribution", J. Lightwave Tech., Vol. LT-7, No. 9, pp. 1329-1342, Sept. 1989.

Appendix A

Response to a tone

In this appendix we derive the output of the semiconductor laser. We demonstrate this calculation for an input tone. The output of a p^{th}-order Volterra system in frequency domain is:

$$Y_p(\omega) = \frac{1}{(2\pi)^{p-1}} \int_{-\infty}^{+\infty} \int_{-\infty}^{+\infty} ... \int_{-\infty}^{+\infty} H_p(\omega - \omega_1 - \omega_2 - ...\omega_p, \omega_1, \omega_2, ..., \omega_p)$$

$$A(\omega - \omega_1 - \omega_2 - ... - \omega_p)A(\omega_1)A(\omega_2)...A(\omega_p)d\omega_1 d\omega_2 ... d\omega_p \qquad (A.1)$$

If we consider a system that is modelled with three Volterra systems: first-order, second-order and third-order Volterra system then the output of such a system is the sum of the output of each Volterra operator. In the frequency domain this can be expressed in the following form:

$$Y(\omega) = H_1(\omega)X(\omega) + \frac{1}{2\pi} \int_{-\infty}^{+\infty} H_2(\omega - \omega_1, \omega_1)x(\omega - \omega_1)x(\omega_1)d\omega_1$$

$$+\frac{1}{(2\pi)^2} \int_{-\infty}^{+\infty} H_3(\omega - \omega_1 - \omega_2, \omega_1, \omega_2)i(\omega - \omega_1 - \omega_2)i(\omega_1)i(\omega_2)d\omega_1 d\omega_2 \qquad (A.2)$$

Suppose that a single-frequency tone is applied to the predistortion block prior to laser. We denoted the kernels Fourier transforms of this block by B_i. Since we have used up to the third-order kernel, the frequency domain description of the output in case of applying a single-frequency tone; $e^{j\omega t}$, is:

$$y(\omega) = B_1(\omega)\delta(\omega-\omega_0) + \frac{1}{(2\pi)}\int_{-\infty}^{+\infty} B_2(\omega-\omega_1,\omega_1)\delta(\omega-\omega_1-\omega_0)\delta(\omega_1-\omega_0)d\omega_1$$

$$+\frac{1}{(2\pi)^2}\int_{-\infty}^{+\infty}\int_{-\infty}^{+\infty} B_3(\omega-\omega_1-\omega_2,\omega_1,\omega_2)\delta(\omega-\omega_1-\omega_2-\omega_0)\delta(\omega_1-\omega_0)\delta(\omega_2-\omega_0)d\omega_1 d\omega_2 \tag{A.3}$$

which becomes:

$$y(\omega) = B_1(\omega_0)\delta(\omega-\omega_0) + \frac{1}{2\pi}B_2(\omega_0,\omega_0)\delta(\omega-2\omega_0)$$

$$+\frac{1}{(2\pi)^2}B_3(\omega_0,\omega_0,\omega_0)\delta(\omega-3\omega_0) \tag{A.4}$$

Now, $y(\omega)$ is considered as the frequency-domain description of the input to the laser, which is again modelled by three Volterra operators. We denote the kernel Fourier transform of the laser by F_i. The output of the laser with $y(\omega)$ as an input is:

$$Z(\omega) = F_1(\omega)y(\omega) + \frac{1}{2\pi}\int_{-\infty}^{+\infty} F_2(\omega-\omega_1,\omega_1)y(\omega-\omega_1)y(\omega_1)d\omega_1$$

$$+\frac{1}{(2\pi)^2}\int_{-\infty}^{+\infty}\int_{-\infty}^{+\infty} F_3(\omega-\omega_1-\omega_2,\omega_1,\omega_2)y(\omega-\omega_1-\omega_2)y(\omega_1)y(\omega_2)d\omega_1 d\omega_2 \tag{A.5}$$

We denote the output of each Volterra operator separately and assume that the total output is the sum of the output of each operator. So each term in eq.(A.5) is calculated, separately.

$$Z(\omega) = Z_1(\omega) + Z_2(\omega) + Z_3(\omega) \tag{A.6}$$

where

$$Z_1(\omega) = F_1(\omega)y(\omega) \tag{A.7}$$

$$Z_2(\omega) = \frac{1}{2\pi}\int_{-\infty}^{+\infty} F_2(\omega-\omega_1,\omega_1)y(\omega-\omega_1)y(\omega_1)d\omega_1 \tag{A.8}$$

$$Z_3(\omega) = \frac{1}{(2\pi)^2}\int_{-\infty}^{+\infty}\int_{-\infty}^{+\infty} F_3(\omega-\omega_1-\omega_2,\omega_1,\omega_2)y(\omega-\omega_1-\omega_2)y(\omega_1)y(\omega_2)d\omega_1 d\omega_2 \tag{A.9}$$

Now, we substitute eq. (A.4) in the above expressions for each output:

$$Z_1(\omega) = F_1(\omega)\left[B_1(\omega_0)\delta(\omega-\omega_0) + \frac{1}{2\pi}B_2(\omega_0,\omega_0)\delta(\omega-2\omega_0) + \frac{1}{(2\pi)^2}B_3(\omega_0,\omega_0,\omega_0)\delta(\omega-3\omega_0)\right]$$

$$= F_1(\omega_0)B_1(\omega_0)\delta(\omega-\omega_0) + \frac{1}{2\pi}F_1(2\omega_0)B_2(\omega_0,\omega_0)\delta(\omega-2\omega_0) + \frac{1}{(2\pi)^2}F_1(3\omega_0)B_3(\omega_0,\omega_0,\omega_0)\delta(\omega-3\omega_0)$$

$$Z_2(\omega) = \frac{1}{2\pi}\int_{-\infty}^{+\infty} F_2(\omega-\omega_1,\omega_1)\left[B_1(\omega_0)\delta(\omega-\omega_1-\omega_0) + \frac{1}{2\pi}B_2(\omega_0,\omega_0)\delta(\omega-\omega_1-2\omega_0) + \frac{1}{(2\pi)^2}B_3(\omega_0,\omega_0,\omega_0)\delta(\omega-\omega_1-3\omega_0)\right]\times$$

$$\times\left[B_1(\omega_0)\delta(\omega_1-\omega_0) + \frac{1}{2\pi}B_2(\omega_0,\omega_0)\delta(\omega_1-2\omega_0) + \frac{1}{2\pi^2}B_3(\omega_0,\omega_o,\omega_0)\delta(\omega_1-3\omega_0)\right]$$

$$= \frac{1}{2\pi}F_2(\omega_0,\omega_0)B_1(\omega_0)^2\delta(\omega-2\omega_0) + \frac{1}{(2\pi)^2}F_2(2\omega_0,\omega_0)B_2(\omega_0,\omega_0)B_1(\omega_0)\delta(\omega-3\omega_0) + \frac{1}{(2\pi)^3}F_2(3\omega_0,\omega_0)B_3(\omega_0,\omega_0,\omega_0)B_1(\omega_0)\delta(\omega-4\omega_0) + \frac{1}{(2\pi)^2}F_2(\omega_0,2\omega_0)B_1(\omega_0)B_2(\omega_0,\omega_0)\delta(\omega-3\omega_0) + \frac{1}{(2\pi)^3}F_2(2\omega_0,2\omega_0)B_2(\omega_0,\omega_0)B_2(\omega_0,\omega_0)\delta(\omega-4\omega_0) + \frac{1}{(2\pi)^4}F_2(3\omega_0,2\omega_0)B_3(\omega_0,\omega_0,\omega_0)B_2(\omega_0,\omega_0)\delta(\omega-5\omega_0)$$

$$+\frac{1}{(2\pi)^3}F_2(\omega_0,3\omega_0)B_1(\omega_0)B_3(\omega_0,\omega_0,\omega_0)\delta(\omega-4\omega_0)$$

$$+\frac{1}{(2\pi)^4}F_2(2\omega_0,3\omega_0)B_2(\omega_0,\omega_0)B_3(\omega_0,\omega_0,\omega_0)\delta(\omega-5\omega_0)$$

$$+\frac{1}{(2\pi)^5}F_2(3\omega_0,3\omega_0){B_3}^2(\omega_0,\omega_0,\omega_0)\delta(\omega-6\omega_0)$$

The same method is used for $Z_3(\omega)$.

$$Z_3(\omega)=\frac{1}{(2\pi)^2}\int_{-\infty}^{+\infty}\int_{-\infty}^{+\infty}F_3(\omega-\omega_1-\omega_2,\omega_1,\omega_2)\Big[B_1(\omega_0)\delta(\omega-\omega_1-\omega_2-\omega_0)$$

$$+\frac{1}{2\pi}B_2(\omega_0,\omega_0)\delta(\omega-\omega_1-\omega_2-2\omega_0)+\frac{1}{(2\pi)^2}B_3(\omega_0,\omega_0,\omega_0)\delta(\omega-\omega_1-\omega_2-3\omega_0)\Big]$$

$$.\Big[B_1(\omega_0)\delta(\omega_1-\omega_0)+\frac{1}{2\pi}B_2(\omega_0,\omega_0)\delta(\omega_1-2\omega_0)+\frac{1}{(2\pi)^2}B_3(\omega_0,\omega_0,\omega_0)\delta(\omega_1-3\omega_0)\Big]$$

$$.\Big[B_1(\omega_0)\delta(\omega_2-\omega_0)+\frac{1}{2\pi}B_2(\omega_0,\omega_0)\delta(\omega_2-2\omega_0)+\frac{1}{(2\pi)^2}B_3(\omega_0,\omega_0,\omega_0)\delta(\omega_2-3\omega_0)\Big]d\omega_1 d\omega_2$$

Computation of this double integral yields the coefficients of δ-functions in multiples of $3\omega_0, 4\omega_0, ..., 9\omega_0$. The final result is obtained in a similar manner as for $Z_2(\omega)$ except there are three δ-functions multiplied in each term. These results have been used in chapter 3.

Appendix B

Frequency spectrum of the output

Frequency spectrum of any signal is the Fourier transform of its autocorrelation function. The autocorrelation of the output signal of a system which is represented by Volterra kernels of first, second and the third order is derived directly by finding the mean of $y(t).y(t-\tau)$. In our case, first the output frequency spectrum of the predistortion block is computed and then it is considered as the input frequency spectrum of the laser. If we denote the input frequency spectrum of the predistortion by $S_a(\omega)$, then output frequency spectrum is:

$$S_y(\omega) = < a(t)^2 > \delta(\omega) + S_a(\omega)\left|B_1(\omega) + \frac{1}{2}\int_{-\infty}^{+\infty} S_a(\lambda)B_3(\omega,\lambda,-\lambda)d\lambda\right|^2$$
$$+\frac{1}{2!}\int_{-\infty}^{+\infty} S_a(\lambda)S_a(\omega-\lambda)|B_2(\lambda,\omega-\lambda)|^2 d\lambda$$
$$+\frac{1}{3!}\int_{-\infty}^{+\infty}\int_{-\infty}^{+\infty} S_a(\lambda)S_a(\gamma)S_a(\omega-\lambda-\gamma)|B_3(\lambda,\gamma,\omega-\lambda-\gamma)|^2 d\lambda d\gamma \qquad (B.1)$$

Now, we substitute $B_2(\omega)$ and $B_3(\omega)$ in eq. (B.1) their equivalent expressions in terms of ω:

$$S_y(\omega) =< a(t)^2 > \delta(\omega) + S_a(\omega)\left|B_1(\omega) + \frac{1}{2}\int_{-\infty}^{+\infty} S_a(\lambda)(6r - 2g\omega^2 + 2j\sigma\omega)d\lambda\right|^2$$
$$+\frac{1}{2!}\int_{-\infty}^{+\infty} S_a(\lambda)S_a(\omega-\lambda)|(-2l + jn\omega + n\omega^2)|^2 d\lambda$$
$$+\frac{1}{3!}\int_{-\infty}^{+\infty}\int_{-\infty}^{+\infty} S_a(\lambda)S_a(\gamma)|(6r + 2j\sigma\omega - 2g\omega^2)|^2 d\lambda d\gamma \qquad (B.2)$$

$$S_y(\omega) =< a(t)^2 > \delta(\omega) + S_a(\omega)\left|B_1(\omega) + \frac{1}{2}(6r - 2g\omega^2 + 2j\sigma v)\int_{-\infty}^{+\infty} S_a(\lambda)d\lambda\right|^2$$

$$+\frac{1}{2!}\left[(-2l + n\omega^2)^2 + m^2\omega^2\right]\int_{-\infty}^{+\infty} S_a(\lambda)S_a(\omega - \lambda)d\lambda$$

$$+\frac{1}{3!}\left[(6r - 2g\omega^2)^2 + 4\sigma^2\omega^2\right]\int_{-\infty}^{+\infty}\int_{-\infty}^{+\infty} S_a(\lambda)S_a(\gamma)S_a(\omega - \lambda - \gamma)d\lambda d\gamma \qquad (B.3)$$

There are two terms in $S_y(\omega)$ that can be written in convolution term integrals :

$$\int_{-\infty}^{+\infty} S_a(\lambda)S_a(\omega - \lambda)d\lambda = S_a(\omega) * S_a(\omega) \qquad (B.4)$$

And also,

$$\int_{-\infty}^{+\infty}\int_{-\infty}^{+\infty} S_a(\lambda)S_a(\gamma)S_a(\omega - \lambda - \gamma)d\lambda d\gamma = S_a(\omega) * S_a(\omega) * S_a(\omega) \qquad (B.5)$$

Therefore, a numerical method can be performed for computation of this expression and its integrals. This is in fact the frequency spectrum of the input of the laser. The Volterra series model of the laser is presented in chapter 3. So, by assuming $S_y(\omega)$ as the input, the frequency spectrum of the final output is:

$$S_c(\omega) =< c(t)^2 > \delta(\omega) + S_y(\omega)\left|F_1(\omega) + \frac{1}{2}\int_{-\infty}^{+\infty} F_3(\omega, \lambda, -\lambda)S_y(\omega - \lambda)\right|^2$$

$$+\frac{1}{2!}\int_{-\infty}^{+\infty} S_y(\lambda)S_y(\omega - \lambda)|F_2(\omega - \lambda, \lambda)|^2 d\lambda$$

$$+\frac{1}{3!}\int_{-\infty}^{+\infty}\int_{-\infty}^{+\infty} S_y(\lambda)S_y(\gamma)S_y(\omega - \lambda - \gamma)|F_3(\lambda, \gamma, \omega - \lambda - \gamma)|^2 d\lambda d\gamma \qquad (B.6)$$

The terms $F_2(\omega,\omega)$ and $F_3(\omega,\omega,\omega)$ can be substituted by their equivalent expressions in terms of B_i functions.

$$\frac{1}{2!}\int_{-\infty}^{+\infty} S_y(\lambda)S_y(\omega - \lambda)|F_2(\omega - \lambda, \lambda)|^2 d\lambda$$

$$= \frac{1}{2!}\int_{-\infty}^{+\infty} S_y(\lambda)S_y(\omega-\lambda)\left|\frac{B_2(\omega-\lambda,\lambda)}{B_1(\omega-\lambda)B_1(\lambda)B_1(\omega)}\right|^2 d\lambda$$

$$= \frac{1}{2!}\frac{\left[(-2l+n\omega^2)^2+m^2\omega^2\right]}{(d-f\omega^2)^2+e^2\omega^2}\int_{-\infty}^{+\infty}\frac{S_y(\lambda)S_y(\omega-\lambda)}{|B_1(\lambda)B_1(\omega-\lambda)|^2}d\lambda$$

$$= \frac{1}{2!}\frac{\left[(-2l+n\omega^2)^2+m^2\omega^2\right]}{(d-f\omega^2)^2+e^2\omega^2}\frac{S_y(\omega)}{|B_1(\omega)|^2} * \frac{S_y(\omega)}{|B_1(\omega)|^2} \qquad (B.7)$$

This is another convolution integral that can be computed by the same numerical method that we used for the convolution integral of $S_y(\omega)$. The third term of $S_c(\omega)$ is:

$$\frac{1}{3!}\int_{-\infty}^{+\infty}\int_{-\infty}^{+\infty} S_y(\lambda)S_y(\gamma)S_y(\omega-\lambda-\gamma)|F_3(\lambda,\gamma,\omega-\lambda-\gamma)|^2 d\lambda d\gamma \qquad (B.8)$$

This term is computed by numerical methods for double integrals. So first $S_y(\omega)$ is computed and then it is considered as the input frequency spectrum to the laser and then $S_c(\omega)$ is computed. Numerical results for these computations were demonstrated in chapter 3.

Appendix C

Expression of model in terms of laser parameters

Volterra transfer functions for laser input-output characteristics are derived in chapter 3. There are constants in these expressions that are formed by laser parameters. In this appendix, we present the list of these constants and the corresponding expressions in terms of laser parameters.

$$d = V[\frac{1}{\Gamma\tau_{ph}} + \frac{1}{a\tau_{ph}\tau_s} - \frac{bS_o}{a^2\tau_s\tau_{ph}} + \frac{b\Gamma\beta N_o}{a^2{\tau_s}^2}]$$

$$e = V[\frac{1}{\Gamma} + \frac{1}{a\tau_s} - \frac{bS_o}{a^2\tau_{ph}} + \frac{b\Gamma\beta N_o}{A^2\tau_s} + \frac{1}{a\tau_{ph}}]$$

$$f = \frac{V}{a}$$

$$l = V[\frac{b}{a^2\tau_s\tau_{ph}} - \frac{\theta S_o}{\tau_s\tau_{ph}} + \frac{\theta\Gamma\beta N_o}{{\tau_s}^2}]$$

$$m = V[\frac{b}{a^2\tau_s} + \frac{2b}{a^2\tau_{ph}} + \frac{2\theta\Gamma\beta N_o}{\tau_s} - \frac{2\theta S_o}{\tau_{ph}}]$$

$$s = \frac{bV}{a^2}$$

$$r = V[\frac{\theta}{\tau_s\tau_{ph}} + \frac{\gamma S_o}{\tau_s\tau_{ph}} - \frac{\gamma\Gamma\beta S_o}{{\tau_s}^2}]$$

$$\sigma = V[\frac{\theta}{\tau_s} + \frac{3\theta}{\tau_{ph}} + \frac{3\gamma S_o}{\tau_{ph}} - \frac{3\gamma\Gamma\beta N_o}{\tau_s}]$$

$$g = V\theta$$

$$a = \Gamma(gS_o + \frac{\beta}{\tau_s} - \epsilon g S_o{}^2 0$$

$$b = \Gamma(g - 2\epsilon g S_o)$$

$$c = -\Gamma\epsilon g$$

$$\theta = \frac{b^2}{a^3} - \frac{c}{a^2}$$

$$\gamma = \frac{2bc}{a^3} - \frac{b^3}{a^4}$$

$$S_o = \frac{\Gamma\tau_{ph}(I_o - I_{th})}{V}$$